PERFORMANCE EVALUATION OF AN ENHANCED CYCLIC SOLVENT PROCESS (ECSP) FOR THIN HEAVY OIL RESERVOIRS

A Thesis

Submitted to the Faculty of Graduate Studies and Research

In Partial Fulfillment of the Requirements

For the Degree of

Master of Applied Science

In

Petroleum Systems Engineering

University of Regina

By

Ping Yang

Regina, Saskatchewan

September 2013

UNIVERSITY OF REGINA

FACULTY OF GRADUATE STUDIES AND RESEARCH

SUPERVISORY AND EXAMINING COMMITTEE

Ping Yang, candidate for the degree of Master of Applied Science in Petroleum Systems Engineering**,** has presented a thesis titled, ***Performance Evaluation of an Enhanced Cyclic Solvent Process (ECSP) for Thin Heavy Oil Reservoirs,*** in an oral examination held on September 13, 2013. The following committee members have found the thesis acceptable in form and content, and that the candidate demonstrated satisfactory knowledge of the subject material.

External Examiner:	Dr. Adisron Aroonwilas, Industrial Systems Engineering
Supervisor:	Dr. Daoyong Yang, Petroleum Systems Engineering
Committee Member:	Dr. Farshid Torabi, Petroleum Systems Engineering
Committee Member:	Dr. Peng Luo, Petroleum Systems Engineering
Chair of Defense:	Dr. Doug Durst, Faculty of Social Work

ABSTRACT

Canada's energy future depends on heavy oil resources, which are mainly located in Western Canada, i.e., Saskatchewan and Alberta, and account for almost half of the total world heavy oil reserves. At present, only 8-9% of the original oil in place (OOIP) can be recovered in such heavy oil reservoirs with the current available technology because the oil is very viscous and contained in thin formations. It has been found that cyclic steam stimulation and steam-assisted gravity drainage (SAGD) and vapour extraction (VAPEX) often do not work for recovering heavy oil in such thin reservoirs. The enhanced cyclic solvent process (ECSP) experimentally shows its potential to increase heavy oil recovery in such thin formations by using methane (CH_4) and propane (C_3H_8) as two separate slugs in a cyclic manner. So far, no comprehensive numerical simulation has been conducted to evaluate the performance of the ECSP in the laboratory- and field-scale.

Pressure-volume-temperature (PVT) tests have been performed for the solvent(s)-heavy oil systems. Then, the PVT properties are simulated by using the CMG WinProp module. For the CH_4-C_3H_8-heavy oil mixture, the swelling factor of heavy oil maintains at a relatively high value for each test temperature, while the measured saturation pressures are also found to have high values. The tuned Peng-Robinson equation of state (PR EOS) (1978) model can be used to reproduce the saturation pressures and swelling factors with an average relative error of 3.68% and 3.76%, respectively, while the modified viscosity model is able to predict the viscosity of solvent(s)-heavy oil systems with an average relative error of 10.74%.

Numerical techniques are developed to history match the ECSP profile in the laboratory scale, while efforts have been made to examine the effects of molecular diffusion, dispersion, and foamy oil behaviour on the ultimate oil recovery. Finally, the operational parameters are optimized by using the orthogonal design method. There exists a good agreement between the experimental and numerical results for each individual ECSP test. As for the diffusion coefficient, a minor impact on the oil recovery is observed while the dispersion coefficient imposes a strong impact. The reaction frequency factor (RFF) for gas exsolution from bubble to gas phase almost shows no influence on the simulated oil recovery. In comparison, the RFFs for gas dissolution and exsolution from oil phase to bubble affect the oil recovery to a larger extent. The injection pressure of CH_4 and minimum production pressure are found to be the most sensitive parameters.

The field-scale simulation is conducted to evaluate the ECSP performance in the Pelican oilfield. Subsequently, the orthogonal design method is applied to optimize the operational parameters. Finally, these optimized operational parameters are selected to predict the production performance. There exists a good agreement between the simulated production profiles and the observed field data. The minimum well bottomhole pressure is found to be the most sensitive parameter while the injection time of CH_4 and C_3H_8 as well as soaking time are also subject to relatively large sensitivities. As for the ECSP performance, the cumulative oil production increases quickly with time once the ECSP is initiated, and then its increasing rate slows down slightly after two years of production. After ECSP treatment, the oil saturation decreases due to good oil production near the wellbore and the exsolution of solution gas from heavy oil.

ACKNOWLEDGEMENTS

I would like to express my sincere gratitude to my academic supervisor, Dr. Daoyong (Tony) Yang, for his strong support, continuous patience, excellent guidance, and valuable advice throughout my graduate studies at the University of Regina.

I would also like to acknowledge the following individuals or organizations for their encouragement and support:

- My past and present research group members: Dr. Huazhou Li, Mr. Sixu Zheng, Mr. Chengyao Song, Miss Min Yang, Mr. Feng Zhang, Ms. Huijuan Sun, Mr. Yin Zhang, Miss Xiaoli Li, Mr. Deyue Zhou, Mr. Yu Shi, and Mr. Zhan Chen, for their useful technical discussions and assistance;
- Natural Sciences and Engineering Research Council (NSERC) of Canada for a Discovery Grant to Dr. Yang;
- Petroleum Technology Research Centre (PTRC) for the innovation fund to Dr. Yang;
- Computer Modelling Group Ltd. for providing the CMG WinProp and STARS simulator;
- Many friends, especially Ms. Jianli Li, Mr. Xinfeng Jia, and Mr. Ryan Wilton for their great friendship during my stay in Regina;
- My parents, Mrs. Zhen Leng and Mr. Shaoqing Yang, my brother, Mr. De Yang, and my parents-in-law, Mrs. Yujie Ma and Mr. Fuguo Zhang, for their continuous support and unconditional love.

DEDICATION

To my dearest parents, Mrs. Zhen Leng and Mr. Shaoqing Yang,

and my beloved husband, Mr. Shuo Zhang

TABLES OF CONTENTS

LIST OF TABLES

LIST OF FIGURES

NOMENCLATURE

Notations

a, b, and c	Coefficients with their respective values listed in TABLE 3-3
b_1, b_2, b_3, b_4, and	To-be-determined coefficients in viscosity correlation
c_f	Rock compressibility, psi^{-1}
c_w	Water compressibility, psi^{-1}
B_g	Gas formation volume factor
B_{gi}	Initial gas formation volume factor
B_o	Oil formation volume factor
B_{oi}	Initial oil formation volume factor
B_w	Water formation volume factor
$BubCH_4$	Methane bubble in oil phase
$BubC_2H_6$	Ethane bubble in oil phase
$BubC_3H_8$	Propane bubble is oil phase
$(CH_4)_L$	Dissolved methane in oil phase
$(C_2H_6)_L$	Dissolved ethane in oil phase
$(C_3H_8)_L$	Dissolved propane in oil phase
$(CH_4)_G$	Methane in gaseous phase
$(C_2H_6)_G$	Ethane in gaseous phase
$(C_3H_8)_G$	Propane in gaseous phase
k_{CH_4}	Reaction frequency factor (RFF) for CH_4 dissolution

m	Ratio of the initial hydrocarbon pore volume of the gas cap to that of the oil
MW	Molecular weight
MW_w	Average molecular weight in weight fraction
MW_n	Average molecular weight in mole fraction
N	Stock tank oil initially in place, m^3
N_{BubCH_4}	$BubCH_4$, mole/m^3
$N_{(CH_4)_G}$	CH_4 concentration in gas phase, mole/m^3
$N_{(CH_4)_L}$	CH_4 concentration in oil phase, mole/m^3
nc	Number of components in the mixture
N_g	Gas concentration, mole/m^3
N_o	Oil concentration, mole/m^3
N_p	Cumulative oil production, m^3
ΔP	Pressure drop, psi
P	Pressure, kPa
P_b	Saturation pressure, kPa
P_c	Critical pressure, kPa
P_i	Initial reservoir pressure, psi
Q	Flow rate, cm^3/min
R	Universal gas constant, 8.314 Pa·m^3/(K·mol)
R_p	Cumulative gas oil ratio
R_s	Solution gas oil ratio

R_{si}	Initial solution gas oil ratio
SF	Swelling factor
SG	Specific gravity
S_{wc}	Connate water saturation
S^2	Variance
t	Time, day
T	Temperature, K
T_b	Normal boiling point, °C,
T_c	Critical temperature, K
T_r	Reduced temperature
v	Molar volume, m^3/kmol
v_{s2}	Molar volume of the total fluid sample, m^3/kmol
v_{s1}	Molar volume of heavy oil at atmospheric pressure and saturation temperature, m^3/kmol
V_c	Critical volume, l/mol
W_e	Cumulative water influx, m^3
W_p	Cumulative water produced, m^3
X	Mole fraction of a solvent in heavy oil
$x_{(CH_4)_{Leqm}}$	Mole fraction of CH_4 in oil phase in equilibrium condition
$x_{(CH_4)_L}$	Mole fraction of CH_4 in oil phase
x_i	Data set
$\bar{x}$	Mean value of the data set

$y_{(CH_4)_G}$	Mole fraction of CH_4 in gas phase
Z	Rackett's compressibility factor

Greek letters

α	Alpha function
δ_{ij}	Binary interaction coefficient between the *i*th component and *j*th component
φ	Rotational coupling coefficient
μ_o	Viscosity of heavy oil at atmospheric pressure, cP
μ	Viscosity, cP
ρ_l	Liquid density, kg/m^3
ρ_o	Density of heavy oil at atmospheric pressure, kg/m^3
ρ_r	Reduced density of the reference substance
ρ_s	Density of liquid solvent, kg/m^3
ω	Acentric factor
Ω_a, Ω_b	EOS parameters

CHAPTER 1 INTRODUCTION

1.1 Thin Heavy Oil Resources

With the rising global demands on energy and depleting conventional oil resources, the heavy oil resources in Western Canada, i.e., Saskatchewan and Alberta, are increasingly important. About 62% of Canada's total heavy oil resources was discovered in Saskatchewan, including 21.4 billion barrels of proved reserves (Bowers and Drummond, 1997). As for these resources, approximately 97% is located in reservoirs with the payzones of less than 10 m, among which about 55% is contained in reservoirs with the payzones of less than 5 m (Saskatchewan Energy and Resources, 2008).

As for Lloydminster area, it is located on the Alberta-Saskatchewan border, containing 19 billion barrels of original oil in place (OOIP) (Alvarez *et al*., 2009) with its production mainly from the middle Mannville Group (Marsh and Hein, 2008). Of this area's OOIP, around 80% is found in formations less than 5 m thick (Alvarez *et al*., 2009).

1.2 Technology Challenges

In the Lloydminster area, the primary recovery is only 4-6% of OOIP due to low solution gas available (about 50 scf/bbl), high oil viscosity and sand production (Adams, 1982), while heavy oil waterfloods all exhibit very poor sweep efficiency because of an adverse mobility ratio, reservoir heterogeneity, variation of oil viscosity, and channelling (Miller, 2006). After primary production and waterflood, only 5-10% of OOIP is

recovered (Liu *et al*., 2006). Thermal and non-thermal enhanced oil recovery (EOR) methods have been attempted to recover heavy oil in the Lloydminster area with limited successes (Jameson, 1973; Miller, 1987; Butler and Jiang, 2000; Dong, *et al*., 2011).

The cyclic steam stimulation (CSS) failed in this area as a result of lacking gravity drainage in the thin reservoirs and steam channelling into nearby water zones (Jameson, 1973). Four steamflooding tests were hampered due to excessive heat losses, channelling resulted by high injection pressure, and mechanical problems (Jameson, 1973; Miller, 1987). As for the *in-situ* combustion, it was not economically feasible due to the operating problems, front control and tremendous quantities of the air required (Jameson, 1973). Steam-assisted gravity drainage (SAGD) could be uneconomical due to high heat loss and low drainage rate (Tavallali *et al*., 2012).

Polymer flooding was found to be unsuccessful because of adverse mobility ratio, incompatibility of the polymer and saline formation water, and severe water channelling through high permeability layers while caustic or alkaline flooding was suspended due to poor economics (Miller, 1987). Due to lack of efficient gravity drainage in thin formations, the extremely low production rate makes the vapour extraction (VAPEX) process uneconomic (Butler and Mokrys, 1991; Zeng *et al*., 2008). Due mainly to the paucity of natural CO_2 sources in the surrounding areas, CO_2 huff-n-puff cannot be considered as the most economically attraction option (Padamsey and Railton, 1993).

Enhanced cyclic solvent process (ECSP) may be a potential technique to recover heavy oil in such thin formations by using CH_4 and C_3H_8 as two separate slugs in a cyclic manner (Yadali Jamaloei *et al*., 2012). So far, no comprehensive numerical simulation has been conducted to evaluate the performance of the ECSP in the

laboratory- and field-scale, though the ECSP tests have experimentally shown good potential on oil recovery.

1.3 Objectives of the Study

The primary purpose of this study is to comprehensively evaluate the performance of ECSP in the laboratory- and field-scale. The detailed objectives are listed as follows,

(1) To study the phase behaviour of solvent(s)-heavy oil systems by conducting PVT tests in order to facilitate understanding the mechanisms of ECSP and prepare the PVT properties for numerical simulations;

(2) To evaluate the ECSP performance by history matching the experimental measurements and optimizing the operational parameters so that the potential of ECSP can be comprehensively examined; and

(3) To evaluate the field-scale ECSP performance by conducting production prediction with the optimized operational parameters.

1.4 Outline of the Thesis

This thesis is consisted of six chapters. More specifically, Chapter 1 is an introduction to the research topic together with the research objectives. Chapter 2 provides an up-to-date literature review on recovery techniques of thin heavy oil reservoirs, mechanisms of cold heavy oil production with sand (CHOPS), phase behaviour of solvent(s)-heavy oil systems, and application of optimization techniques in oil and gas production. Chapter 3 describes the experimental setup and procedures for

conducting PVT tests, presents the experimental results, and performs PVT simulations by using the CMG WinProp module. Chapter 4 focuses on sandpack ECSP experiments, history matching the experimental measurements, and examines the effects of molecular diffusion, dispersion, and non-equilibrium solubility with foamy oil behaviour on the ultimate oil recovery. Also, the operational parameters are then optimized to maximize oil recovery. Chapter 5 evaluates the ECSP performance in the Pelican oilfield by predicting production with the optimized operational parameters. Chapter 6 summarizes scientific findings of this research and provides several recommendations for future studies.

CHAPTER 2 LITERATURE REVIEW

Canada's energy future depends on heavy oil resources, which are mainly located in Western Canada, i.e., Saskatchewan and Alberta, and account for almost half of the total world heavy oil reserves. At present, only 8-9% of the original oil in place (OOIP) can be recovered in the heavy oil reservoirs in Western Canada with the current technology available because the oil is very viscous and contained in thin reservoirs. As for the proved heavy oil reserves in Saskatchewan, about 97% is contained in reservoirs with the payzones of less than 10 m, among which 55% is located in reservoirs with the payzones of less than 5 m (Saskatchewan Energy and Resources, 2008).

In Saskatchewan, heavy oil production mainly originated from the Lindberg and the southern Cold Lake oil sand area as well as Lloydminster area. Located on the Alberta-Saskatchewan border as shown in **FIGURE 2-1**, the Lloydminster area contains 19 billion barrels of OOIP (Alvarez *et al.*, 2009) with its production mainly from the middle Mannville Group (Marsh and Hein, 2008). The reservoirs in Lloydminster area are relatively shallow with depth ranging from 500 to 600 m and temperatures around 22°C (Alvarez *et al.,* 2009). Such shallow reservoirs are characterized as very fine to fine grains with relatively clean quartz unconsolidated sand bodies. The formation permeability is in the range of 100 to 5,000 mD, while the porosity spans from 29 to 35% (Adams, 1982; Alvarez *et al.,* 2009). On average, the oil gravity is about 13 to 17 °API, though dead oil viscosities can attain as high as 40,000 mPa·s (Alvarez *et al.,* 2009).

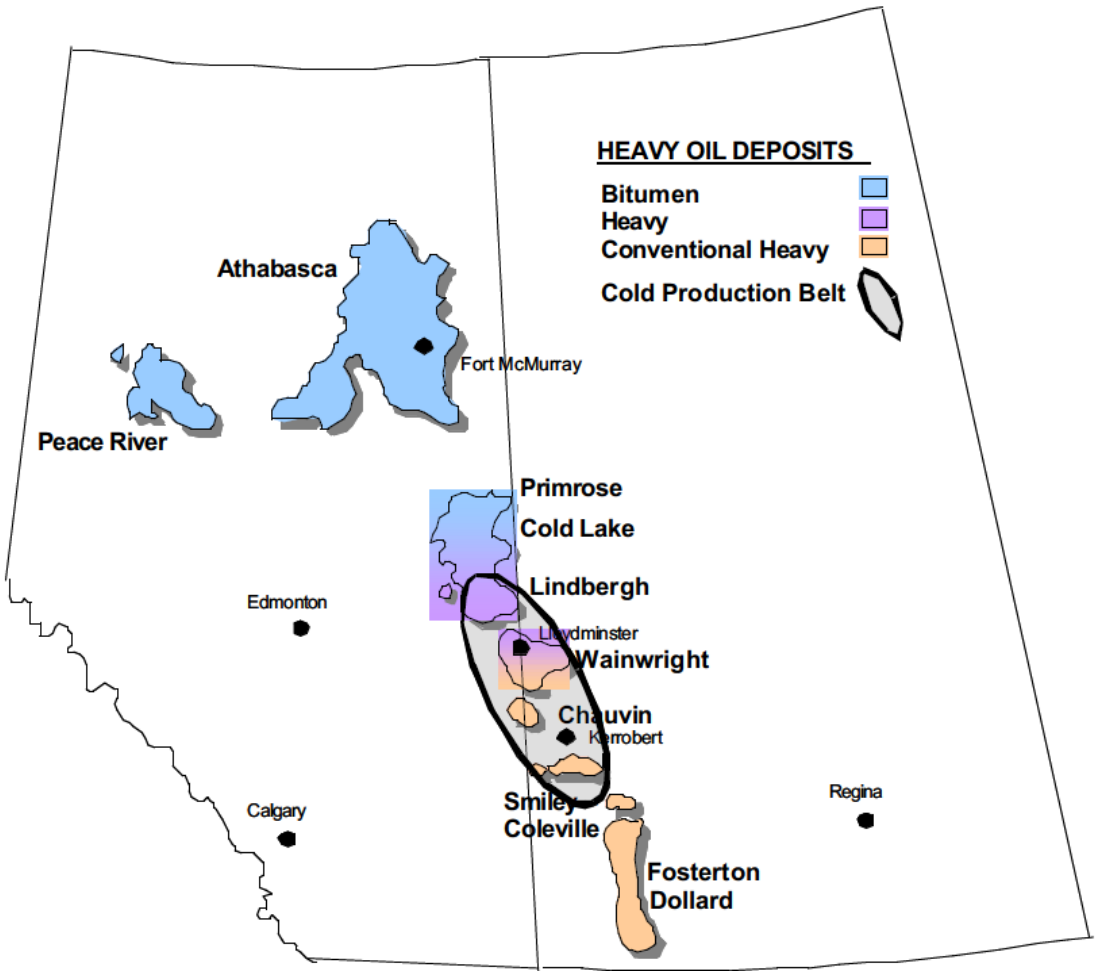

FIGURE 2-1: Heavy oil deposits in Saskatchewan and Alberta with an indication of the cold production belt surrounding Lloydminster area (Sawatzky *et al.*, 2002)

2.1 Recovery Techniques

In Lloydminster area, the first oil well was completed in 1938, but the actual commercial production did not commence until in 1943. In 1945, its total oil production was only 50,000 barrels for the whole year, but the refinery capacity reached 2,500 b/d for the following year with the development of Husky Oil Company. By 1955, the annual oil production is about 3,000,000 barrels. In 1973, there were about 1,700 active oil, gas, and service wells in the region with oil production about 35,000 b/d (Jameson, 1973). In 2012, the annual crude oil production in Lloydminster area is about 20,000,000 barrels (CAPP, 2013).

2.1.1 Primary depletion

Primary drive mechanisms in the Lloydminster area include solution gas drive, rock compaction, and possibly limited edge water drive (Adams, 1982). Due to low solution gas available (about 50 scf/bbl), high oil viscosity and sand production, the primary recovery is only 4-6% of OOIP. In general, a well can produce several hundred barrels of sand over its lifespan, though different sand control methods, including screens, sand consolidation, and gravel packs, have been tried but failed (Jameson, 1973).

In addition to the laboratory depletion tests with a 2 m long sandpack, Chen and Maini (2005) utilized the CMG black oil simulator (IMEX) and thermal simulator (STARS) to history match the depletion experiments. Due to the existence of foamy oil, the STARS simulator was found to provide more accurate history matching results,

though further efforts are required to conduct field-scale simulations to identify the mechanisms governing associated the depletion process.

2.1.2 Waterflooding

Since 1965, waterflooding has been generally used with different pattern arrays (Jameson, 1973). After implementing waterflooding in the Aberfeldy Sparky, Big Gully McLaren/Waseca, Golden Lake Waseca/Sparky, Gully Lake Waseca, Lashburn Waseca and Northminster Sparky formations, the ultimate oil recovery remains low and less than 10% of the OOIP due mainly to the adverse mobility ratio of water and oil (Adams, 1982). In 1992, a heavy oil waterflooding project including more than 200 wells was initiated at the Golden Lake field with poor performance because some wells suffered from premature water breakthrough and others showed no response at all (Forth *et al*., 1996). Heavy oil waterfloods in Western Canada all exhibit very poor sweep efficiency because of an adverse mobility ratio, reservoir heterogeneity, variation of oil viscosity, and channelling (Miller, 2006).

Numerous attempts have been made to evaluate and predict the waterflooding performance for Canadian heavy oil pools (Kasrale *et al*., 1993; Ko *et al*., 1995). Due to the substantial assumptions made to achieve a good history match, the predictive accuracy of the reservoir simulators is greatly compromised (Miller, 2006).

2.1.3 EOR methods

After primary production and waterflood, only 5-10% of OOIP is recovered (Liu *et al*., 2006). Thermal and non-thermal EOR methods have been considered to recover

heavy oil in the Lloydminster area (Jameson, 1973; Miller, 1987; Butler and Jiang, 2000; Dong *et al*., 2011). Thermal EOR methods include CSS, steam drive, *in-situ* combustion, and SAGD, while non-thermal EOR methods are further subdivided into polymer floods, caustic flooding, and solvent-based methods.

1) Thermal methods

In 1965-1966, thirty-two CSS tests were performed in the Lloydminster area, but very few of them were found to be economic (Miller, 1987). The CSS failed in this area as a result of lacking gravity drainage in the thin reservoirs and steam channelling into nearby water reservoirs (Jameson, 1973). However, performance of the Pikes Peak pilot has been successful due to its thicker formations (7-28 m), though the bottom water was highly detrimental to its performance (Milha, 1986). In general, the CMG STARS simulator is usually used to evaluate performance of the thermal heavy oil recovery process due to its incorporation of the thermal cracking and burning reactions (Ambastha and Kumar, 1999). By evaluating the corresponding performance in a typical Cold Lake formation, CSS process is found to be uneconomical if the payzone is less than 11 m (Chang, 2013).

Four steamflooding tests were piloted in the Sparky formation and one in the Waseca formation, all of which were hampered due to excessive heat losses, channelling resulted from high injection pressure, and mechanical problems (Jameson, 1973; Miller, 1987). In 1984, a steamflooding project was initiated in the Pikes Peak and subsequently has expanded to 219 active, 10 observation and 8 salt water disposal wells by mid-2001

(Wong *et al*., 2003). The STARS simulator was used to evaluate the well configurations for steamflooding in thin heavy oil formations. Due to the limited contribution by gravity drainage, it was not feasible to combine horizontal and vertical wells in this regard (Zan *et al*., 2010).

As for the *in-situ* combustion, it was not economically feasible due to the operating problems, front control and tremendous quantities of the air required (Jameson, 1973). Since 1969, *in-situ* combustion pilots have been tested for 17 years in the Golden Lake and for 14 years in the Aberfeldy Sparky formation, respectively. Technical problems such as water influx, gas channelling, high sand cuts, and corrosion failed these two pilots (Miller, 1987). Although numerical simulations were performed to history match the experimental low-temperature oxidation behaviour, more efforts need to develop an accurate simulator for the *in-situ* combustion process due to its complexity in thermal cracking and kinetics (Freitag, 2010).

Due to the notion that higher heat loss and lower drainage rate in thin reservoirs could make the process uneconomical, SAGD has not obtained adequate attention for Lloydminster type of reservoir (Tavallali *et al*., 2012). Also, effect of well configuration on SAGD was examined, while the multi-lateral pattern was considered as the optimum well configuration for the thin reservoirs in Lloydminster.

2) Non-thermal methods

In order to improve the mobility ratio, polymer flooding was used with higher sweep

efficiency, though the additional oil recovery can only attain 4% of OOIP (Miller, 1987). Polymer flooding has not seen extensive applications due mainly to the relatively high cost of polymer (Jameson, 1973). Polymer flooding was conducted in the Blackfoot Sparky reservoir from 1964-1967 and found to be unsuccessful because of adverse mobility ratio, incompatibility of the polymer and saline formation water, and severe water channelling through high permeability layers, while similar problems encountered in the Aberfeldy Sparky reservoir (Miller, 1987).

Caustic or alkaline flooding was suspended in the Wainwright Sparky field in 1983 due to poor economics (Miller, 1987). Laboratory experiments were conducted to enhance oil recovery by applying alkaline for the Pelican Lake reservoir (Arhuoma *et al*., 2009a; b; Dong *et al*., 2011). It was found that the optimum concentration was 0.6 wt% NaOH to achieve the maximum recovery of 15% OOIP in the laboratory experiments, but it is still needed to be piloted for field performance.

The inherent mechanisms should be taken into account in order to numerically simulate the chemical flooding in an accurate and reliable manner (Thomas *et al*., 2001). As for alkaline flooding in heavy oil reservoirs, the increase in oil recovery is due mainly to the *in-situ* formation of water-in-oil (W/O) emulsions because of its blockage of the high permeability zones (Arhuoma *et al*., 2009b). According to field-scale simulation by using the STRAS simulator, polymer flooding is more efficient when combining with parallel horizontal wells since both injectivity of the viscous polymer solution and oil production rate can be increased in the East Bodo reservoir, Lloydminster (Wassmuth *et al*., 2009).

Numerous attempts have been made to develop solvent-based processes to recover heavy oil, among which the VAPEX process has gained a considerable attention over the past two decades (Butler and Mokrys, 1991; Butler and Jiang, 2000; James *et al*., 2008). As for the VAPEX processes, the vapourized hydrocarbon solvents are injected into heavy oil or bitumen reservoirs via an upper horizontal well, while the solvent-diluted oil drains to a horizontal production well by gravity. Due to lack of efficient gravity drainage in thin formations, the extremely low production rate makes the VAPEX an uneconomic process (Butler and Mokrys, 1991; Zeng *et al*., 2008). The STARS simulator was used to capture the mechanisms including diffusion/dispersion and viscous fingering in the VAPEX experiments, which was an important finding for accurately predicting field performance (Cuthiell *et al*., 2003).

As for the thin heavy oil formation, the cyclic solvent process (CSP) has been proposed and tested in laboratories and fields in order to accelerate the production rate (Lim *et al*., 1995; 1996; Dong *et al*., 2006; Ivory *et al*., 2010). Different types of gas can be used for the CSP with the most common ones being as CO_2, flue gas, and produced hydrocarbon gas (Olenick *et al*., 1992; Lim *et al*., 1995; 1996; Srivastava and Huang, 1997; Srivastava *et al*., 1999; Dong *et al*., 2006; Ivory *et al*., 2010; Yadali Jamaloei *et al*., 2012). For most heavy oil reservoirs in Western Canada, CO_2 huff-n-puff cannot be considered as the most economically attraction option due mainly to the paucity of natural CO_2 sources in the surrounding areas (Padamsey and Railton, 1993).

The GEM simulator was applied to simulate the CSP in heavy oil reservoirs with solvent composition of 40 mol% CH_4 and 60 mol% C_3H_8. It was found that molecular diffusion did not affect the production profile obviously, while the main mechanisms

were dominated by the gas drive and dilution effect of solvent (Qi and Polikar, 2005). In the numerical simulations of CSP with solvent composition of 28 vol% C_3H_8 and 72 vol% CO_2, the experimental production data was well matched when diffusion, dispersion, and foamy oil behaviour were considered (Ivory *et al*., 2010; Chang and Ivory, 2012). This method shows a great potential to recovery heavy oil, but it is still needed to be piloted for field performance. In order to perform the CSP effectively in the oilfields, operation parameters should be optimized based on the simulation results under different conditions.

Considering the readily available acquisition, the produced hydrocarbon gas is used to conduct the CSP in order to restore the solution-gas-drive mechanism through repressurizing the reservoirs and make use of viscosity reduction by solvent after termination of either primary depletion or waterflooding (Dong *et al*., 2006). However, the pressure restored by CH_4 injection can be quickly depleted by CH_4 production. Also, the viscosity reduction is not significant due to the low solubility of CH_4 in heavy oil at low or intermediate pressures, while, during the production cycle, the crude oil regains its high viscosity as the dissolved CH_4 leaves the oil (Yadali Jamaloei *et al*., 2012; 2013).

To tackle this problem, the enhanced cyclic solvent process (ECSP) is introduced to recover *in-situ* heavy oil and bitumen in thin formations by using CH_4 and C_3H_8 as two separate slugs in a cyclic manner. As for the ECSP injection cycles, CH_4 as the more-volatile solvent fingers in the oil to provide paths for C_3H_8 as the more-soluble solvent to mix with oil. During the ECSP production cycles, CH_4 provides driving force (expansion) via decreasing the reservoir pressure while some portion of C_3H_8 stays in the oil to maintain the oil viscosity low. A high oil recovery is achieved in the ECSP for six

cycles from the laboratory experiments (Yadali Jamaloei *et al*., 2012). So far, no comprehensive numerical simulation has been conducted to evaluate the performance of the ECSP in the laboratory- and field-scale.

2.2 Cold Heavy Oil Production with Sand (CHOPS)

Cold heavy oil production with sand (CHOPS) appeared as a viable production method for the heavy oil reservoirs by taking the advantage of progressive cavity (PC) pumps in the middle to late 1980s (Sawatzky *et al*., 2002). In western Canada, CHOPS has been mostly applied in thin (2-10 m) and shallow (400-600 m) formations. According to Husky's experience, the primary CHOPS recovery is about 8% of OOIP (Coskuner *et al*., 2013).

The mechanisms of CHOPS can be classified in two categories, i.e., geomechanical effects and fluid effects (Denbina *et al*., 2001). Geomechanical effects refer to the enlarged drainage radius including wormholes, dilated zones or possibility cavities, sand grain flow, liberation of pore blocking materials and clean up of drilling damage, while fluid effects are mainly resulted from foamy oil behaviour (Chugh *et al*., 2000). In practice, the formation of wormholes is considered to be the dominant factor. Numerous attempts have been made to model and simulate the wormhole network generation and growth models as well as foamy oil behaviour (Pan *et al*., 2010).

2.3 Phase Behaviour

The phase behaviour data of solvent-heavy oil systems play an important role in

simulating the solvent-based heavy oil recovery processes. A cubic equation of state (EOS) is generally used to predict solvent solubility, liquid viscosity, phase densities, and phase boundaries. For heavy oil, the existing correlations cannot predict these quantities accurately, thus, for any specific solvent-heavy oil systems, the EOS needs to be properly tuned to match the experimental data (Luo, 2009).

2.3.1 Solubility

Numerous solubility data are available for solvent-heavy oil systems including solubility of CO_2 in the Athabasca bitumen and Utah tar sands (Deo *et al*., 1991), solubility of CH_4, CO_2, C_2H_6, C_3H_8, and n-C_4H_{10} in Cold Lake or Lloydminster heavy oil (Frauenfeld *et al*., 2002; Li *et al*., 2013; Li and Yang, 2013), and solubility of CO_2/C_3H_8 in Athabasca bitumen (Badamchi-Zadeh *et al*., 2009).

Mehrotra and Svrcek (1982) developed an empirical correlation to calculate the solubilities of N_2, CH_4 and CO_2 in Athabasca bitumen with an average deviation of 6.3% for the 71 solubility data, but the correlation is only valid for this specific bitumen. Mehrotra *et al*. (1989) used the PR EOS to determine solubilities of CO, CO_2, N_2, CH_4, and C_2H_6 in Wabasca bitumen by treating the bitumen as three pseudo-components and adjusting the binary interaction parameters (BIP) through the experimental data. In this case, a total of 73 solubility data is well matched with the average deviation of 9.1%. However, the BIP is still a to-be-determined parameter for any other heavy oil or bitumen. Currently, CMG WinProp simulator can be used to determine the solubility of a given solvent by tuning the EOS to match the experimental data (Yazdani and Maini, 2010).

2.3.2 Viscosity

As for the solvent-based heavy oil processes, the major oil recovery mechanism is the viscosity reduction due to solvent dissolution. There are massive viscosity data available for solvent-heavy oil systems in the literature including Athabasca bitumen saturated with N_2, CO_2, CH_4 or a synthetic combustion gas (Mehrotra and Svrcek, 1982), Cold Lake or Lloydminster heavy oil saturated with CH_4, CO_2, C_2H_6, C_3H_8 or n-C_4H_{10} (Frauenfeld *et al*., 2002, Li and Yang, 2013), and Lloydminster heavy oil saturated with C_3H_8 or a solvent mixture (Luo and Gu, 2005, Li *et al*., 2013; Li and Yang, 2013).

Mehrotra and Svrcek (1982) developed an empirical correlation to determine the viscosity of Athabasca bitumen saturated with N_2, CH_4 or CO_2 with an average deviation of 6.7% for the 71 viscosity data, but this correlation is only limited to Athabasca bitumen with the temperature in the range of 20-110°C and the pressure less than 10 MPa. The viscosity data for mixtures of a heavy oil sample collected from Canada's heavy oil reserves and n-decane were used to evaluate the log mixing rule, power-law mixing rule, and the Lederer's mixing rule with the finding that the mixing rule proposed by Lederer is the best (Barrufet and Setiadarma, 2003). As for the Lloydminster area heavy oil, the Lobe's mixing rule is found to be generally superior to other mixing rules in evaluating solvent-saturated heavy oil viscosities (Li, 2013).

2.3.3 Oil-swelling factor

Due to solvent dissolution, the oil swells after solvent contacts with crude oil (Jha, 1986; Bijeljic *et al*., 2003). The oil-swelling factor is defined as the ratio of the heavy oil saturated with solvent at saturation pressure and saturation temperature to the volume of

the original oil at atmospheric pressure and saturation temperature (Teja and Sandler, 1980). It is usually measured in a visual PVT cell with an on-line viscometer (Jha, 1986; Li *et al*., 2013). As for the solvent-heavy oil systems, some data of oil-swelling factor are available (Jha, 1986; Yang and Gu, 2005; 2006; 2007; Li *et al*., 2013; Li and Yang, 2013).

2.3.4 Diffusion and dispersion

Diffusion refers to the random movement of molecules from one part of a system with high concentration to another with low concentration (Ganapathy, 2009; Marufuzzaman, 2010). The molecular diffusion coefficient varies with temperature, pressure, and concentration (Abukhalifeh, 2010). Nevertheless, the diffusion coefficients of pure gases, including CO_2, CH_4, C_2H_6, and C_3H_8 in different bitumens and heavy oils, are normally considered to be constant and fall within the order of 10^{-9} to 10^{-10} m^2/s (Simant and Anil, 2002; Yang and Gu, 2006; Abukhalifeh, 2010; Li, 2013).

The fluid spreading phenomenon through a porous medium is called dispersion, which is a combination of convective dispersion and molecular diffusion (Abukhalifeh, 2010). Dispersion coefficient is often regarded as a constant with 2-3 orders of magnitude higher than the molecular diffusivity (Lim *et al*., 1996; Nghiem *et al*., 2001; El-Haj *et al*., 2009), though it also depends on concentration (Abukhalifeh, 2010).

2.4 Optimization Techniques

Generally, oil production can be increased by 3-25% if focused and continuous

optimization is adopted (Satter and Thakur, 1994). Early optimization studies on reservoir development referred to simple reservoir models, so linear programming techniques were applied (Chen, 2012). A linear programming model was developed to maximize profit by scheduling oil production (Lee and Aronofsky, 1958) and optimize the development plan for a multi-reservoir pipeline system (Bohannon, 1970), respectively. As for the latter, the main variables include number of development wells to be drilled each year, annual production rate from each reservoir, and timing of major capital investments. A multi-objective linear programming model on injection oilfield recovery system was presented to maximize the oil recovery with minimum investment (Xiao *et al*., 1998).

Due to the fact that both the objective function together with its constraint should be linear if the linear programming method is applied, the nonlinear production system is approximated by a system with linear functions (Chen, 2012). Therefore, the application of sophisticated reservoir simulators is limited greatly by such approximation.

Multivariate optimization of production systems was performed by using nonlinear optimization techniques on single-well production (Carroll III and Horne, 1992). Genetic algorithm (GA) was applied to optimize the design and operations for a multi-well production system (Fujii and Horne, 1995). It was found that, for the multiphase network flow problem, multiple solutions may exist, but the legitimate solution was not selected. GA is also useful to deal with the objective function with irregular surface. The production schedule for a group of linked oil and gas fields was optimized by GA in order to maximize the net present value (NPV). GA is found to be suitable to solve such

problems compared to the sequential quadratic programming technique, simulated annealing techniques, and GA combined with local search (Harding *et al*., 1996).

As a special case of GA, orthogonal array (OA) is widely used to design experiments, and it has been considered as the most efficient design because it can handle multiple factors and cover the factor space with fewer runs (Hedayat *et al*., 1999; Wu *et al*., 2001; Kalla and White, 2007). For example, there are 6 factors including injection volume, injection pressure, injection rate, soaking time, well-bottom pressure, and production rate, each of which has five levels (Yang *et al*., 2011). In this case, an OA ($25, 5^6, 2$) was generated and it requires only 25 runs instead of 15,625 runs for a full factorial design.

2.5 Summary

As for the thin formations in Lloydminster area, thermal EOR methods are generally not applicable due to excessive heat losses to overburden and underburden zones. Polymer flooding was found to be unsuccessful because of adverse mobility ratio, incompatibility of the polymer and saline formation water, and severe water channelling, while caustic or alkaline flooding was suspended due to poor economics. As for the VAPEX, the extremely low production rate makes it uneconomic due to lack of efficient gravity drainage in thin formations.

Experimentally, the ECSP shows its potential to increase heavy oil recovery in such thin formations by using CH_4 and C_3H_8 as two separate slugs in a cyclic manner. So far,

no comprehensive numerical simulation has been conducted to evaluate the performance of the ECSP in the laboratory- and field-scale.

The phase behaviour data of solvent-heavy oil systems play an important role in simulating the solvent-based heavy oil recovery processes. For any specific solvent-heavy oil systems, the EOS needs to be properly tuned to match the experimental data. The CMG STARS simulator was usually used to simulate the solvent-based processes, while diffusion, dispersion, and foamy oil behaviour were considered in history matching the experimental data in order to capture the dominant mechanisms, which was an important finding for accurately predicting field performance. In order to perform the solvent-based processes effectively in the oilfields, operation parameters need to be optimized based on the simulation results under different conditions. In this case, OA method may be a good choice due to its high efficiency of designing experiments.

CHAPTER 3 PHASE BEHAVIOUR

For a given solvent-heavy oil system, the associated phase behaviour is the fundamental to match either the experimental data or design the field development scheme. In this chapter, PVT tests have been performed for the C_3H_8-heavy oil systems, CH_4-C_3H_8-heavy oil systems, and C_2H_6-C_3H_8-heavy oil systems under reservoir conditions, respectively (Yang *et al*., 2013). Then, the PVT properties are simulated by using the CMG WinProp module.

3.1 PVT Experiments

3.1.1 Materials

The heavy oil sample, collected from the Lloydminster area in Saskatchewan, Canada, has molecular weight of 389 g/mol measured with the freezing point depression method and specific gravity of 0.9749. The reservoir temperature and pressure are 291-293 K and 1,800-2,400 kPa, respectively. The compositional analysis result of the Lloydminster heavy oil (see **TABLE 3-1**) is measured with the simulated distillation method by using gas chromatography. Physical properties of this heavy oil sample, including density and viscosity, are tabulated in **TABLE 3-2**. The measured density of the heavy oil can be reproduced by the following equation,

$$\rho_o(T, P_o) = -0.6486T + 1162.3162 \qquad [3\text{-}1]$$

where ρ_o is the density of heavy oil at atmospheric pressure in kg/m^3 and T is the temperature in K. The correlation coefficient for this fit is R^2=0.9998.

TABLE 3-1: Compositional analysis result of the heavy oil sample

Component	wt%	Component	wt%
C_1	0.000	C_{32}	1.550
C_2	0.000	C_{33}	1.267
C_3	0.000	C_{34}	1.120
C_4	0.000	C_{35}	1.547
C_5	0.000	C_{36}	1.733
C_6	0.000	C_{37}	1.000
C_7	0.000	C_{38}	0.983
C_8	1.407	C_{39}	1.717
C_9	1.093	C_{40}	1.600
C_{10}	1.433	C_{41}	0.900
C_{11}	1.976	C_{42}	1.025
C_{12}	2.091	C_{43}	1.475
C_{13}	2.625	C_{44}	1.540
C_{14}	2.625	C_{45}	0.985
C_{15}	3.083	C_{46}	0.895
C_{16}	2.667	C_{47}	1.000
C_{17}	2.600	C_{48}	1.000
C_{18}	2.800	C_{49}	0.900
C_{19}	2.600	C_{50}	0.880
C_{20}	2.333	C_{51}	0.900
C_{21}	2.583	C_{52}	0.880
C_{22}	1.717	C_{53}	0.830
C_{23}	2.167	C_{54}	0.830
C_{24}	1.867	C_{55}	0.780
C_{25}	2.000	C_{56}	0.690
C_{26}	1.867	C_{57}	0.690
C_{27}	1.887	C_{58}	0.800
C_{28}	1.913	C_{59}	0.700
C_{29}	1.667	C_{60}	0.750
C_{30}	1.629	C_{61+}	18.750
C_{31}	1.655		
		Total	100.000

TABLE 3-2: Physical properties of heavy oil sample

Temperature, K	Viscosity, cP	Density, kg/m^3
288.15	4820	974.9
298.15	1620	969.0
308.15	718	962.6
323.15	253	952.6

The measured viscosity data is fitted by the following equation with a correlation coefficient of R^2= 0.9993,

$$\log_{10}\left[\log_{10}\left(\mu_o\right)\right] = -3.7033\log_{10}\left(T\right) + 9.6728 \qquad [3\text{-}2]$$

where μ_o is the viscosity of heavy oil at atmospheric pressure in cP and T is the temperature in K.

Methane, ethane, and propane (Praxair, Canada) used in the PVT tests have the purities of 99.97 mol%, 99.0 mol%, and 99.99 wt%, respectively. The density of liquid C_2H_6 and C_3H_8 is determined from the following correlation (Yaws, 2003),

$$\log_{10}\left(\frac{\rho_s}{1000}\right) = \log_{10}\left(a\right) - \log_{10}\left(b\right)\left(1 - \frac{T}{T_c}\right)^c \qquad [3\text{-}3]$$

where ρ_s is the density of liquid solvent in kg/m^3, a, b, and c are the coefficients with their respective values listed in **TABLE 3-3**, and T_c is the critical temperature of solvent in K. For a given solvent, the above equation is only applicable below the critical value. As such, it cannot be used to calculate the density of CH_4 because CH_4 is in the supercritical condition at the experimental temperature.

3.1.2 Experimental setup

All the PVT measurements for the solvent(s)-heavy oil systems are conducted by using a mercury-free DBR PVT system (PVT-0150-100-200-316-155, DBR, Canada) as shown in **FIGURE 3-1**. The PVT cell equipped in the PVT system has an inner diameter of 3.177 cm and a total length of 20.320 cm, while it can be operated at pressures up to 69000 kPa and over the temperature range of 238.15 K to 473.15 K. A

TABLE 3-3: Coefficient values in Equation [3-3]

Solvent	*a*	*b*	*c*
C_2H_6	0.2009	0.2733	0.2933
C_3H_8	0.2215	0.2774	0.2870

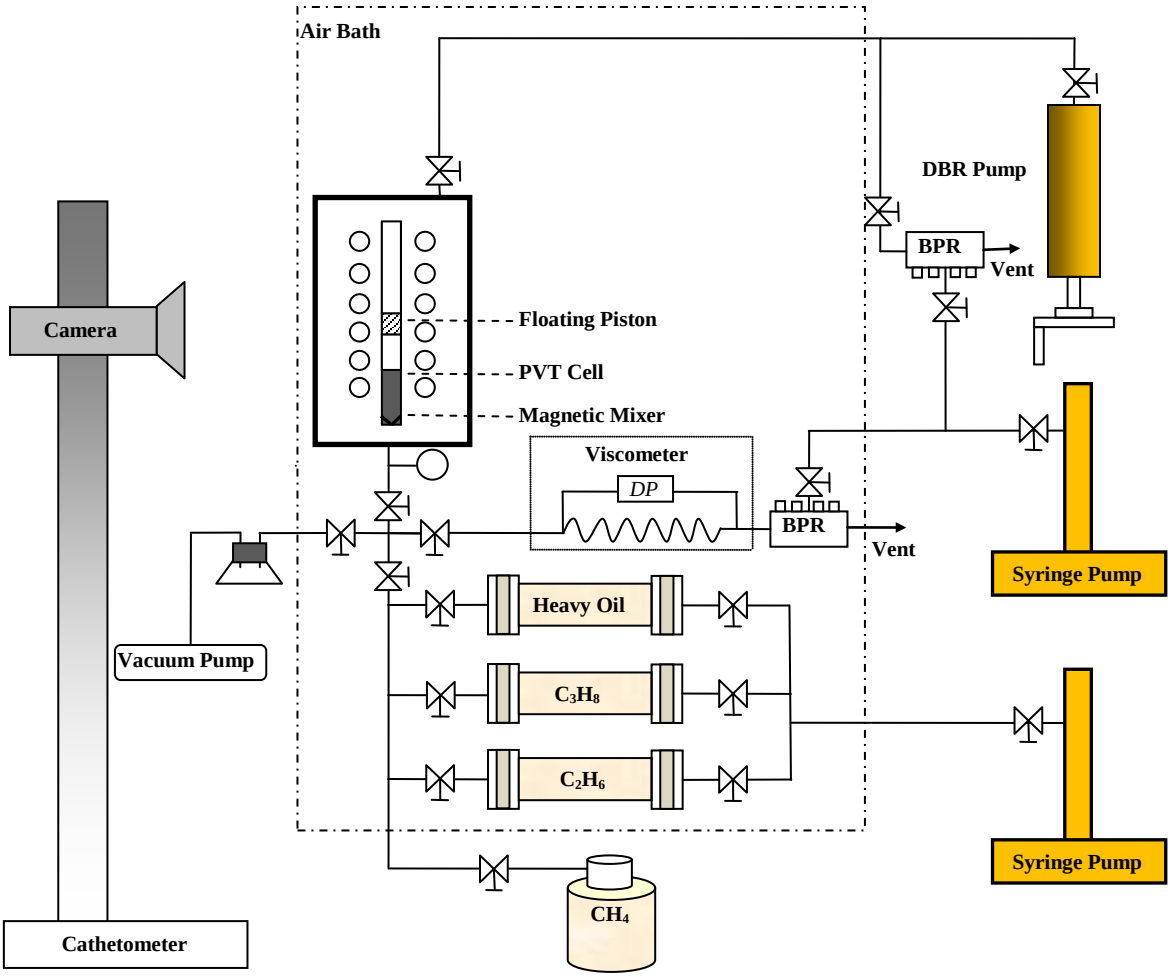

FIGURE 3-1: Experimental setup for conducting the PVT measurements for solvent(s)-heavy oil systems.

floating piston in the PVT cell isolates the test sample from the hydraulic oil. The cell pressure is controlled by using a high-pressure automatic positive-displacement pump (PMP-0500-1-10-MB-316-M4-C0, DBR, Canada). A video-based digital cathetometer with a resolution of 0.002 cm allows direct and accurate measurements of the cell volume. A high-precision test gauge (Model No.: 2089, Ashcroft) with an accuracy of 0.05% of full scale 13790 kPa (i.e., 2000 psia) is attached to the inlet tubing of the PVT cell for pressure measurement. The heavy oil, ethane, and propane are pressurized in three transfer cylinders, while the high-pressure methane can be directly discharged from the gas cylinder. One syringe pump (500 HP, Teledyne ISCO Inc., USA) is used to displace the fluid in the cylinder to the PVT cell, while the other syringe pump applies back pressure for the customized-capillary viscometer. Temperature in the air-bath can be controlled with an accuracy of ±0.1 K. The house-made capillary viscometer can be used to measure the viscosity of fluid sample at the saturation pressures.

A customized-capillary viscometer is constructed and connected to the PVT cell for determining viscosity of the solvent(s)-heavy oil mixture at saturation conditions. The capillary tube is a 3 m long stainless steel tubing (Swagelok, Canada) with an inner diameter (ID) of 0.069 in (0.175 cm) and a wall thickness of 0.028 in (0.071 cm). Two standard viscosity fluids, i.e., S60 and S20 (Cannon Instrument Company, USA), are used as standard viscosity liquids to calibrate the capillary viscometer. The following simplified Poiseuille equation is obtained (Li *et al*., 2013),

$$\mu = (14.3671 - 0.0324T)\frac{\Delta P}{Q} \qquad [3\text{-}4]$$

where μ is viscosity in cP, ΔP is differential pressure in kPa, and Q is flow rate in cm^3/min. The capillary viscometer has an overall accuracy of ±6%.

3.1.3 Experimental procedures

1) C_3H_8-heavy oil systems (Feeds #1-2)

The experimental procedure for conducting phase behaviour measurements for C_3H_8-heavy oil systems is briefly described as follows. Prior to each test, the PVT cell and the tubings are cleaned with kerosene, dried, and then evacuated. Next, a certain amount of liquid propane is injected into the PVT cell. The density of liquid propane in the PVT cell is calculated via Equation [3-3], while its volume is measured with the cathetometer. Subsequently, a certain amount of heavy oil is injected into the PVT cell while the magnetic mixer is kept on. The volume of the injected heavy oil equals to the total volume minus the volume of the injected solvent, assuming that volume change of the heavy oil-solvent mixture is neglected. The temperature of the air-bath is set to be 20.0±1.0°C for at least 12 h prior to any measurement while keeping the magnetic mixer on.

In this study, the continuous depressurization method is used to measure the saturation pressure and swelling factor (Badamchi-Zadeh, *et al.*, 2009; Li *et al.*, 2013). Starting from high-pressure liquid phase, the C_3H_8-heavy oil mixture is depressurized with a withdrawal rate of 3 cm^3/h by using the positive-displacement pump. The pressure can be directly read from the pressure gauge, while the mixture volume can be obtained from the cathetometer. Both saturation pressure and mixture volume at the saturation

pressure can be obtained from the transitioning point on the pressure-volume curve recorded. The swelling factor at a given temperature is determined to be the mixture volume at saturation point divided by the volume of heavy oil at atmospheric pressure and a given temperature. Once measurements at the current temperature are completed, the temperature is increased to another higher level and the continuous depressurization method is applied to perform the corresponding measurements.

After saturation pressure and swelling factor measurements are accomplished, the temperature is reduced to the lowest test temperature. Then the mixture is displaced into the customized-capillary viscometer by using the displacement pump at a given flow rate. The differential pressure is recorded when it reaches a stable value. Thus, Equation [3-4] is used to determine the viscosity of the solvent(s)-saturated heavy oil.

2) CH_4-C_3H_8-heavy oil systems (Feeds #3-4)

Since methane exists as a supercritical fluid at test temperatures, its density cannot be determined by using Equation [3-3]. In this study, with regard to the PVT test for the CH_4-C_3H_8-heavy oil system, a given amount of liquid propane is injected into the PVT cell first. Its mass can be determined once the volume is read from the cathetometer and its density is calculated by using Equation [3-3]. Then the high-pressure methane is injected into the PVT cell. Subsequently, the continuous depressurization method is applied to determine the saturation pressure for the CH_4-C_3H_8 mixture.

The PR EOS (1978) in the CMG WinProp module is used to match the measured saturation pressure by varying the mole fractions of methane and propane in the mixture.

The true mole fractions of methane and propane are the ones which can provide an accurate match between the calculated and measured saturation pressure. Heavy oil is finally added to the solvent mixture at a pressure just above the saturation pressure of the solvent mixture so that the overall composition can be achieved. The experimental procedure for conducting phase behaviour measurements for the C_3H_8-heavy oil system is also applied for the CH_4-C_3H_8-heavy oil system. Note that the viscosity of the saturated-fluids cannot be determined by using Equation [3-4] due to the unstable differential pressure at the test conditions.

3) C_2H_6-C_3H_8-heavy oil systems (Feeds #5-6)

With regard to the PVT test for the C_2H_6-C_3H_8-heavy oil systems, a given amount of liquid propane is injected into the PVT cell first. Its mass can be determined once the volume is read from the cathetometer and its density is calculated by using Equation [3-3]. Then, ethane is injected into the PVT cell at a pressure just above its vapour pressure. The mass of the injected liquid ethane can be determined from the volume reading and density equation again. Similarly, the experimental procedure for conducting phase behaviour measurements for the C_3H_8-heavy oil system has been followed to obtain the phase behaviour data of the C_2H_6-C_3H_8-heavy oil mixtures.

3.2 Preparation of PVT Properties

The CMG WinProp simulator is used to simulate the phase behaviour of solvent(s)-heavy oil systems. The PR EOS (1978) can be expressed as follows,

$$P = \frac{RT}{v-b} - \frac{a}{v(v+b)+b(v-b)} \qquad [3\text{-}5]$$

$$a = a_c \alpha\left(T_r, \omega\right) \qquad [3\text{-}6a]$$

$$a_c = \frac{0.457235 R^2 T_c^2}{P_c} \qquad [3\text{-}6b]$$

and

$$b = \frac{0.0777969 R T_c}{P_c} \qquad [3\text{-}6c]$$

where $\alpha\left(T_r, \omega\right)$ is the alpha function dependent on both the reduced temperature T_r and the acentric factor ω, P is the pressure in kPa, T is the temperature in K, v is the molar volume in m^3/kmol, R is the universal gas constant, 8.314 Pa·m^3/(K·mol), P_c is the critical pressure in kPa, and T_c is the critical temperature in K.

The Soave-type alpha function used in the PR EOS is given by (Peng and Robinson, 1976),

$$\alpha = \left[1 + \left(0.37464 + 1.54226\omega - 0.26992\omega^2\right)\left(1 - T_r^{0.5}\right)\right]^2 \qquad [3\text{-}7]$$

A new form of the alpha function for $\omega > 0.49$ was later proposed by Robinson and Peng (1978),

$$\alpha = \left[1 + \left(0.3796 + 1.485\omega - 0.1644\omega^2 + 0.01667\omega^3\right)\left(1 - T_r^{0.5}\right)\right]^2 \qquad [3\text{-}8]$$

For a mixture system, the following van der Waals mixing rule is used,

$$a = \sum_{i=1}^{nc}\sum_{j=1}^{nc} x_i x_j \left(1 - \delta_{ij}\right)\sqrt{a_i a_j} \qquad [3\text{-}9a]$$

$$b = \sum_{i=1}^{nc} x_i b_i \qquad [3\text{-}9b]$$

where *nc* is the number of components in the mixture, x_i is the molar percentage of the *i*th component in the mixture, a_i and b_i are calculated from Equations [3-6a] and [3-6c] for the *i*th component, respectively, and δ_{ij} is the binary interaction coefficient between the *i*th component and the *j*th component.

In the CMG WinProp module, two viscosity correlations (i.e., the Pedersen corresponding states viscosity correlation and Jossi-Stiel-Thodos (JST) correlation) may be chosen. Unlike the JST technique, the Pedersen correlation does not depend on having accurate density predictions (CMG WinProp, 2011) so that the modified Pedersen correlation is used to determine the viscosity of solvent(s)-heavy oil mixture (Pedersen and Fredenslund, 1987), i.e.,

$$\frac{\mu_{mix}(P,T)}{\mu_o(P_o,T_o)} = \left(\frac{T_{c,mix}}{T_{c,o}}\right)^{-1/6}\left(\frac{P_{c,mix}}{P_{c,o}}\right)^{2/3}\left(\frac{MW_{mix}}{MW_o}\right)^{1/2}\left(\frac{\varphi_{mix}}{\varphi_o}\right) \qquad [3\text{-}10]$$

where μ is viscosity in cP, T_c is critical temperature in K, P_c is critical pressure in kPa, MW is molecular weight, and φ is rotational coupling coefficient. The subscript "mix" refers to the mixture, while the subscript "o" refers to the reference substance, i.e., methane. The molecular weight of the mixture can be determined from (Pedersen and Fredenslund, 1987),

$$MW_{mix} = b_1\left(MW_w^{\,b2} - MW_n^{\,b2}\right) + MW_n \qquad [3\text{-}11]$$

where MW_w and MW_n are the average molecular weight in weight fraction and mole fraction, respectively. The rotational coupling coefficient is determined by

$$\varphi = 1 + b_3 \rho_r^{\,b4} MW^{b5} \qquad [3\text{-}12]$$

where ρ_r is the reduced density of the reference substance. In Equations [3-11] and [3-12], b_1, b_2, b_3, b_4, and b_5 are the to-be-determined coefficients by matching the measured viscosity data.

The swelling factor of a fluid sample can be calculated with the following equation (Teja and Sandler, 1980; Li and Yang, 2013),

$$SF = \frac{v_{s2}}{v_{s1}} \times \frac{1}{1 - X} \qquad [3\text{-}13]$$

where SF is swelling factor, v_{s2} is molar volume of the total fluid sample in m^3/kmol, v_{s1} is the molar volume of heavy oil at atmospheric pressure and saturation temperature in m^3/kmol, and X is mole fraction of a solvent in heavy oil.

The heavy oil is characterized with 7 pseudo-components (see **TABLE 3-4**) after lumping with the Whitson method (Whitson, 1983). The experimental data of one CH_4-C_3H_8-heavy oil system (Feed #3), including saturation pressure (P_b), liquid density (ρ_l), and swelling factor (SF) at saturation pressures for three different temperatures, are used to regress the parameters in the PR EOS. The regressed parameters include the molecular weight of the last two pseudo-components, binary interaction parameters (BIPs) between methane and each pseudo-component, and the BIPs between propane and each pseudo-component.

The measured data of one C_2H_6-C_3H_8-heavy oil system (Feed #5), including the saturation pressures and swelling factors at saturation pressures for three different temperatures, are used to regress the BIPs of ethane with each pseudo-component. The

TABLE 3-4: Pseudo-components of heavy oil after lumping

Pseudo-component	mol%
C_{8-11}	15.64
C_{12-15}	19.48
C_{16-21}	21.64
C_{22-29}	15.21
C_{30-41}	12.20
C_{42-56}	7.78
C_{57+}	8.05

liquid viscosity (μ_l) at the bubble-point pressure at the lowest experimental temperature for Feed #5 together with the viscosities of crude oil (μ_o) at atmospheric pressure for four different temperatures are used to tune the Pedersen viscosity correlation. After tuning the PR EOS (1978) model and the modified Pedersen (1987) corresponding states viscosity model with the measured PVT data, the PVT properties are well prepared for performing the corresponding simulation.

3.3 Results and Discussion

3.3.1 Experimental measurements

FIGUREs 3-2 to **3-4** show the measured pressure-volume curves at the lowest temperatures for the C_3H_8-heavy oil systems (Feeds #1 and 2), CH_4-C_3H_8-heavy oil systems (Feeds #3 and 4), and C_2H_6-C_3H_8-heavy oil systems (Feeds #5 and 6), respectively, where both saturation pressures together with the corresponding mixture volumes can be obtained from the transitioning points.

The constant-composition expansion (CCE) test results (i.e., saturation pressure (P_b), swelling factor (SF), and viscosity) for the C_3H_8-heavy oil systems, CH_4-C_3H_8-heavy oil systems, and C_2H_6-C_3H_8-heavy oil systems are presented in **TABLEs 3-5** to **3-7**, respectively.

TABLE 3-5 shows that a large swelling factor together with a reduced viscosity can be obtained when a large amount of propane is dissolved in heavy oil. The saturation pressure increases when more propane is dissolved in heavy oil at the same temperature, leading to a simultaneous increase in the swelling factor.

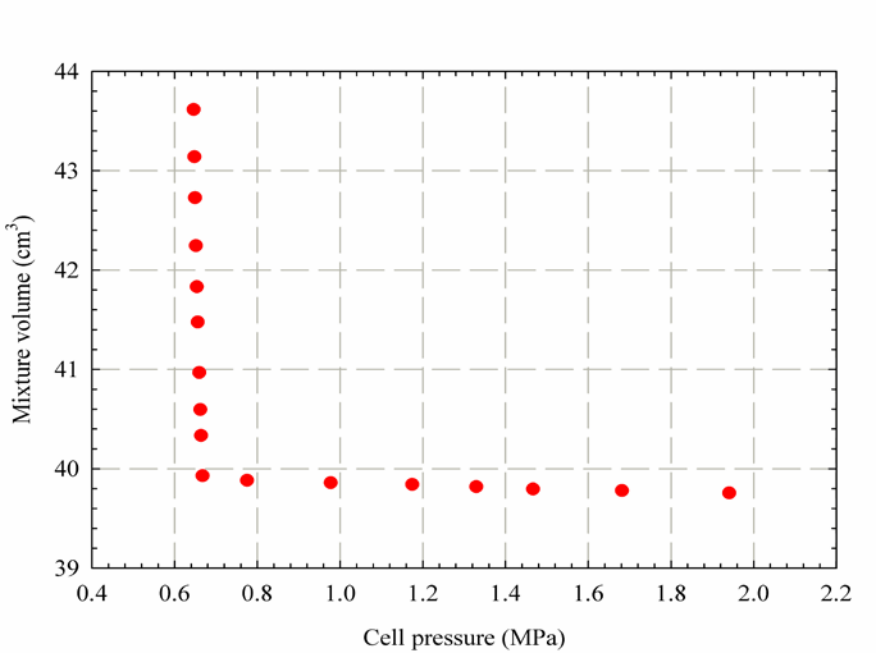

(a)

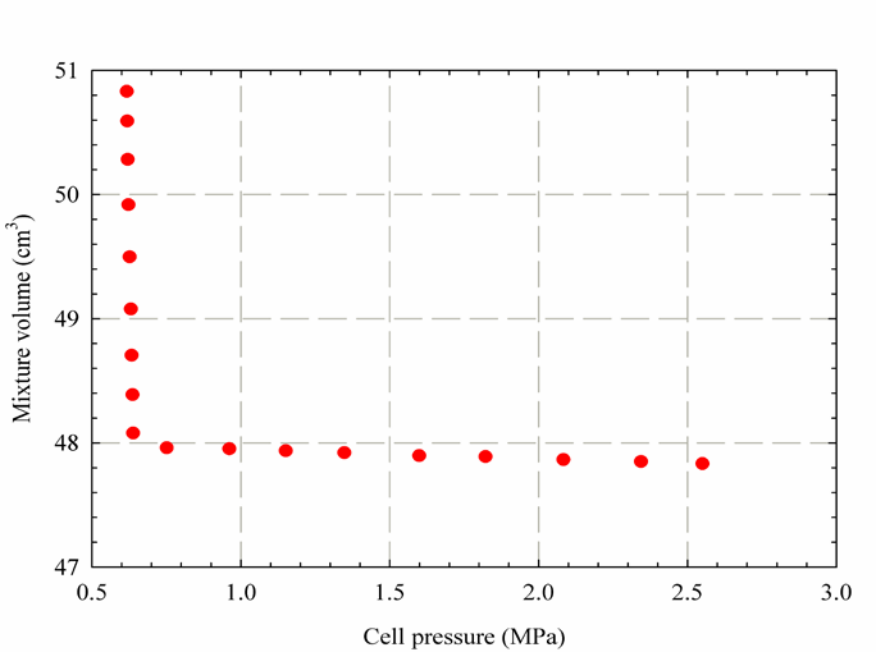

(b)

FIGURE 3-2: Measured P-V relations for the C_3H_8-heavy oil systems: **(a)** Feed #1 at 20.7°C and **(b)** Feed #2 at 20.6°C

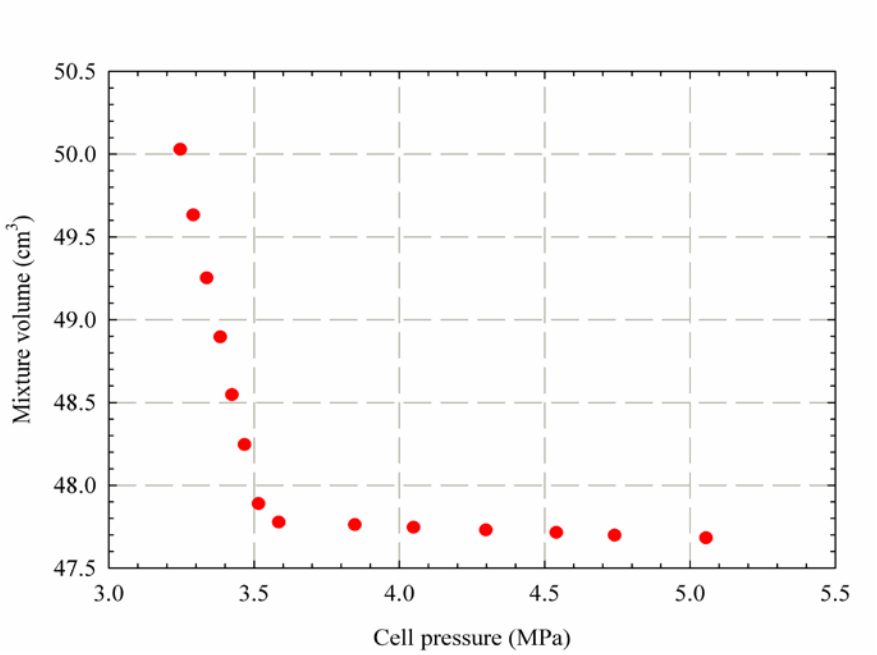

(a)

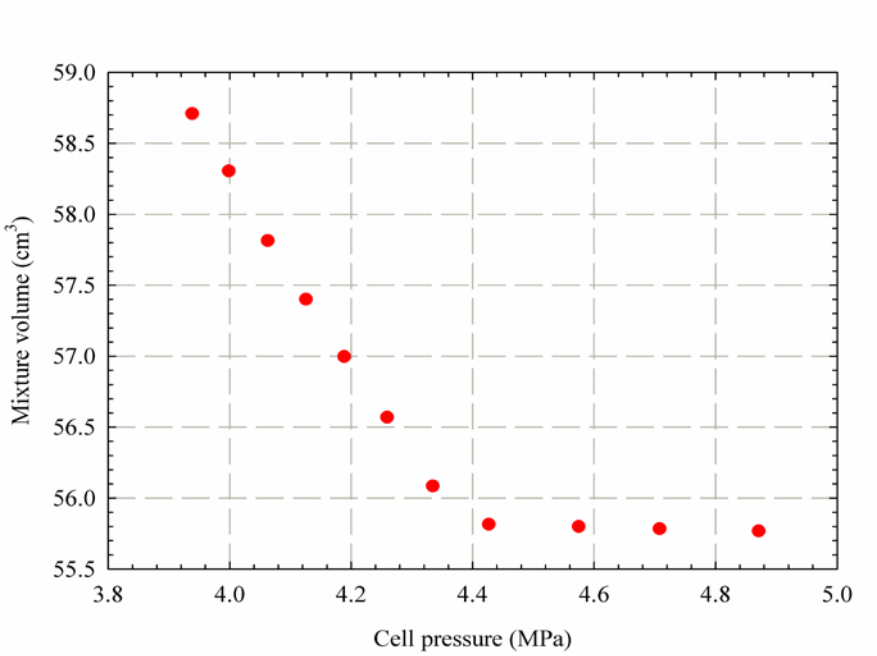

(b)

FIGURE 3-3: Measured P-V relations for the CH_4-C_3H_8-heavy oil systems: **(a)** Feed #3 at 20.5°C and **(b)** Feed #4 at 20.5°C

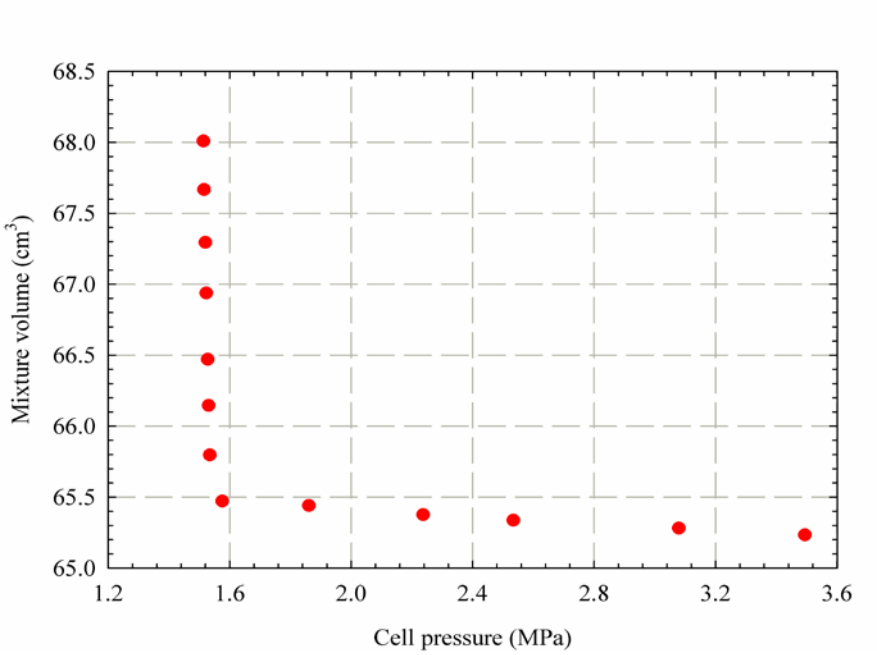

(a)

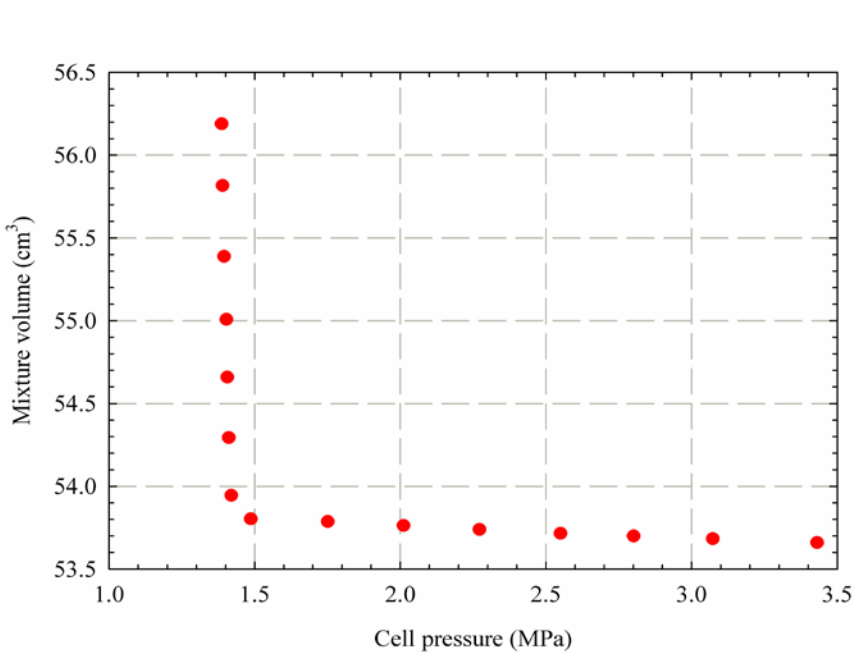

(b)

FIGURE 3-4: Measured P-V relations for the C_2H_6-C_3H_8-heavy oil systems: **(a)** Feed #5 at 20.2°C and **(b)** Feed #6 at 20.0°C

TABLE 3-5: CCE test results for the C_3H_8-heavy oil systems

Feed	C_3H_8 mol%	Heavy oil mol%	T, °C	P_b, kPa	Swelling factor	Viscosity at P_b, cP
#1	57.94	42.06	20.7	664.9	1.304	31.6
			35.0	913.9	1.312	
			49.5	1228.7	1.324	
#2	53.87	46.13	20.6	637.4	1.227	60.7
			35.1	862.3	1.229	
			49.5	1134.9	1.230	

TABLE 3-6: CCE test results for the CH_4-C_3H_8-heavy oil systems

Feed	CH_4 mol%	C_3H_8 mol%	Heavy oil mol%	T, °C	P_b, kPa	Swelling factor	Viscosity at P_b, cP
#3	10.67	53.97	35.36	20.5	3526.7	1.404	/
				35.0	4054.4	1.412	
				49.5	4678.2	1.415	
#4	13.81	49.52	36.67	20.5	4368.5	1.362	/
				35.0	4981.5	1.370	
				49.5	5683.7	1.377	

TABLE 3-7: CCE test results for the C_2H_6-C_3H_8-heavy oil systems

Feed	C_2H_6 mol%	C_3H_8 mol%	Heavy oil mol%	T, °C	P_b, kPa	Swelling factor	Viscosity at P_b, cP
#5	27.75	33.65	38.60	20.2	1531.3	1.358	25.9
				34.8	2026.4	1.363	
				49.5	2644.7	1.370	
#6	22.29	39.68	38.03	20.0	1421.1	1.367	20.0
				35.0	1866.2	1.372	
				49.5	2403.3	1.379	

As for the solvent-based techniques for recovering heavy oil, CH_4, C_2H_6, and C_3H_8 function differently. As can be seen from **TABLE 3-6**, for the same CH_4-C_3H_8-heavy oil mixture, the swelling factor of heavy oil maintains at a high value for each test temperature. Also, if more solvent is dissolved in heavy oil, a larger swelling factor of heavy oil can be achieved. A larger swelling factor is particularly beneficial for recovering more oil. In addition, the saturation pressure increases greatly with the temperature, indicating that the solvent solubility decreases significantly when the temperature increases at the same pressure. As can also be seen from **TABLE 3-6**, the measured saturation pressures are found to have high values, indicating that the dissolved methane can come out of solution and provides sufficient solution-gas driving energy in certain solvent-based schemes when the reservoir pressure drops. Meanwhile, the heavy oil viscosity can still be maintained to be low even at a low pressure during its production cycle because C_3H_8 has a high solubility even at low pressures (see **TABLE 3-5**).

As for the C_2H_6-C_3H_8-heavy oil systems with the results shown in **TABLE 3-7**, the saturation pressures do not present high values like those for the CH_4-C_3H_8-heavy oil systems due mainly to the higher solubility of C_2H_6 than that of CH_4. If ethane and propane are both injected into the reservoir, the dissolved ethane will still stay in the reservoir when the reservoir pressure decreases, so it will not provide sufficient solution-gas driving energy. In this case, ethane acts like propane to reduce viscosity of the reservoir fluid (see **TABLE 3-5**).

3.3.2 Simulation of PVT properties

The simulated PVT properties for Feeds #1-6 are presented in **TABLEs 3-8** to **3-13**. It can be found that the tuned PR EOS (1978) model can be used to reproduce the saturation pressures and swelling factors with an average relative error of 3.68% and 3.76%, respectively, while the modified Pedersen (1987) corresponding states viscosity model is able to predict the viscosity of solvent(s)-heavy oil systems with an average relative error of 10.74%. Considering the fact that the customized-capillary viscometer has an overall accuracy of ±6%, the average relative error resulted from the viscosity prediction falls in the range of 4.74-16.74%.

TABLEs 3-14 and **3-15** show the properties of each component and the matrix for the BIPs in the PR EOS (1978) model after regression, respectively. **TABLE 3-16** tabulates parameters in the modified Pedersen (1987) corresponding states viscosity model which are obtained by matching the measured viscosity data. Subsequently, the aforementioned parameters are incorporated in the CMG STARS simulator to perform history matching of the sandpack experimental results, which will be detailed in Chapter 4.

3.4 Summary

The continuous depressurization method is used to measure the saturation pressures and swelling factors, while a customized-capillary viscometer is constructed and connected to the PVT cell for determining viscosity of the solvent(s)-heavy oil mixtures at saturation conditions. For the C_3H_8-heavy oil system, a large swelling factor together

TABLE 3-8: Simulated PVT results for the C_3H_8-heavy oil system (Feed #1)

Parameter	Measured	Simulated	Relative error, %
P_b at 20.7°C, kPa	664.9	615.4	7.45
P_b at 35.0°C, kPa	913.9	856.5	6.28
P_b at 49.5°C, kPa	1228.7	1160.1	5.58
SF at 20.7°C	1.304	1.268	2.75
SF at 35.0°C	1.312	1.274	2.88
SF at 49.5°C	1.324	1.281	3.27
μ_l at 20.7°C, cP	31.6	35.7	13.10

TABLE 3-9: Simulated PVT results for the C_3H_8-heavy oil system (Feed #2)

Parameter	Measured	Simulated	Relative error, %
P_b at 20.6°C, kPa	637.4	574.6	9.85
P_b at 35.1°C, kPa	862.3	800.9	7.12
P_b at 49.5°C, kPa	1134.9	1078.5	4.97
SF at 20.6°C	1.227	1.227	0.00
SF at 35.1°C	1.229	1.232	0.25
SF at 49.5°C	1.230	1.237	0.60
μ_l at 20.6°C, cP	60.7	55.2	9.03

TABLE 3-10: Simulated PVT results for the CH_4-C_3H_8-heavy oil system (Feed #3)

Parameter	Measured	Simulated	Relative error, %
P_b at 20.5°C, kPa	3526.7	3516.2	0.30
P_b at 35.0°C, kPa	4054.4	4065.7	0.28
P_b at 49.5°C, kPa	4678.2	4678.3	0.00
SF at 20.5°C	1.404	1.334	5.01
SF at 35.0°C	1.412	1.341	5.01
SF at 49.5°C	1.415	1.349	4.65
ρ_l at 20.5°C, kg/m^3	820.1	827.9	0.95
ρ_l at 35.0°C, kg/m^3	808.1	818.3	1.26
ρ_l at 49.5°C, kg/m^3	797.8	808.2	1.30

TABLE 3-11: Simulated PVT results for the CH_4-C_3H_8-heavy oil system (Feed #4)

Parameter	Measured	Simulated	Relative error, %
P_b at 20.5°C, kPa	4368.5	4534.9	3.81
P_b at 35.0°C, kPa	4981.5	5176.7	3.92
P_b at 49.5°C, kPa	5683.7	5873.6	3.34
SF at 20.5°C	1.362	1.308	3.99
SF at 35.0°C	1.370	1.315	4.05
SF at 49.5°C	1.377	1.321	4.03

TABLE 3-12: Simulated PVT results for the C_2H_6-C_3H_8-heavy oil system (Feed #5)

Parameter	Measured	Simulated	Relative error, %
P_b at 20.2°C, kPa	1531.3	1537.0	0.38
P_b at 34.8°C, kPa	2026.4	2029.5	0.15
P_b at 49.5°C, kPa	2644.7	2618.9	0.97
SF at 20.2°C	1.358	1.283	5.49
SF at 34.8°C	1.363	1.290	5.33
SF at 49.5°C	1.370	1.298	5.28
μ_l at 20.2°C, cP	25.9	27.0	4.32
μ_o at 15.0°C, cP	4820.0	4078.9	15.38
μ_o at 25.0°C, cP	1620.0	1666.4	2.86
μ_o at 35.0°C, cP	718.0	757.1	5.44
μ_o at 50.0°C, cP	253.0	273.9	8.27

TABLE 3-13: Simulated PVT results for the C_2H_6-C_3H_8-heavy oil system (Feed #6)

Parameter	Measured	Simulated	Relative error, %
P_b at 20.0°C, kPa	1421.1	1345.4	5.33
P_b at 35.0°C, kPa	1866.2	1801.4	3.47
P_b at 49.5°C, kPa	2403.3	2329.7	3.06
SF at 20.0°C	1.367	1.296	5.20
SF at 35.0°C	1.372	1.303	5.00
SF at 49.5°C	1.379	1.311	4.94
μ_l at 20.0°C, cP	20.0	25.5	27.52

TABLE 3-14: Parameters for the PR EOS (1978) model after regression

	P_c (atm)	T_c (K)	ω	MW	Vol. shift	Z (Rackett)	V_c (l/mol)	Ω_a	Ω_b	SG	T_b (°C)	Parachor
CH_4	45.40	190.60	0.01	16.04	-0.15	0.29	0.10	0.46	0.08	0.30	-161.45	77.00
C_2H_6	48.20	305.40	0.10	30.07	-0.10	0.28	0.15	0.46	0.08	0.36	-88.65	108.00
C_3H_8	41.90	369.80	0.15	44.10	-0.07	0.28	0.20	0.46	0.08	0.51	-42.05	150.30
C_{8-11}	20.81	612.13	0.48	137.42	0.25	0.25	0.59	0.46	0.08	0.73	169.55	390.93
C_{12-15}	16.23	687.93	0.65	193.00	0.29	0.24	0.80	0.46	0.08	0.78	248.67	530.04
C_{16-21}	13.04	758.39	0.85	260.36	0.32	0.23	1.05	0.46	0.08	0.82	325.26	680.43
C_{22-29}	10.52	835.35	1.12	358.21	0.34	0.23	1.31	0.46	0.08	0.87	409.86	863.33
C_{30-41}	8.87	911.79	1.27	495.25	0.32	0.23	1.51	0.46	0.08	0.92	492.42	1048.66
C_{42-56}	8.00	982.15	1.37	541.92	0.26	0.22	1.59	0.46	0.08	0.98	564.65	1167.09
C_{57+}	7.79	1055.82	1.41	781.53	0.11	0.24	1.60	0.46	0.08	1.04	632.58	1044.43

Note:

P_c is critical pressure in atm, T_c is critical temperature in K, ω is acentric factor, *MW* is molecular weight, Vol. shift is volume translation (dimensionless), *Z* is Rackett's compressibility factor, V_c is critical volume in l/mol, Ω_a and Ω_b are EOS parameters, *SG* is specific gravity, T_b is normal boiling point in °C, and Parachor is interfacial tension (IFT) parameter.

TABLE 3-15: BIP matrix of the PR EOS (1978) model after regression

	CH_4	C_2H_6	C_3H_8	C_{8-11}	C_{12-15}	C_{16-21}	C_{22-29}	C_{30-41}	C_{42-56}	C_{57+}
CH_4	0.000	0.003	0.008	0.000	0.000	0.141	0.400	0.200	0.006	0.000
C_2H_6	0.003	0.000	0.002	0.031	0.046	0.000	0.000	0.027	0.159	0.133
C_3H_8	0.008	0.002	0.000	0.018	0.031	0.108	0.000	0.002	0.137	0.000
C_{8-11}	0.000	0.031	0.018	0.000	0.002	0.006	0.011	0.147	0.017	0.017
C_{12-15}	0.000	0.046	0.031	0.002	0.000	0.001	0.004	0.006	0.008	0.008
C_{16-21}	0.141	0.000	0.108	0.006	0.001	0.000	0.001	0.002	0.003	0.003
C_{22-29}	0.400	0.000	0.000	0.011	0.004	0.001	0.000	0.000	0.000	0.000
C_{30-41}	0.200	0.027	0.002	0.147	0.006	0.002	0.000	0.000	0.000	0.000
C_{42-56}	0.006	0.159	0.137	0.017	0.008	0.003	0.000	0.000	0.000	0.000
C_{57+}	0.000	0.133	0.000	0.017	0.008	0.003	0.000	0.000	0.000	0.000

TABLE 3-16: Parameters in the modified Pedersen (1987) corresponding states viscosity model

MW mixing rule coefficient (b_1)	0.000188
MW mixing rule exponent (b_2)	2.589096
Coupling factor correlation coefficient (b_3)	0.007083
Coupling factor correlation density exponent (b_4)	2.659500
Coupling factor correlation MW exponent (b_5)	0.372280

with a reduced viscosity can be obtained when a large amount of propane is dissolved in heavy oil. The saturation pressure increases when more propane is dissolved in heavy oil at the same temperature, leading to a simultaneous increase in the swelling factor. For the CH_4-C_3H_8-heavy oil mixture, the swelling factor of heavy oil maintains at a relatively high value for each test temperature. For the CH_4-C_3H_8-heavy oil systems, the measured saturation pressures are found to have high values, indicating that the solution methane comes out of solution easily. Meanwhile, the heavy oil viscosity can still be maintained to be low at a low pressure because C_3H_8 has a high solubility even at low pressures. As for the C_2H_6-C_3H_8-heavy oil systems, the saturation pressures do not present high values as those for the CH_4-C_3H_8-heavy oil systems. This indicates that the dissolved ethane will still stay in the reservoir when the reservoir pressure decreases if ethane and propane are both injected into a reservoir. As such, solution-gas driving energy may not be sufficient, though ethane acts like propane to reduce viscosity of the reservoir fluid.

The parameters in the PR EOS are regressed using the experimentally measured saturation pressures, liquid densities, and swelling factors for the CH_4-C_3H_8-heavy oil system and the C_2H_6-C_3H_8-heavy oil system, respectively. The modified Pedersen (1987) corresponding states viscosity model is tuned by using the measured liquid viscosity of the C_2H_6-C_3H_8-heavy oil system together with the viscosities of the crude oil. The tuned PR EOS (1978) model can be used to reproduce the saturation pressures and swelling factors with an average relative error of 3.68% and 3.76%, respectively. The modified Pedersen (1987) corresponding states viscosity model is able to predict the viscosity of solvent(s)-heavy oil systems with an average relative error of 10.74%.

CHAPTER 4 NUMERICAL SIMULATION OF EXPERIMENTAL ECSP MEASUREMENTS

In this chapter, two series of experiments on the enhanced cyclic solvent processes (ECSPs) are conducted in a visual long sandpack (Dong *et al*., 2013). Subsequently, numerical techniques are developed to history match the experimental measurements, identifying the inherent mechanisms associated with the ECSP. Also, efforts have been made to examine the effects of molecular diffusion, dispersion, and non-equilibrium solubility with foamy oil behaviour on the ultimate oil recovery. Finally, the operational parameters are optimized for maximizing oil recovery by using the orthogonal design method.

4.1 Experimental

4.1.1 Materials

The heavy oil is the same as that used for PVT tests with its physical properties tabulated in **TABLE 3-2**. CH_4, C_2H_6, C_3H_8, and N_2 are supplied by Praxair with purities of 99.99 mol%, 99.0 mol%, 99.99 wt%, and 99.99 mol%, respectively. Crystalline silica sand (CAS# 14808-60-7) has been used to pack the visual coreholder.

4.1.2 Experimental setup

The experimental setup comprises of a visual sandpack, flow pressure gauges, an oil injection system, a gas injection system, a back pressure regulator (BPR) unit for

adjusting the production pressure, an oil-gas separator, and an effluent gas meter as shown in **FIGURE 4-1** (Dong *et al*., 2013).

The visual sandpack and flow pressure gauges are the main components of the setup. The visual sandpack packed with crystalline silica is a relatively long porous medium that resembles a thin formation. The pressure along the sandpack is monitored by three digital pressure gauges. The physical properties of the visual sandpack for ECSPs #1 and 2 are presented in **TABLE 4-1** (Dong *et al*., 2013). ECSP #1 injects CH_4 and C_2H_6 alternatively, while ECSP #2 uses CH_4 and C_3H_8 as solvents.

The oil injection system includes an oil transfer vessel and a high-precision low-rate HPLC pump (515, Waters). This pump is used to inject the warm crude oil at 45°C into the sandpack. During saturating the sandpack with heavy oil, sandpack, oil vessel, and flow lines are continuously heated to 65°C and controlled by a digital temperature controller (CN4116-R1-R2, Omega).

The gas injection system consists of three gas cylinders containing CH_4, C_2H_6, and C_3H_8, respectively, regulators, and digital programmable mass flow meters and totalizers (FMA 4000, Omega) to display the flow rate and the total amount of gas injected into the sandpack. The BPR unit consists of a BPR, a nitrogen cylinder, a regulator to adjust the production pressure, and two pressure gauges. The amount of the recovered oil and gas are recorded continuously by the oil-gas separator and effluent gas meter, respectively.

4.1.3 Experimental procedures

The visual sandpack is first packed with crystalline silica, and then tested for leakage

TABLE 4-1: Physical properties of the sandpack (Dong *et al*., 2013)

Parameter	ECSP #1 ($CH_4 + C_2H_6$)	ECSP #2 ($CH_4 + C_3H_8$)
Length, m	1.013	1.013
Width, m	0.049	0.049
Depth, m	0.032	0.032
Porosity	0.39	0.39
Permeability, Darcy	28.3	25.0
Initial oil saturation, %	82.6	73.9
Initial gas saturation, %	17.4	26.1

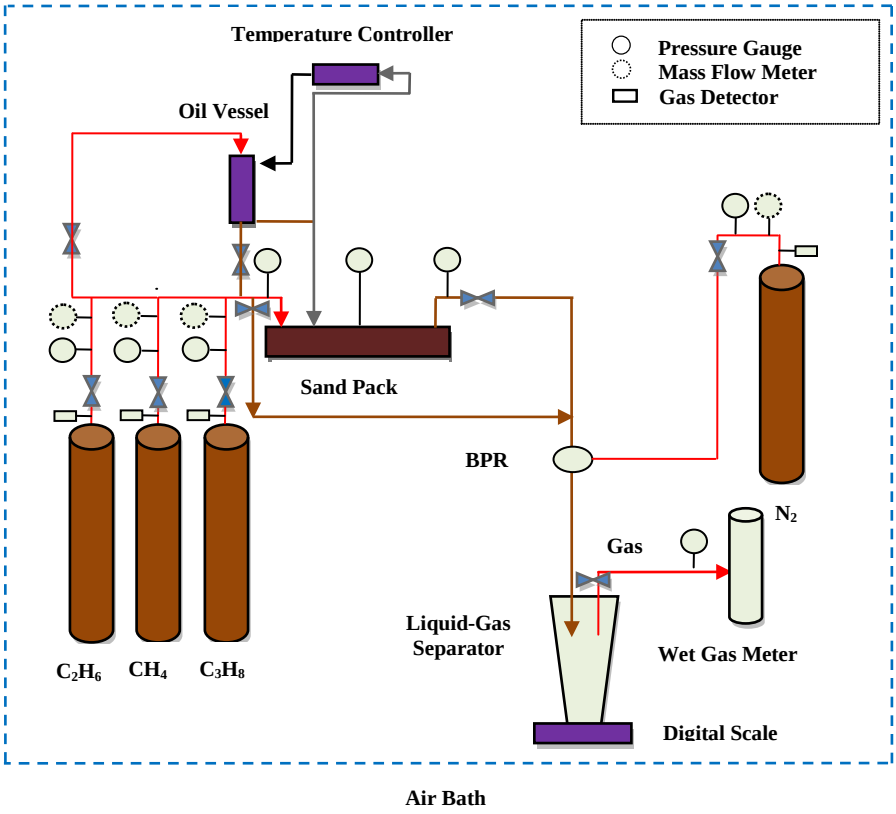

FIGURE 4-1: Experimental setup for conducting the ECSP tests (Dong *et al.*, 2013)

by using CH_4. Subsequently, the warm crude oil at 45°C and CH_4 are sequentially injected into the sandpack. Once completed, the warm sandpack is cooled to the experimental temperature (22°C). The initial oil and gas saturations in the sandpack are presented in **TABLE 4-1**.

Once the sandpack reaches the designed experimental temperature (i.e., 22°C), the desired volumes of CH_4 slug or CH_4/C_3H_8 slugs (for primary depletion), or CH_4/C_2H_6 slugs or CH_4/C_3H_8 slugs (for ECSP cycles) are injected into the system in a cyclic manner. Once the gas injection is finished, the injection valve is closed and the soaking period begins in the sandpack. After the pressure of the sandpack reaches a steady value, production from the sandpack inlet is commenced (i.e., simulating a single-well ECSP). During the production cycle, the amount of oil and gas production is measured continuously. This procedure is repeated for the two series of ECSP test, i.e., ECSP #1: CH_4-C_2H_6 and ECSP #2: CH_4-C_3H_8.

As for the two ECSP tests, each of which consists of six cycles, the visual long sandpack is first filled with CH_4-heavy oil mixture to mimic the primary depletion phase. After the primary depletion, CH_4 is employed as the volatile hydrocarbon gas slug, while C_2H_6 or C_3H_8 is used as the more soluble solvent slug. The injection of the CH_4 slug can be either followed by the C_2H_6 or C_3H_8 slug.

4.2 Numerical Simulation

4.2.1 Numerical model

The CMG STARS simulator (Version 2011) is used to simulate the ECSP tests in the

physical model with a gridblock of $5\times5\times3$ as shown in **FIGURE 4-2**. This numerical model has the same dimension and properties as the sandpack physical model.

4.2.2 PVT properties

In Chapter 3, the parameters in the PR EOS (1978) model and the modified Pedersen (1987) corresponding states viscosity model have been regressed. Subsequently, the tuned parameters in these two models are incorporated in the CMG STARS simulator to perform history matching of the sandpack experimental measurements.

Since dispersion is a combination of convective dispersion and molecular diffusion, the diffusion coefficient and dispersion coefficient cannot be added in the CMG STARS simulator simultaneously (Abukhalifeh, 2010; CMG STARS, 2011). Also, the predicted recovery rate only using molecular diffusion in the mathematical models is lower than the experimental one observed in the VAPEX experiments (Dunn *et al*., 1989; Das and Butler, 1998). As such, the oil-phase dispersion coefficient is adjusted to history match the experiments results obtained from the ECSP tests.

The non-equilibrium gas dissolution of CH_4, C_2H_6, and C_3H_8 in heavy oil is represented by the following equations (Ivory *et al*., 2010; CMG STARS, 2011; Chang and Ivory, 2012), respectively,

$$(CH_4)_G + (CH_4)_L \rightarrow 2(CH_4)_L \qquad [4\text{-}1]$$

$$(C_2H_6)_G + (C_2H_6)_L \rightarrow 2(C_2H_6)_L \qquad [4\text{-}2]$$

$$(C_3H_8)_G + (C_3H_8)_L \rightarrow 2(C_3H_8)_L \qquad [4\text{-}3]$$

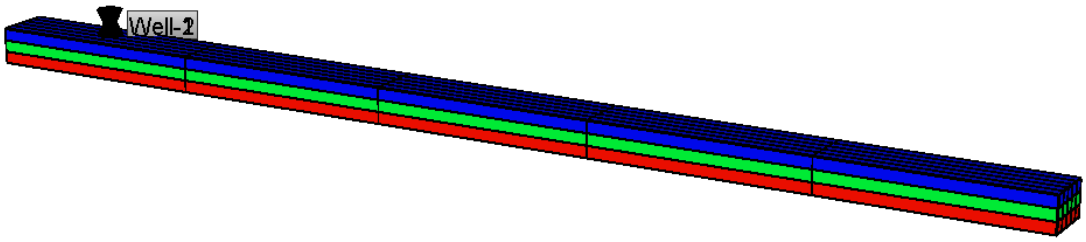

FIGURE 4-2: Numerical model used to simulate the experimental ECSP tests

where $(CH_4)_L$ is dissolved methane in oil phase; $(C_2H_6)_L$ is dissolved ethane in oil phase; $(C_3H_8)_L$ is dissolved propane in oil phase; $(CH_4)_G$ is methane in gaseous phase; $(C_2H_6)_G$ is ethane in gaseous phase; and $(C_3H_8)_G$ is propane in gaseous phase.

The dissolution rate of CH_4 for isothermal condition is,

$$\frac{\partial N_{(CH_4)_L}}{\partial t} = k_{CH_4} N_O \left(x_{(CH_4)_{Leqm}} - x_{(CH_4)_L} \right) N_g y_{(CH_4)_G} \quad [4\text{-}4]$$

where k_{CH_4} is the reaction frequency factor (RFF) for CH_4 dissolution in $m^3/(gmole \cdot day)$; $N_{(CH_4)_L}$ is CH_4 concentration in oil phase, $mole/m^3$; t is the time, day; N_O is the oil concentration, $mole/m^3$; $x_{(CH_4)_{Leqm}}$ is the mole fraction of CH_4 in oil phase in equilibrium condition; $x_{(CH_4)_L}$ is the mole fraction of CH_4 in oil phase; N_g is the gas concentration, $mole/m^3$; and $y_{(CH_4)_G}$ is the mole fraction of CH_4 in gas phase. This dissolution rate equation can also be applied for either C_2H_6 or C_3H_8.

The non-equilibrium gas exsolution (i.e., released from the solution) with the formation of foamy oil in the oil phase is represented by (Ivory *et al*., 2010; CMG STARS, 2011; Chang and Ivory, 2012),

$$(CH_4)_L \rightarrow BubCH_4 \rightarrow (CH_4)_G \quad [4\text{-}5]$$

$$(C_2H_6)_L \rightarrow BubC_2H_6 \rightarrow (C_2H_6)_G \quad [4\text{-}6]$$

$$(C_3H_8)_L \rightarrow BubC_3H_8 \rightarrow (C_3H_8)_G \quad [4\text{-}7]$$

where $BubCH_4$ is methane bubble in oil phase, $BubC_2H_6$ is ethane bubble in oil phase, and $BubC_3H_8$ is propane bubble is oil phase.

The exsolution rate for CH_4 from oil phase to bubble at isothermal conditions is:

$$\frac{\partial N_{Bub\,CH_4}}{\partial t} = k_{CH_4} N_O x_{(CH_4)_L} \quad [4\text{-}8]$$

where N_{BubCH_4} is $BubCH_4$ in mole/m^3.

The exsolution rate for CH_4 from bubble to gas phase at isothermal conditions is:

$$\frac{\partial N_{(CH_4)_G}}{\partial t} = k_{CH_4} N_{Bub\,CH_4} \quad [4\text{-}9]$$

where $N_{(CH_4)_G}$ is CH_4 concentration in gas phase, mole/m^3. These exsolution rate equations can also be used for either C_2H_6 or C_3H_8.

4.3 Results and Discussion

4.3.1 Experimental measurements

TABLE 4-2 and **TABLE 4-3** summarize the experimental conditions used in the tests together with the experimental results for the two ECSP tests (Dong *et al*., 2013).

The ultimate oil recovery for ECSPs #1 and 2 is measured to be 18.7% and 41.1% of the original oil in place (OOIP), respectively. During the ECSP tests, CH_4 slug is first injected into the sandpack. Due to the viscous fingering, CH_4 fingers in the oil to provide paths for the following C_2H_6 or C_3H_8 slug in order to achieve a better mixing effect with oil. As for the ECSP production cycles, CH_4 provides a driving force when the reservoir pressure is reduced, while partial C_2H_6 or C_3H_8 is retained in the oil to keep the oil viscosity at low level and swell the oil as well.

Due to the higher solubility of C_3H_8 than C_2H_6 at the same condition, the oil viscosity

TABLE 4-2: Experimental conditions and results for ECSP #1 test (Dong *et al*., 2013)

Run	Depletion	Cycle 1	Cycle 2	Cycle 3	Cycle 4	Cycle 5	Cycle 6
C_2H_6 injected scm^3	-	1481.7	1133.1	828.5	845.0	790.7	569.4
C_2H_6 injection pressure, psig	-	500.0	500.0	500.0	500.0	500.0	500.0
CH_4 injected, scm^3	3684.9	1933.9	2221.9	2577.2	2904.1	3137.4	3319.4
CH_4 injection pressure, psig	500.0	500.0	500.0	500.0	500.0	500.0	500.0
Initial oil, g	496.8	488.4	472.1	452.0	433.5	420.3	410.0
Soaking time, hr	72.0	21.5	21.8	22.4	22.5	22.3	22.8
Sandpack pressure before soaking, psig	485.0	485.0	485.0	485.0	485.0	485.0	485.0
Sandpack pressure after soaking, psig	319.2	377.1	413.4	429.5	436.9	441.4	451.6
Final sandpack pressure, psig	69.1	129.6	174.1	181.3	190.5	209.5	228.4
Production time, min	15.0	15.0	15.0	15.0	15.0	15.0	15.0
Oil recovered, g	8.4	16.3	20.1	18.5	13.2	10.3	6.1

TABLE 4-3: Experimental conditions and results for ECSP #2 test (Dong *et al*., 2013)

Run	Depletion	Cycle 1	Cycle 2	Cycle 3	Cycle 4	Cycle 5	Cycle 6
C_3H_8 injected scm^3	1146.5	497.1	505.8	568.3	601.0	623.1	608.5
C_3H_8 injection pressure, psig	105.0	105.0	105.0	105.0	105.0	105.0	105.0
CH_4 injected, scm^3	4448.2	5227.1	6171.0	7181.5	8012.5	8695.8	9257.5
CH_4 injection pressure, psig	500.0	500.0	500.0	500.0	500.0	500.0	500.0
Initial oil, g	444.2	417.3	384.7	349.8	321.1	297.5	278.1
Soaking time, hr	72.0	23.5	23.1	22.8	22.7	22.5	22.3
Sandpack pressure before soaking, psig	485.0	485.0	485.0	485.0	485.0	485.0	485.0
Sandpack pressure after soaking, psig	309.8	423.2	431.5	434.5	438.1	440.3	441.9
Final sandpack pressure, psig	63.1	68.2	69.3	70.9	72.2	74.5	78.5
Production time, min	15.0	15.0	15.0	15.0	15.0	15.0	15.0
Oil recovered, g	26.9	32.6	34.9	28.7	23.6	19.4	16.3

can be reduced to a larger degree and a larger swelling factor of heavy oil can be achieved if C_3H_8 is used instead of C_2H_6. A larger swelling factor is particularly beneficial for recovering more oil in the ECSP test because more mobile oil saturation together with an increased oil-phase relative permeability can be achieved *in-situ* in the reservoir due to the swollen volume of heavy oil. Therefore, the recovery factor is significantly enhanced when C_2H_6 is replaced with C_3H_8.

It can be seen from **TABLEs 4-2** and **4-3** that the oil recovery peaks in the early cycles, while it drops in the subsequent cycles due mainly to the significant reduction of initial oil saturation in the later cycles, especially near the production well. As for the later ECSP cycles, the rate of pressure depletion decreases during the soaking time as a result of the decrease in the rate of gas dissolution, resulting in less oil swelling and viscosity reduction. This factor also contributes to the decrease of oil recovery for the later cycles.

As for ECSP #2, CH_4 is injected as the more volatile solvent, while C_3H_8 is injected as the more soluble solvent. It can be concluded that, the dominant recovery mechanisms of ECSP #2 are solution gas drive due to the more volatile solvent (i.e., CH_4), viscosity reduction, and swelling effect due to the enhanced dissolution of more soluble solvent (i.e., C_3H_8) in heavy oil.

4.3.2 Numerical simulations

1) History matching

The oil/water relative permeability does not affect the simulation results because of

no water in the sandpack. **FIGUREs 4-3** and **4-4** show the oil/gas relative permeability as a function of liquid saturation used to simulate performance of ECSPs #1 and 2.

FIGUREs 4-5 and **4-6** present the history matching results of cumulative oil production and production pressure obtained from the numerical simulations for ECSPs #1 and 2. Obviously, there exists a good agreement between the experimental measurements and numerical simulation results, indicating that the mechanisms of solution gas drive, viscosity reduction, and swelling effect governing the ECSP have been well captured by the tuned numerical model.

After history matching the experiments results obtained from the ECSP tests, an oil-phase dispersion coefficient of 5.0×10^{-8} m^2/s is determined. Also, the following parameters that describe the non-equilibrium solubility with foamy oil behaviour are obtained: the RFF of 0.2 $m^3/(gmole.day)$ for gas dissolution, 2 day^{-1} for gas exsolution from oil phase to bubble, and 2×10^{-3} day^{-1} for gas exsolution from bubble to gaseous phase.

Based on both the experimental and simulation results, it is found that a higher oil recovery factor is achieved in ECSP #2 (i.e., CH_4-C_3H_8 pair) than in ECSP #1 (i.e., CH_4-C_2H_6 pair). Distribution of gas saturation may account for the rather different recovery efficiency of these two ECSP tests. Subsequent numerical simulations are carried out to compare the distribution of gas saturation in the sandpack after soaking of Cycle #1 for these two ECSP tests.

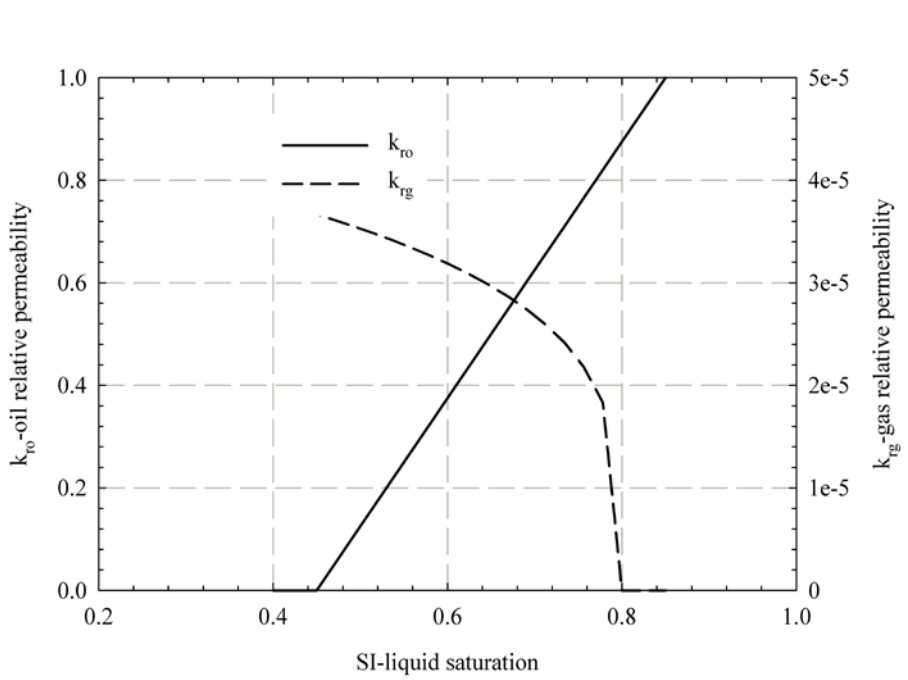

FIGURE 4-3: Oil-gas relative permeability curves tuned for simulating ECSP #1

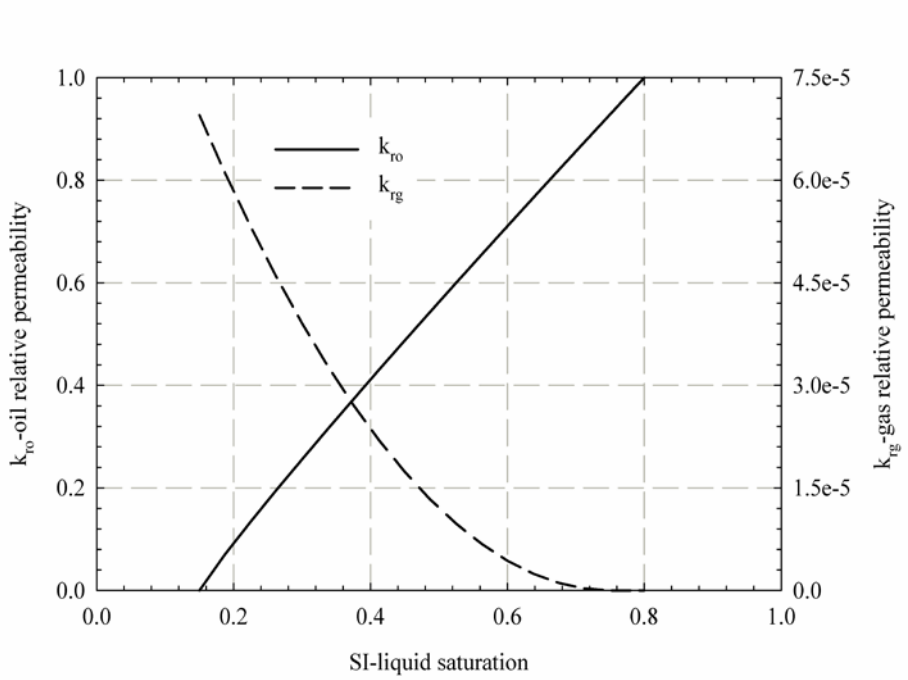

FIGURE 4-4: Oil-gas relative permeability curves tuned for simulating ECSP #2

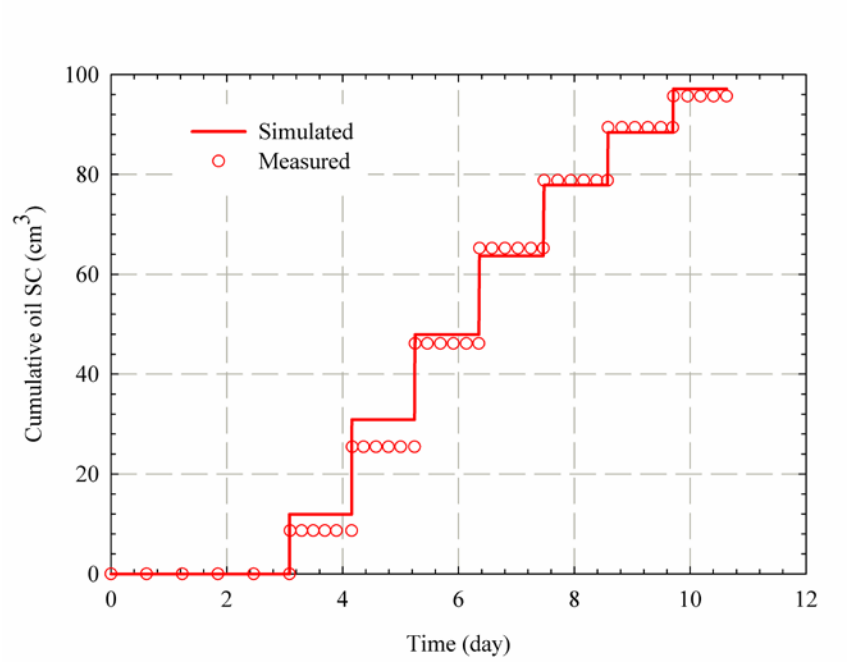

(a)

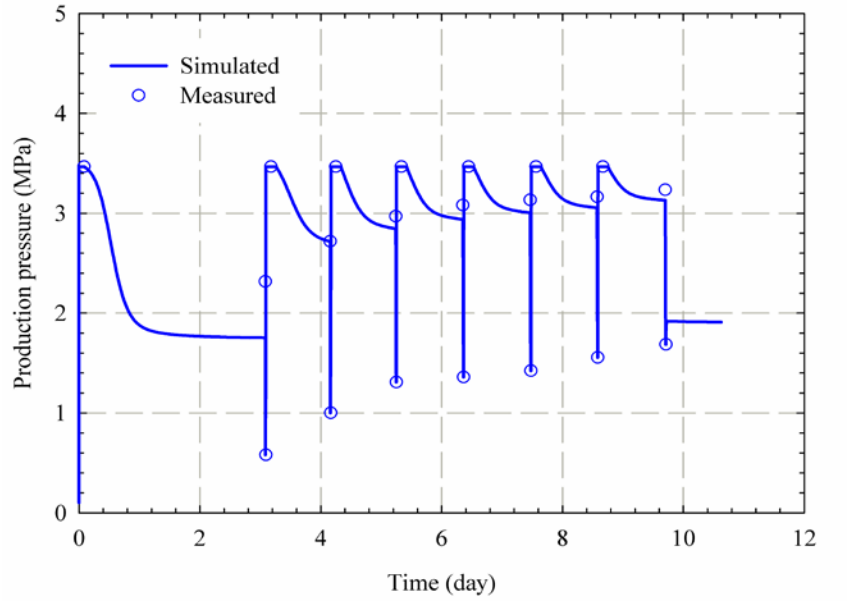

(b)

FIGURE 4-5: History matching results of **(a)** cumulative oil production and **(b)** production pressure for ECSP #1

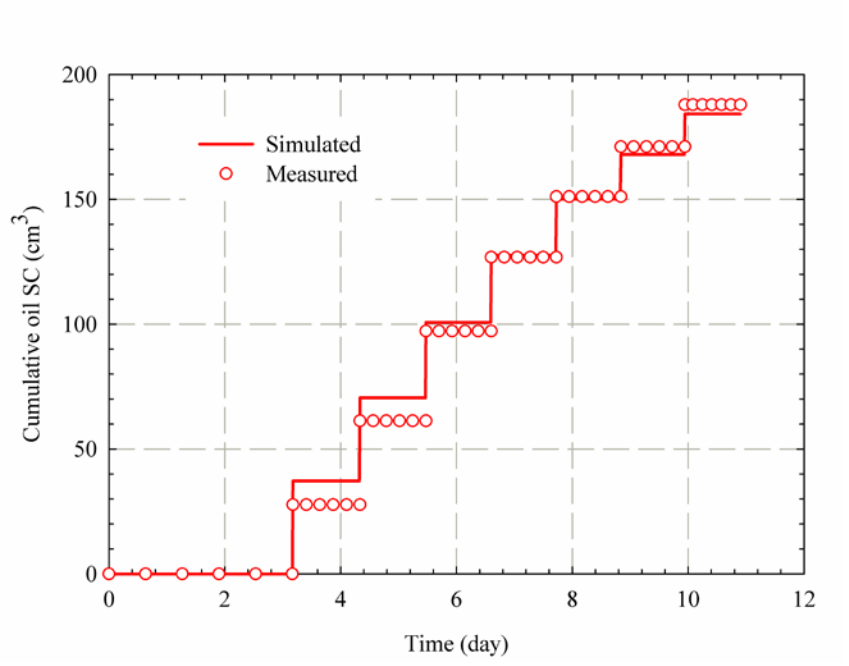

(a)

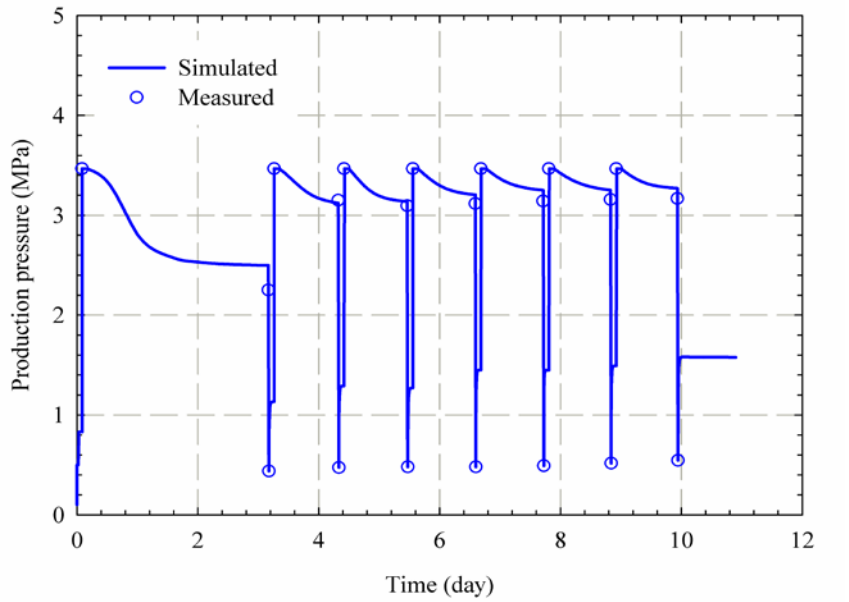

(b)

FIGURE 4-6: History matching results of **(a)** cumulative oil production and **(b)** production pressure for ECSP #2

2) Gas saturation

FIGURE 4-7 shows the distribution of gas saturation in the three layers of the sandpack at the end of the soaking process of Cycle #1 in ECSPs #1 and 2, respectively. It can be seen from **FIGURE 4-7** that gas penetrates into the sandpack faster in ECSP #2 than ECSP #1. In ECSP #2, the deeper penetration of gas into the sandpack and larger gas saturation in the sandpack result in a larger contact area between the solvents and heavy oil so that more solvents can be dissolved in the heavy oil. Gas override effect can also be observed in these two ECSP tests, implying that, as for field application, the bottom layer other than all the layers of the production zone should be perforated in order to reduce the solvent requirements.

Based on the simulation results with the tuned PR EOS model, C_3H_8 is found to be more soluble in heavy oil than C_2H_6 at the same pressure and temperature, while C_2H_6 is more soluble in heavy oil than CH_4 at the same pressure and temperature. In addition, based on the modified Pedersen (1987) corresponding states viscosity model, even if the same amount of solvent is dissolved, C_3H_8 can reduce the viscosity to a larger degree than either CH_4 or C_2H_6. Therefore, in order to efficiently reduce the viscosity of the crude oil, utilizing a C_3H_8 slug in the ECSP is capable of significantly enhancing the heavy oil recovery efficiency.

The following explanations are provided to more reasonably account for the superior recovery efficiency achieved in ECSP #2 test (i.e., CH_4-C_3H_8 pair). CH_4 is in supercritical state at the experimental temperature and has a smaller solubility compared to C_3H_8. However, if the pressure is high enough, CH_4 and C_3H_8 can be completely

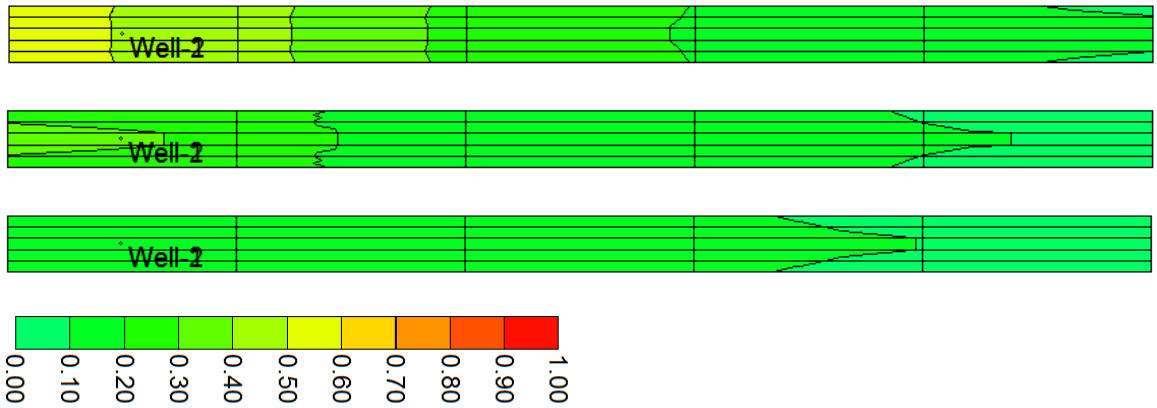

(a)

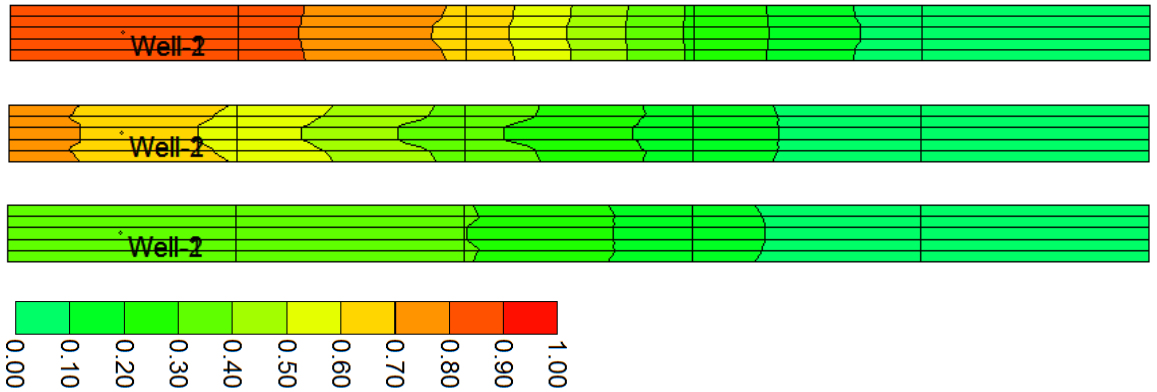

(b)

FIGURE 4-7: Distribution of gas saturation in the sandpack at the end of the soaking process of Cycle #1 in **(a)** ECSP #1 and **(b)** ECSP #2

dissolved in heavy oil.

Once production begins and sandpack pressure drops below the bubblepoint pressure, the dissolved CH_4/C_3H_8 gas comes out of solution in the form of nucleated gas bubbles (Zhao *et al*., 2011). As the pressures are reduced further, these gas bubbles grow larger in size. Such growth is driven by mass transfer from the liquid phase to the gas phase as well as volume expansion due to the decreasing pressure. Small gas bubbles can flow with the oil, while large bubbles become trapped at pore throats. The trapped bubbles continue to grow and eventually become larger than the pore size and occupy some pore spaces. The continued growth of these bubbles and coalescence of the adjoining bubbles eventually result in the formation of a continuous gas phase within the reservoir. The gas then starts to flow into the production well at an increasing rate.

Since the CH_4/C_3H_8 mobility is significantly greater than that of oil, the gas production rate is much higher than that of oil. Consequently, the rapid production of gas results in a rapid decline in pressure. As the pressure declines, some C_3H_8 can still be dissolved in the heavy oil, maintaining the heavy oil viscosity at low levels. This is attributed to the fact that C_3H_8 has relatively large solubility compared to CH_4 or C_2H_6 at the same conditions.

3) Effect of molecular diffusion coefficient

TABLE 4-4 compares the ultimate oil recovery resulted from using five different molecular diffusion coefficients in the ECSP #2, where the diffusion coefficients of CH_4 and C_3H_8 are assumed to be the same (Ivory *et al*., 2010; Chang and Ivory, 2012), while

TABLE 4-4: Ultimate oil recoveries with different molecular diffusion coefficients

Simulation run No.	Diffusion coefficient 10^{-10} m^2/s	Oil recovery %
1	1	36.7
2	5	38.1
3	10	38.3
4	50	38.5
5	100	39.3

the dispersion coefficient is not considered. The RFFs for gas dissolution, gas exsolution from oil phase to bubble, and gas exsolution from bubble to gaseous phase are found to be 0.2 $m^3/(gmole{\cdot}day)$, 2 day^{-1}, and 2×10^{-3} day^{-1}, respectively. In general, the oil recovery is found to increase with the diffusion coefficient. When the diffusion coefficients are in the order of 10^{-9} to 10^{-10} m^2/s, a minor impact on the oil recovery is imposed.

4) Effect of dispersion coefficient

TABLE 4-5 shows the oil recoveries simulated with ten different dispersion coefficients in the ECSP #2. The dispersion coefficients of CH_4 and C_3H_8 are assumed to be the same (Ivory *et al*., 2010; Chang and Ivory, 2012). The RFFs for gas dissolution, gas exsolution from oil phase to bubble, and gas exsolution from bubble to gaseous phase are 0.2 $m^3/(gmole{\cdot}day)$, 2 day^{-1}, and 2×10^{-3} day^{-1}, respectively.

It can be seen from **TABLE 4-5** that the dispersion coefficient demonstrates a strong effect on oil recovery, especially when the dispersion coefficient is in the order of 10^{-6} to 10^{-8} m^2/s. The oil recovery factor first increases with the dispersion coefficient, and then tends to level off when dispersion coefficient falls into the order of 10^{-6} m^2/s. Spreading or mixing of solvent in oil phase is determined by dispersion. Larger dispersion coefficients result in higher mixing, which is beneficial for recovering oil (Boustani and Maini, 2001; Shrivastava, 2003). Thus, oil recovery factor increases with the dispersion coefficient. When the dispersion coefficient increases up to certain value (i.e., in the order of 10^{-6} m^2/s), however, the solvent is fully mixed, and then the oil recovery stops increasing.

TABLE 4-5: Ultimate oil recoveries with different dispersion coefficients

Simulation run No.	Dispersion coefficient 10^{-8} m^2/s	Oil recovery %
1	1	39.2
2	5	40.4
3	10	43.0
4	50	51.7
5	100	54.3
6	500	59.9
7	1000	60.7
8	2000	61.8
9	5000	62.4
10	7000	62.4

5) Non-equilibrium solubility with foamy oil behaviour

In these simulations, an oil-phase dispersion coefficient of 5.0×10^{-8} m^2/s is used. **TABLE 4-6** shows the ultimate oil recovery simulated with different RFFs. The RFFs of CH_4 and C_3H_8 are assumed to be the same (Ivory *et al*., 2010; Chang and Ivory, 2012). It can be seen from **TABLE 4-6** that the reaction RFF for gas exsolution from bubble to gas phase almost shows no influence on the simulated oil recovery. In comparison, the RFFs for gas dissolution and exsolution from oil phase to bubble affect the simulated oil recovery to a larger extent. This is because gas dissolution and exsolution from oil phase to bubble determine the bubble creation and foamy oil drive (Ivory *et al*., 2010; Chang and Ivory, 2012).

4.3.3 Optimization of operational parameters

The orthogonal design method is used in this study to optimize the operational parameters in ECSP #2 including a depletion process and 6 cycles. The following parameters are chosen as the variables that need to be optimized: the injection pressure and injection time of C_3H_8, the injection pressure and injection time of CH_4, the soaking time, and the minimum production pressure which is controlled by the BPR. **TABLE 4-7** shows the five-level values for each of these 6 parameters.

A $L_{25}5^6$ scheme is employed in the orthogonal design. The results of orthogonal design experiments are presented in **TABLE 4-8**. **FIGURE 4-8** shows the factor index for the orthogonal design. According to **TABLE 4-8** and **FIGURE 4-8**, it can be concluded that the highest recovery efficiency can be achieved when: 1) the injection

TABLE 4-6: Ultimate oil recoveries with different reaction frequency factor

Simulation run No.	RFF dissolution $m^3/(gmole \cdot day)$	RFF exsolution from oil phase to bubble, day^{-1}	RFF exsolution from bubble to gaseous phase day^{-1}	Oil recovery factor, %
1	0.02	0.2	0.0002	39.8
2	0.02	0.2	0.0020	39.8
3	0.02	0.2	0.0200	39.5
4	0.02	2.0	0.0002	41.0
5	0.02	2.0	0.0020	41.1
6	0.02	2.0	0.0200	41.2
7	0.02	20.0	0.0002	41.6
8	0.02	20.0	0.0020	41.5
9	0.02	20.0	0.0200	41.7
10	0.20	0.2	0.0002	44.0
11	0.20	0.2	0.0020	44.0
12	0.20	0.2	0.0200	43.6
13	0.20	2.0	0.0002	40.4
14	0.20	2.0	0.0020	40.5
15	0.20	2.0	0.0200	40.7
16	0.20	20.0	0.0002	40.0
17	0.20	20.0	0.0020	40.0
18	0.20	20.0	0.0200	40.3
19	2.00	0.2	0.0002	39.4
20	2.00	0.2	0.0020	39.2
21	2.00	0.2	0.0200	39.7
22	2.00	2.0	0.0002	36.4
23	2.00	2.0	0.0020	36.7
24	2.00	2.0	0.0200	36.7
25	2.00	20.0	0.0002	40.5
26	2.00	20.0	0.0020	40.0
27	2.00	20.0	0.0200	40.9

TABLE 4-7: Five levels of the six influencing parameters

Injection pressure of C_3H_8, kPa	Injection time of C_3H_8, h	Injection pressure of CH_4, kPa	Injection time of CH_4 , h	Soaking time, h	Minimum production pressure, kPa
450.0	0.5	2200.0	0.5	6.0	101.0
580.0	1.0	2900.0	1.0	12.0	300.0
830.0	2.0	3550.0	2.0	24.0	500.0
1150.0	5.0	5300.0	5.0	36.0	881.0
1200.0	10.0	7000.0	10.0	48.0	1000.0

TABLE 4-8: Orthogonal experimental design and corresponding simulation results

Simulation run No.	Injection pressure of C_3H_8 kPa	Injection time of C_3H_8, h	Injection pressure of CH_4 kPa	Injection time of CH_4, h	Soaking time, h	Minimum production pressure kPa	Ultimate oil recovery %
1	450.0	0.5	2200.0	0.5	6.0	101.0	38.5
2	450.0	1.0	2900.0	1.0	12.0	300.0	42.9
3	450.0	2.0	3550.0	2.0	24.0	500.0	43.5
4	450.0	5.0	5300.0	5.0	36.0	881.0	48.5
5	450.0	10.0	7000.0	10.0	48.0	1000.0	59.0
6	580.0	0.5	2900.0	2.0	36.0	1000.0	30.8
7	580.0	1.0	3550.0	5.0	48.0	101.0	49.4
8	580.0	2.0	5300.0	10.0	6.0	300.0	54.9
9	580.0	5.0	7000.0	0.5	12.0	500.0	61.3
10	580.0	10.0	2200.0	1.0	24.0	881.0	21.8
11	830.0	0.5	3550.0	10.0	12.0	881.0	38.9
12	830.0	1.0	5300.0	0.5	24.0	1000.0	47.2
13	830.0	2.0	7000.0	1.0	36.0	101.0	69.9
14	830.0	5.0	2200.0	2.0	48.0	300.0	33.8
15	830.0	10.0	2900.0	5.0	6.0	500.0	35.8
16	1150.0	0.5	5300.0	1.0	48.0	500.0	52.4
17	1150.0	1.0	7000.0	2.0	6.0	881.0	57.0
18	1150.0	2.0	2200.0	5.0	12.0	1000.0	19.6
19	**1150.0**	**5.0**	**2900.0**	**10.0**	**24.0**	**101.0**	**55.2**
20	1150.0	10.0	3550.0	0.5	36.0	300.0	51.3
21	1200.0	0.5	7000.0	5.0	24.0	300.0	66.6
22	1200.0	1.0	2200.0	10.0	36.0	500.0	30.9
23	1200.0	2.0	2900.0	0.5	48.0	881.0	28.6
24	1200.0	5.0	3550.0	1.0	6.0	1000.0	32.6
25	1200.0	10.0	5300.0	2.0	12.0	101.0	62.1

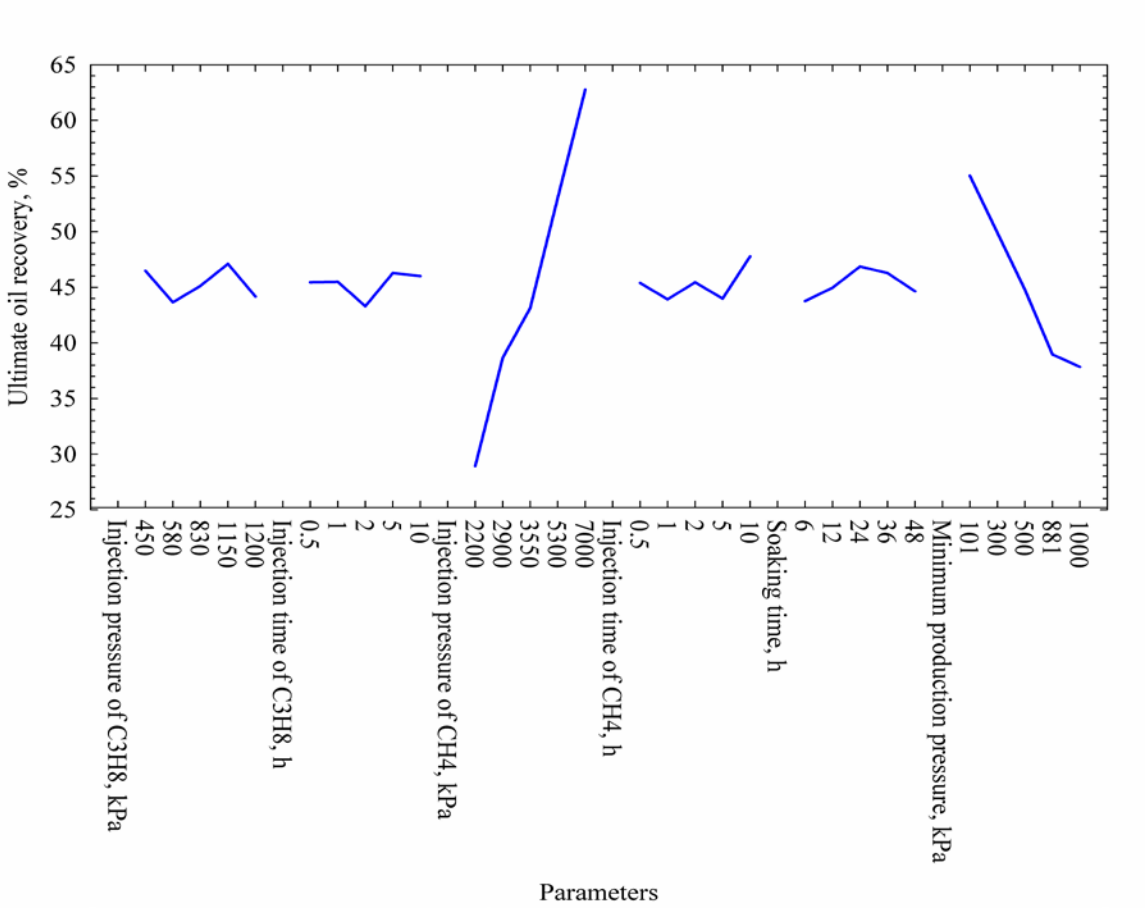

FIGURE 4-8: Factor index for the orthogonal design

pressure of C_3H_8 is 1150.0 kPa and the injection time of C_3H_8 is 5.0 hour; 2) the injection pressure and time of CH_4 are 7000.0 kPa and 10.0 hours, respectively; 3) the soaking time is 24.0 hours; and 4) the minimum production pressure is 101.0 kPa.

Statistical analysis of the ultimate oil recovery (e.g., variance) resulted from these parameters should be considered in the orthogonal design. Variance is defined as a measure of the distance for each value in the data set from the mean, which can be used to analyze the sensitivity of each factor in orthogonal design (Yang *et al*., 2011).

The variance can be calculated by the following formula (Efron and Stein, 1981),

$$S^2 = \frac{1}{N}\sum_{i=1}^{N}(x_i - \bar{x})^2 \qquad [4\text{-}10]$$

where S^2 is the variance, x_i is the data set, $\bar{x}$ is mean value of the data set, and N is size of the data set.

The variances of the ultimate oil recovery resulted from injection pressure and injection time of C_3H_8, injection pressure and injection time of CH_4, soaking time and minimum production pressure are calculated to be 1.7×10^{-4}, 1.1×10^{-4}, 136.3×10^{-4}, 2.0×10^{-4}, 1.3×10^{-4}, and 42.4×10^{-4}, respectively. Therefore, the injection pressure of CH_4 and minimum production pressure are found to be the most sensitive parameters. The other remaining parameters are less sensitive due to the small variances resulted from them.

When the injection pressure of C_3H_8, injection time of C_3H_8, injection pressure of CH_4, injection time of CH_4, soaking time, and minimum production pressure are set as 1150.0 kPa, 5.0 hour, 2900.0 kPa, 10.0 hour, 24.0 hour and 101.0 kPa, respectively, the ultimate oil recovery of the present laboratory-scale ECSP test can reach a high value of

55.2% of OOIP (i.e., Simulation Run #19 in **TABLE 4-8**), demonstrating a great potential for improving heavy-oil recovery through the ECSP technique.

4.4 Summary

Two series of ECSP test are conducted in a visual long sandpack. The ultimate oil recovery for the two ECSP tests using CH_4-C_2H_6 and CH_4-C_3H_8 are measured to be 18.7% and 41.1%, respectively. The ECSP performance is enhanced significantly when C_2H_6 is replaced with C_3H_8 because C_3H_8 has a higher solubility at the same condition and can reduce the oil viscosity and swell the oil to a larger degree. The dominant mechanisms of ECSP using CH_4-C_3H_8 to enhance oil recovery are solution gas drive due to the more volatile solvent (i.e., CH_4), viscosity reduction, and swelling effect due to the enhanced dissolution of more soluble solvent (i.e., C_3H_8) in heavy oil.

The CMG STARS simulator is used to conduct the numerical simulations of experimental measurements. There exists a good agreement between the experimental and numerical results for each individual ECSP test, indicating that the mechanisms governing the ECSP has been largely captured in the numerical simulations. As for ECSP #2, the deeper penetration of gas into the sandpack and larger gas saturation in the sandpack result in a larger contact area between solvent and heavy oil so that more solvent can be dissolved in the heavy oil.

Although oil recovery increases with the molecular diffusion coefficient, a minor impact on the oil recovery is observed when the diffusion coefficients are in the order of 10^{-9} to 10^{-10} m^2/s. The dispersion coefficient imposes a strong impact on the oil recovery

factor, especially when the dispersion coefficient is in the order of 10^{-6} to 10^{-8} m^2/s. The oil recovery factor first increases with the dispersion coefficient, and then tends to level off when dispersion coefficient falls in the order of 10^{-6} m^2/s. Larger dispersion coefficients result in higher mixing, which is beneficial for recovering oil. However, when the dispersion coefficient increases up to certain value (i.e., in the order of 10^{-6} m^2/s), the solvent is fully mixed so that the oil recovery reaches its maximum. The reaction frequency factor for gas exsolution from bubble to gas phase almost shows no influence on the simulated oil recovery. In comparison, the reaction frequency factors for gas dissolution and exsolution from oil phase to bubble affect the simulated oil recovery to a larger extent. This is because gas dissolution and exsolution from oil phase to bubble determine the bubble creation and foamy oil drive.

The orthogonal design method is used to optimize the operational parameters in ECSP #2. The highest recovery efficiency can be achieved when: 1) the injection pressure of C_3H_8 is 1150.0 kPa and the injection time of C_3H_8 is 5.0 hour; 2) the injection pressure and time of CH_4 are 7000.0 kPa and 10.0 hours, respectively; 3) the soaking time is 24.0 hours; and 4) the minimum production pressure is 101.0 kPa. The variances of the ultimate oil recovery resulted from injection pressure and injection time of C_3H_8, injection pressure and injection time of CH_4, soaking time and minimum production pressure are calculated to be 1.7×10^{-4}, 1.1×10^{-4}, 136.3×10^{-4}, 2.0×10^{-4}, 1.3×10^{-4}, and 42.4×10^{-4}, respectively. Therefore, the injection pressure of CH_4 and minimum production pressure are found to be the most sensitive parameters.

CHAPTER 5 PERFORMANCE EVALUATION OF FIELD-SCALE ECSP APPLICATION

In this chapter, the field-scale simulation is conducted to evaluate the performance of ECSP in the Pelican oilfield. A three-dimensional (3-D) geological model is constructed based on the petrophysical properties of the Wabiskaw formation mined from AccuMap. The CMG STARS simulator (Version 2011) is employed to perform history matching of the production profile in the targeted area. Subsequently, the orthogonal design method with a $L_{25}5^6$ scheme is applied to optimize the operational parameters. Finally, such optimized operational parameters are selected to predict the performance of 13 wells in this area for 5 and half years with 30 cycles.

5.1 Field Background

The Pelican oilfield (see **FIGURE 5-1**) is located 250 km north of Edmonton, Alberta, covering an area of 530 km^2 and lies in the middle of the Wabiskaw oil sands deposit (Fontaine *et al*., 1993; Fossey *et al*., 1997). The Wabiskaw sandstone formation comprises part of the lower cretaceous Mannville Group of Alberta and was deposited in a marine environment (Grabowski *et al*., 2005). The depth of reservoir is about 400 m, with *in-situ* fluid temperature of about 291-293 K and oil gravity of 9-15°API. The Wabiskaw sands contain the members "A", "B", and "C", among which the Wabiskaw "A" sand is the primary heavy-oil bearing formation with an average net pay of 5.0 m (Fontaine *et al*., 1993). The initial reservoir pressure, permeability, average porosity, and

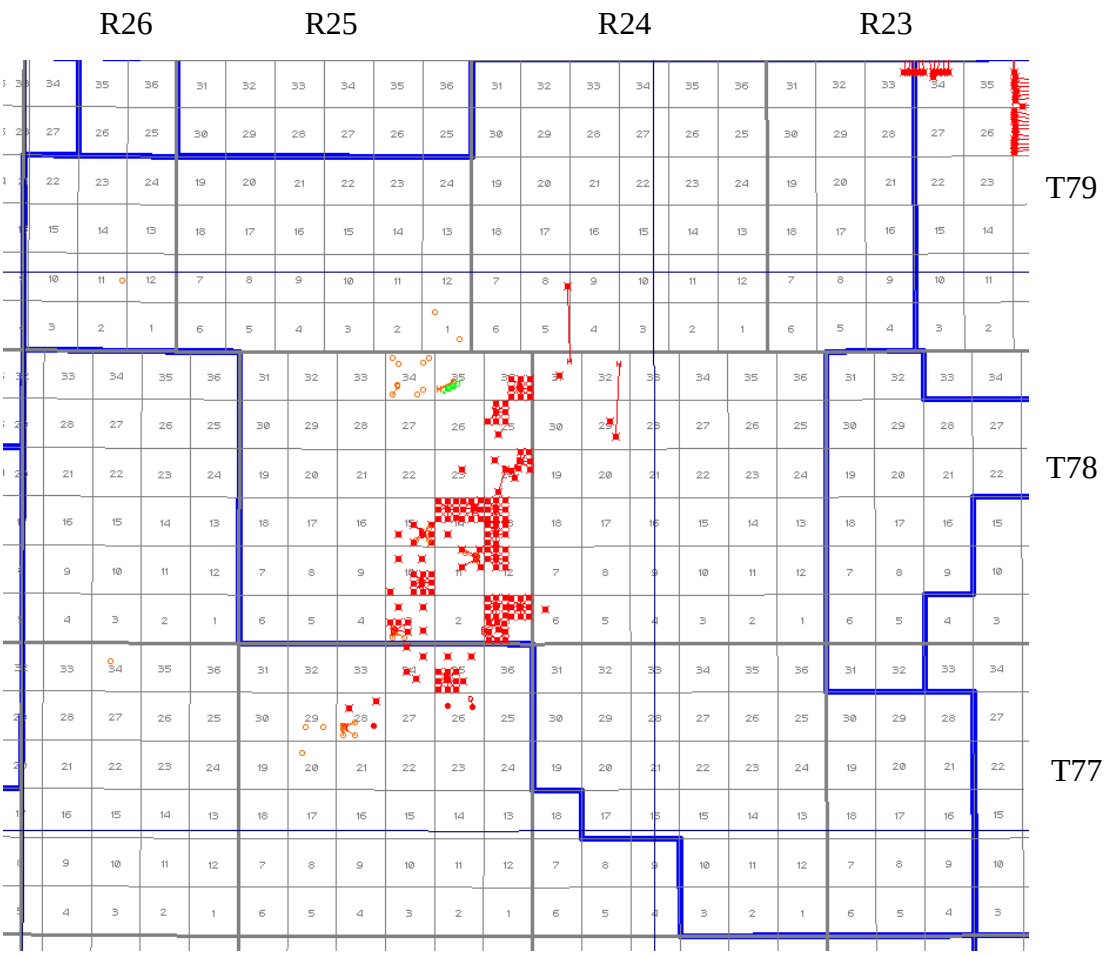

FIGURE 5-1: Detailed areal map of the Pelican oilfield

initial average oil saturation of the Wabiskaw "A" formation are 1,800-2,400 kPa, 300-3,000 mD, 30%, and 70%, respectively. The viscosity of the dead oil produced from the Wabiskaw "A" formation falls in the range of 1,000-25,000 cP (West, 2012).

5.2 Numerical Simulation

5.2.1 Reservoir geological model

As shown in **FIGURE 5-2**, an area of 6.4 km^2 enclosing 17 wells is selected as the targeted area for this study. The geological model is constructed based on the petrophysical properties of the Wabiskaw formation. The payzone depth and thickness in the targeted area can be mined from AccuMap, which are interpolated to construct the geological model of the whole formation with a grid block of 32×20×10. For each grid block, both of the length and width are 100 m while the thickness is variable as shown in **FIGURE 5-3**. The reservoir temperature and its initial pressure are set at 293 K and 2400 kPa, respectively. The oil properties used are the same as those measured in the laboratory. As for the porosity, permeability, and oil saturation, they can be obtained from the core analysis data for 5 wells in AccuMap, including W-00/02-10, W-00/04-10, W-00/10-10, W-00/11-10, and W-00/16-11. Subsequently, the formation properties of other locations in the reservoir geological model are interpolated based on the data from these 5 wells by applying the Gaussian geostatistical simulation method.

5.2.2 Production and pressure data

The targeted area considered in the study includes 17 wells, among which wells W-

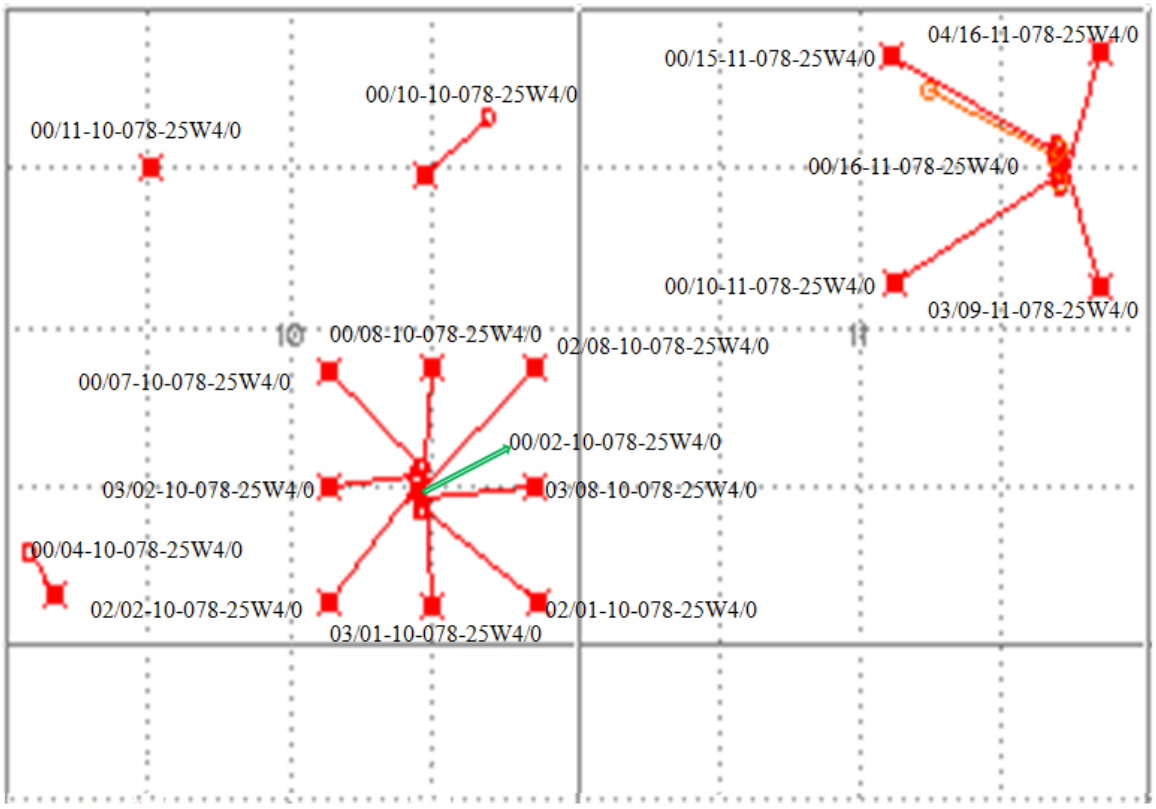

FIGURE 5-2: Well patterns used in numerical simulation in the Pelican oilfield

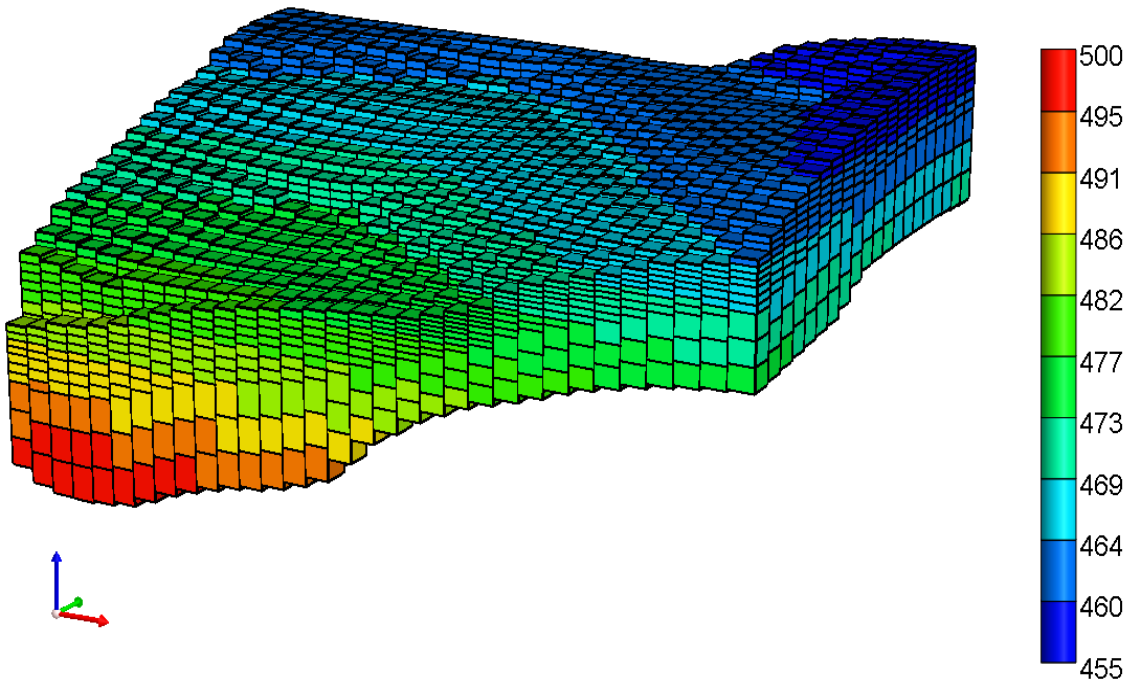

FIGURE 5-3: 3D reservoir geological model of the targeted area in the Pelican oilfield

00/15-11, W-04/16-11, W-03/09-11, and W-00/10-11 commenced producing after September 31, 2011. Based on the production data for these 4 wells, it was found that gas injection is initiated to enhance heavy oil recovery from October 1, 2011. The monthly production data of the other 13 wells, including cumulative oil production, cumulative water production, and cumulative gas production are obtained from AccuMap.

Due to the lack of the measured pressure data available, the material balance method is used to achieve this purpose as outlined below (Dake, 2010),

$$N_p[B_o + (R_p - R_s)B_g] = N(B_o - B_{oi}) + N(R_{si} - R_s)B_g + mNB_{oi}\left(\frac{B_g}{B_{gi}} - 1\right) + (1+m)NB_{oi}\left(\frac{c_w S_{wc} + c_f}{1 - S_{wc}}\right)\Delta p + (W_e - W_p)B_w \quad [5\text{-}1]$$

where N_p is the cumulative oil production in m^3, B_o, B_g, and B_w are the formation volume factor for oil, gas, and water, respectively, R_p is the cumulative gas oil ratio, R_s is the solution gas oil ratio, B_{oi} is the initial oil formation volume factor, R_{si} is the initial solution gas oil ratio, m is the ratio of the initial hydrocarbon pore volume of the gas cap to that of the oil, N is the stock tank oil initially in place in m^3, B_{gi} is the initial gas formation volume factor, c_w is the water compressibility in psi^{-1}, S_{wc} is the connate rater saturation, c_f is rock compressibility in psi^{-1}, ΔP is the pressure drop in psi, W_e is the cumulative water influx in m^3, and W_p is the cumulative water produced in m^3.

The above equation can be rewritten as,

$$N_p[B_o + (R_p - R_s)B_g] = NB_{oi}\left[\frac{\dfrac{(B_o - B_{oi}) + (R_{si} - R_s)B_g}{B_{oi}} + m\left(\dfrac{B_g}{B_{gi}} - 1\right) + (1+m)\left(\dfrac{c_w S_{wc} + c_f}{1 - S_{wc}}\right)\Delta p}{}\right] + (W_e - W_p)B_w \quad [5\text{-}2]$$

The bubble-point pressure for this oil is calculated to be 1400 kPa with the CMG WinProp module. According to the production data retrieved from AccuMap, the reservoir pressure is maintained above the bubble-point pressure because an almost constant gas/oil ratio (about 13.5 scf/bbl) is observed until the end of September, 2011. Assuming that R_s=R_{si}=R_p (i.e., there is no initial gas cap), m=0, and water flux, W_e=0, Equation [5-2] can be simplified as,

$$N_p B_o = NB_{oi}\left[\frac{(B_o - B_{oi})}{B_{oi}} + \frac{(c_w s_{wc} + c_f)}{1 - S_{wc}}\Delta p\right] - W_p B_w \qquad [5\text{-}3]$$

The isothermal oil compressibility is given by,

$$c_o = -\frac{1}{V_o}\frac{dV_o}{dp} = -\frac{1}{B_o}\frac{dB_o}{dp} \approx \frac{-(B_{oi} - B_o)}{B_{oi}\Delta p} = \frac{(B_o - B_{oi})}{B_{oi}\Delta p} \qquad [5\text{-}4]$$

Combing Equations [5-3] and [5-4], the material balance equation can be further simplied as

$$N_p B_o = NB_{oi}\left[c_o + \left(\frac{c_w S_w + c_f}{1 - S_{wc}}\right)\right]\Delta p - W_p B_w \qquad [5\text{-}5]$$

Considering that $\Delta p = p_i - p(t)$, the average reservoir pressure during production process can be calculated using the following equation,

$$P(t) = P_i - \frac{N_p B_o + W_p B_w}{NB_{oi}\left[c_o + (\frac{c_w S_w + c_f}{1 - S_{wc}})\right]} \qquad [5\text{-}6]$$

where P_i is the initial reservoir pressure in psi and $P(t)$ is the current pressure in psi.

The following parameter values obtained from the CMG WinProp module are used in the calcualtions: $B_o \approx 1$ due to the small solution gas-oil ratio (GOR), $B_w \approx 1$,

$c_w = 0.8 \times 10^{-7}\ psi^{-1}$, and $c_o = 3.5 \times 10^{-6}\ psi^{-1}$. The compressibility factor of rock is set as $c_f = 2.5 \times 10^{-6}\ psi^{-1}$.

5.3 Results and Discussion

5.3.1 History matching

The production data of the 13 wells from December 1, 2010 to September 31, 2011 show that the fluids from these 13 wells were produced via primary recovery. Therefore, in this study, history matching is performed only for these 13 wells which experienced natural production via pressure depletion. Considering the fact that the oil properties used in this field-scale simulation are the same as those used in experimental simulation, the following parameters determined by the experimental history matching are also chosen for the field-scale simulation: the oil-phase dispersion coefficient of 5.0×10^{-8} m^2/s for CH_4 and C_3H_8, the RFF of 0.2 $m^3/(gmole.day)$ for gas dissolution, 2 day^{-1} for gas exsolution from oil phase to bubble, and 2×10^{-3} day^{-1} for gas exsolution from bubble to gaseous phase.

The measured oil production rates are used as the input constraints for the production wells. The oil-water and liquid-gas relative permeability curves used in the simulations are plotted in **FIGURE 5-4**. **FIGURE 5-5** presents history matching result of the average reservoir pressure, while **FIGURE 5-6** shows history matching results of the cumulative oil production, cumulative water production, and cumulative gas production, respectively. As can be seen from **FIGUREs 5-5** and **5-6**, there exists a good agreement between the simulated production profiles and the observed field data.

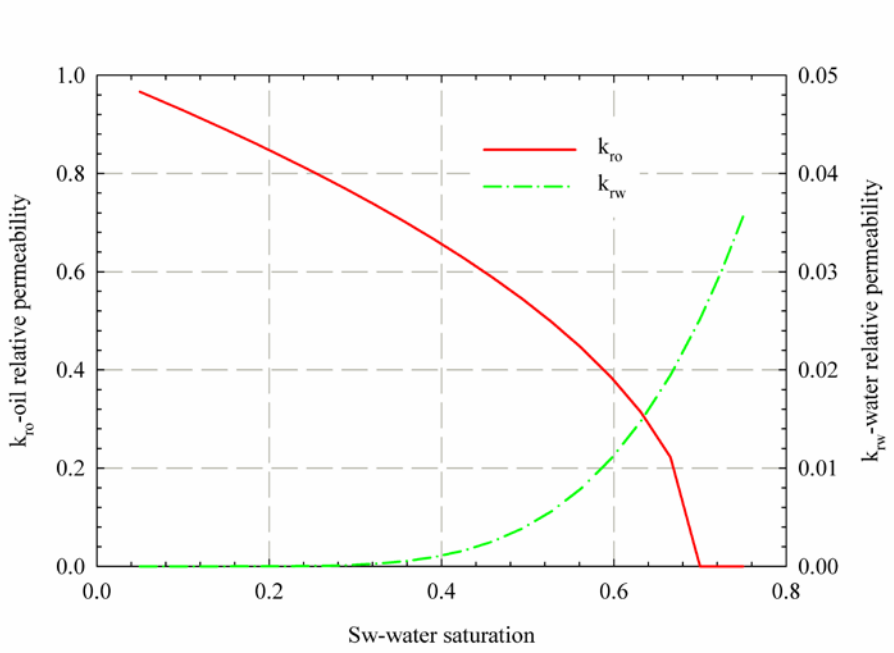

(a)

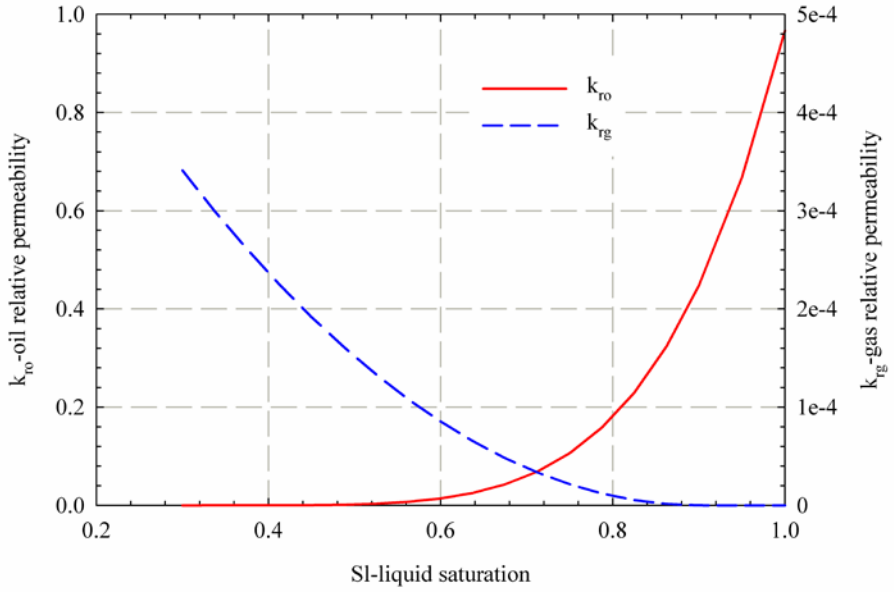

(b)

FIGURE 5-4: Relative permeability curves of **(a)** oil-water system and **(b)** oil-gas system

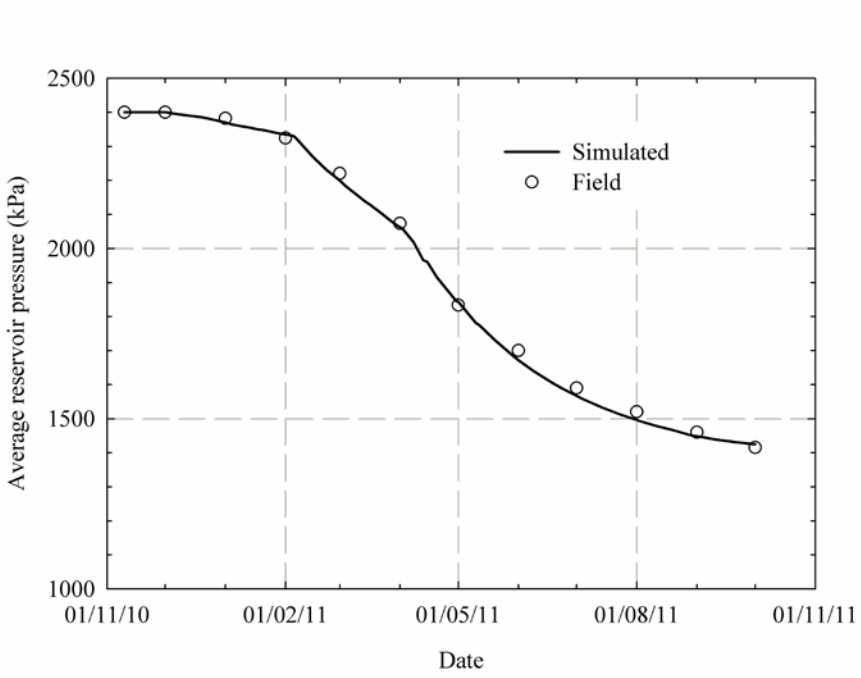

FIGURE 5-5: History matching result of the average reservoir pressure

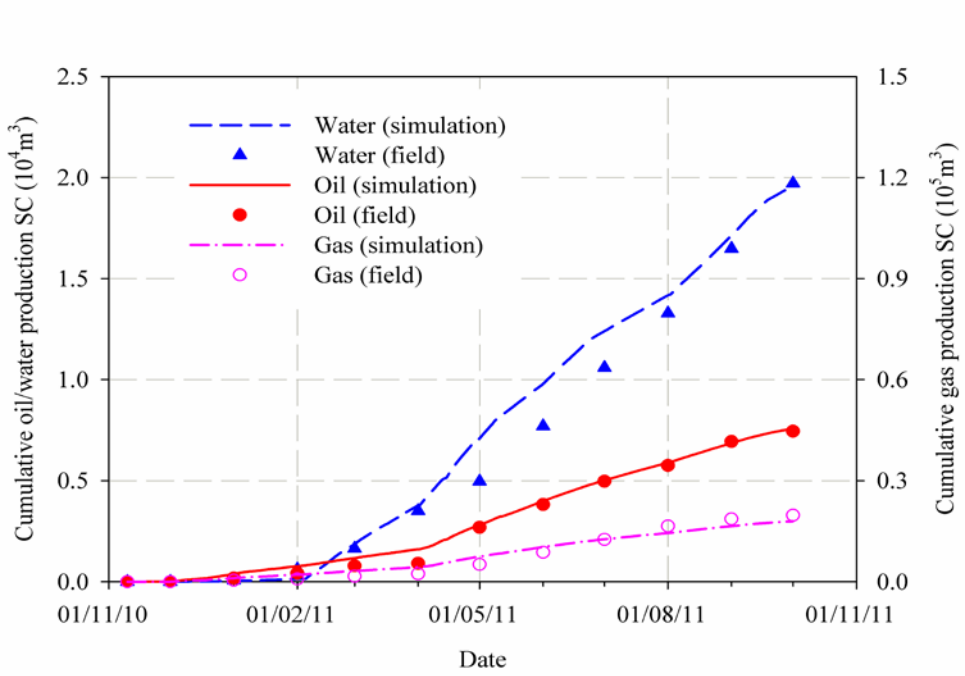

FIGURE 5-6: History matching results of the cumulative oil production, water production, and gas production

The upper 5 layers in Wabiskaw "A" formation are the major producing payzones, among which the top layer is not perforated in most of the 13 wells. As such, **FIGURE 5-7** shows the oil saturation distribution in the second upper layer before and after primary-depletion production, respectively. As can be seen from **FIGURE 5-7**, due to the low recovery factor (0.05% of OOIP) achieved in the primary recovery stage, the oil saturation distribution in the second layer remains almost unchanged.

FIGURE 5-8 depicts the pressure distribution in the second upper layer before and after depletion production, respectively. As can be seen, although the primary oil recovery is only 0.05% of OOIP, the reservoir pressure has experienced a significant decline from 2400 kPa to the bubble-point pressure (about 1400 kPa), indicating that there is only a small amount of solution gas dissolved in heavy oil which can only provide limited natural reservoir energy.

5.3.2 Optimization of operational parameters

The performance of the ECSP using CH_4-C_3H_8 is numerically simulated and predicted by using the CMG STAR simulator (Version 2011). During the simulation, synergetic mechanisms for improving heavy oil recovery are included, i.e., solution-gas-drive caused by CH_4 injection, viscosity reduction together with swelling effect due to C_3H_8 dissolution, and the foamy oil behaviour due to the released solvent from heavy oil. Based on the laboratory experiments, the ECSP scheme with CH_4-C_3H_8 pair is chosen as the suitable scheme for the targeted area.

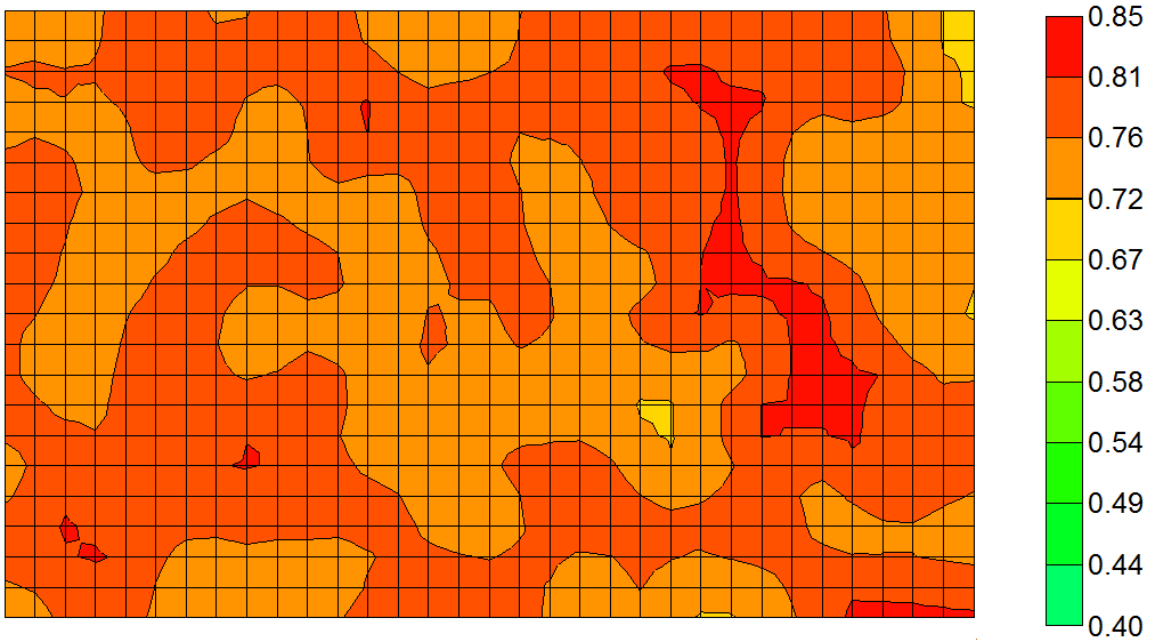

(a)

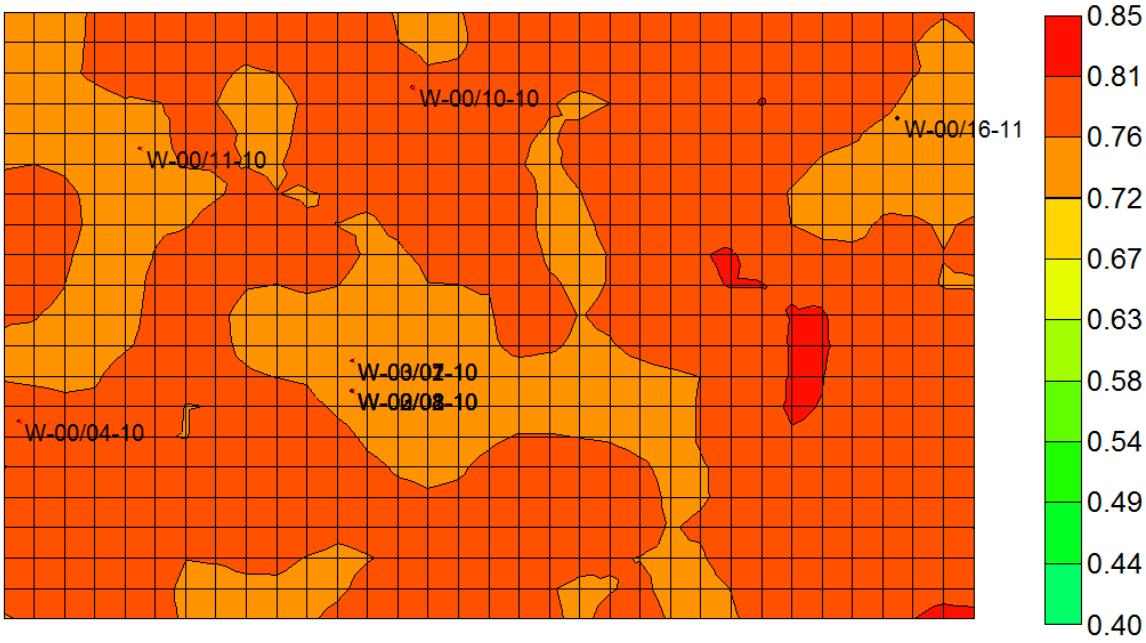

(b)

FIGURE 5-7: Oil saturation distribution in the second layer **(a)** before and **(b)** after primary-depletion production

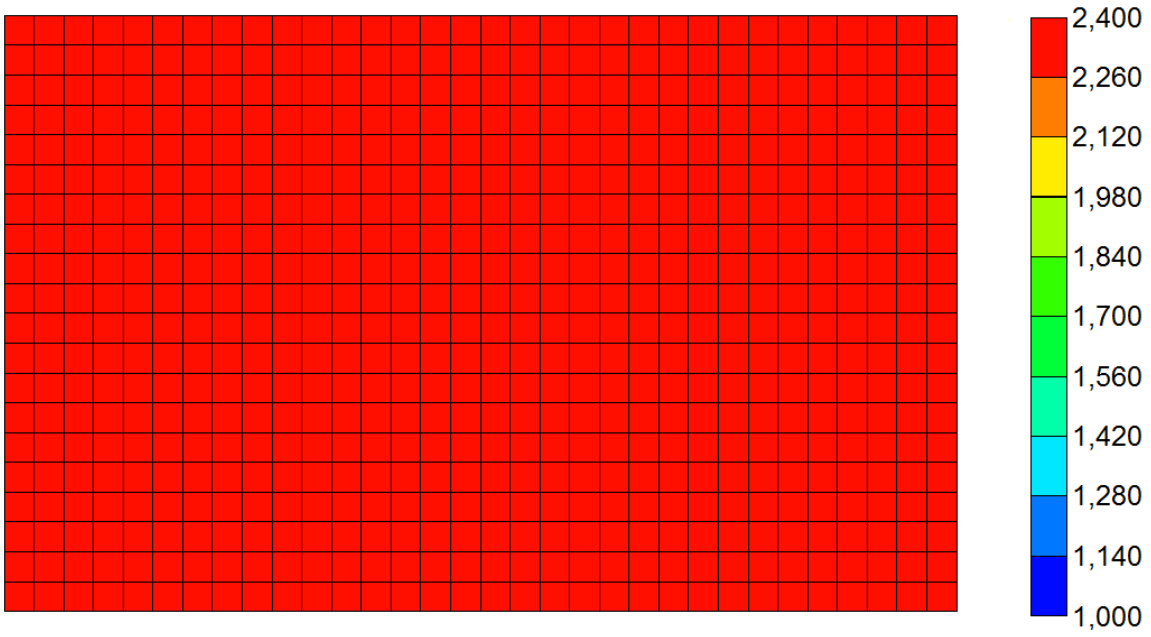

(a)

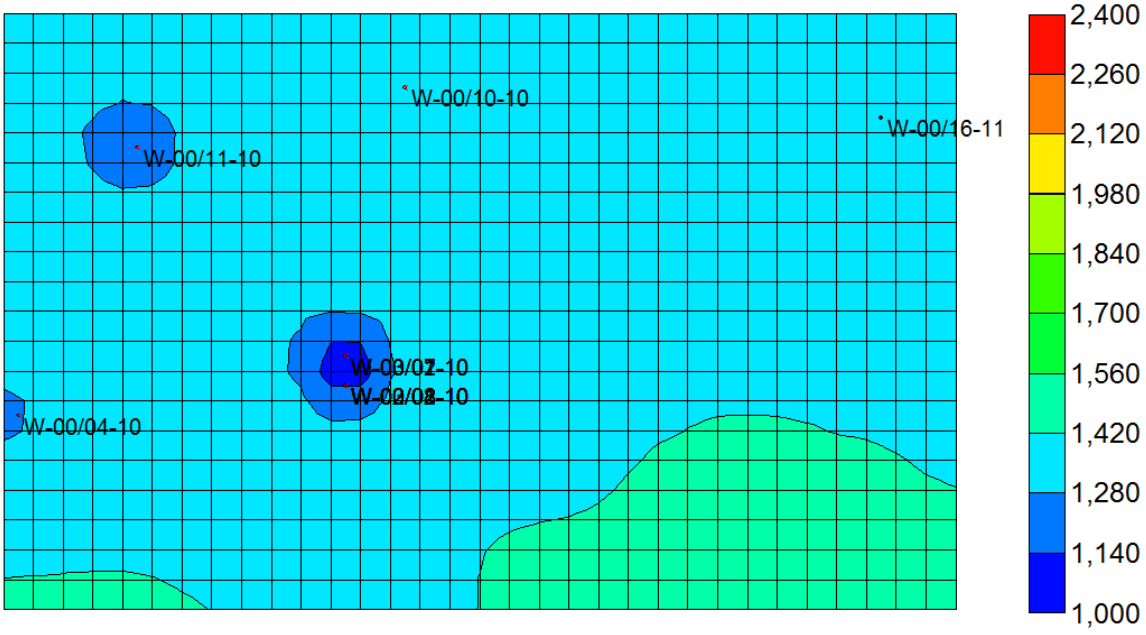

(b)

FIGURE 5-8: Pressure distribution in the second layer **(a)** before and **(b)** after primary-depletion production

The orthogonal design method (Yang *et al*., 2011) is used to optimize the operational parameters in the CH_4-C_3H_8 ECSP scheme. The following parameters are chosen as the to-be-optimized variables: injection rate and injection time of CH_4, injection rate and injection time of C_3H_8, soaking time, and minimum well bottomhole pressure. **TABLE 5-1** shows the five-level values for each of these 6 parameters. A $L_{25}5^6$ scheme is employed in the orthogonal design. The objective function is the cumulative oil production from December 1, 2010 to September 1, 2012. The results of simulation based on the orthogonal-experiment design are presented in **TABLE 5-2**.

FIGURE 5-9 shows the factor index for the orthogonal design. According to **TABLE 5-2** and **FIGURE 5-9**, it can be concluded that the highest recovery efficiency can be achieved when the injection rate of CH_4 is 200-500 Sm^3/day, the injection time of CH_4 is 2 days, the injection rate of C_3H_8 is 100 Sm^3/day, the injection time of C_3H_8 is 3 days, the soaking time is 3 days, and the minimum well bottomhole pressure is 200 kPa, respectively.

Statistical analysis of the cumulative oil (e.g., variance) resulted from these parameters should be considered in the orthogonal design to understand the relative sensitivity of the cumulative oil production to different influencing parameters. The variances of the cumulative oil resulted from injection rate and injection time of CH_4, injection rate and injection time of C_3H_8, soaking time, and minimum well bottomhole pressure are calculated to be $2.0\times10^4\,m^6$, $17.8\times10^4\,m^6$, $5.5\times10^4\,m^6$, $27.3\times10^4\,m^6$, $30.8\times10^4\,m^6$, and $70.7\times10^4\,m^6$, respectively. The larger the variance is, the more sensitive the parameter will be (Yang *et al*., 2011). Therefore, the minimum well

TABLE 5-1: Five levels of the six influencing parameters

Injection rate of CH_4 Sm^3/day	Injection time of CH_4, day	Injection rate of C_3H_8 Sm^3/day	Injection time of C_3H_8, day	Soaking time, day	Minimum well bottomhole pressure, kPa
200	2	100	2	3	200
500	3	200	3	7	300
1000	5	300	5	10	500
2000	7	400	7	14	800
3000	9	500	9	21	1000

TABLE 5-2: Orthogonal experiment design and simulation results

Simulation run No.	Injection rate of CH_4 Sm^3/day	Injection time of CH_4 day	Injection rate of C_3H_8 Sm^3/day	Injection time of C_3H_8 day	Soaking time day	Minimum well bottomhole pressure, kPa	Cumulative oil production m^3
1	200	2	100	2	3	200	25087
2	200	3	200	3	7	300	24270
3	200	5	300	5	10	500	22273
4	200	7	400	7	14	800	20574
5	200	9	500	9	21	1000	18279
6	500	2	200	5	14	1000	21188
7	500	3	300	7	21	200	22083
8	500	5	400	9	3	300	23006
9	500	7	500	2	7	500	22626
10	500	9	100	3	10	800	21552
11	1000	2	300	9	7	800	21047
12	1000	3	400	2	10	1000	21803
13	1000	5	500	3	14	200	22823
14	1000	7	100	5	21	300	21275
15	1000	9	200	7	3	500	21932
16	2000	2	400	3	21	500	22426
17	2000	3	500	5	3	800	21350
18	2000	5	100	7	7	1000	20847
19	2000	7	200	9	10	200	22102
20	2000	9	300	2	14	300	22174
21	3000	2	500	7	10	300	22383
22	3000	3	100	9	14	500	22001
23	3000	5	200	2	21	800	20850
24	3000	7	300	3	3	1000	21850
25	3000	9	400	5	7	200	22382

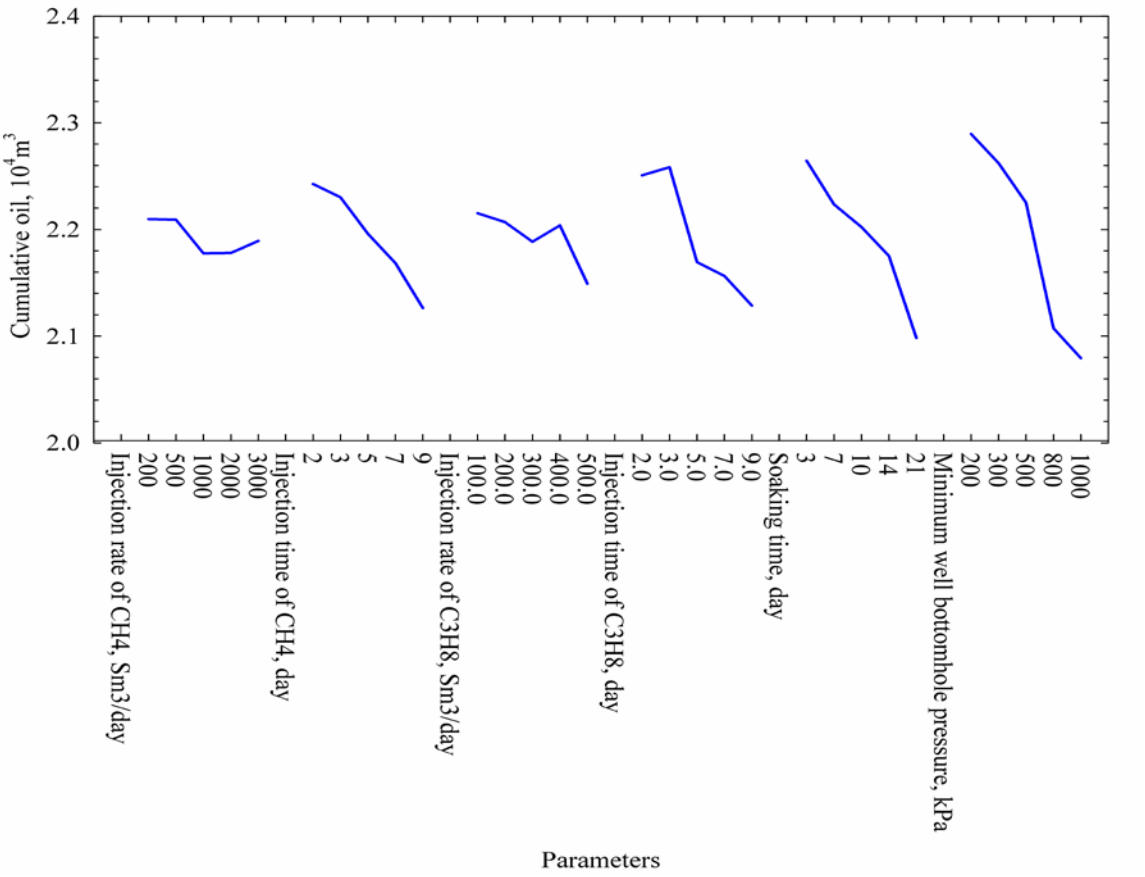

FIGURE 5-9: Factor index for the orthogonal design

bottomhole pressure is the most sensitive parameter and should be carefully set at a proper value for each specific scenario. The injection time of CH_4 and C_3H_8, and soaking time are also subject to relatively large sensitivities and hence should be carefully selected as well. The injection rates of CH_4 and C_3H_8 are less sensitive parameters due to the small variances resulted from them.

5.3.3 Performance prediction

Based on the orthogonal experiment design, the following operational parameters for the ECSP using CH_4-C_3H_8 are selected to be used in the 13 wells: the injection rate of CH_4 is 200 Sm^3/day, the injection time of CH_4 is 2 days, the injection rate of C_3H_8 is 100 Sm^3/day, the injection time of C_3H_8 is 3 days, the soaking time is 3 days, and the minimum well bottomhole pressure is 200 kPa. Subsequently, these parameters are incorporated into the history-matched reservoir model to predict the future field production performance for the ECSP.

FIGURE 5-10 presents the prediction results of cumulative oil production and cumulative water production during the 30 cycles of the ECSP from October 1, 2011 to May 5, 2017 compared to the production via primary recovery through the whole time. Due to the insufficient natural energy, both the cumulative oil production and cumulative water production via primary recovery increase slowly with time. Obviously, the cumulative oil production is found to increase quickly with time since the ECSP is initiated. Afterwards, the increasing rate in cumulative oil production slows slightly after 2 years of production. Meanwhile, the cumulative water production is increased with

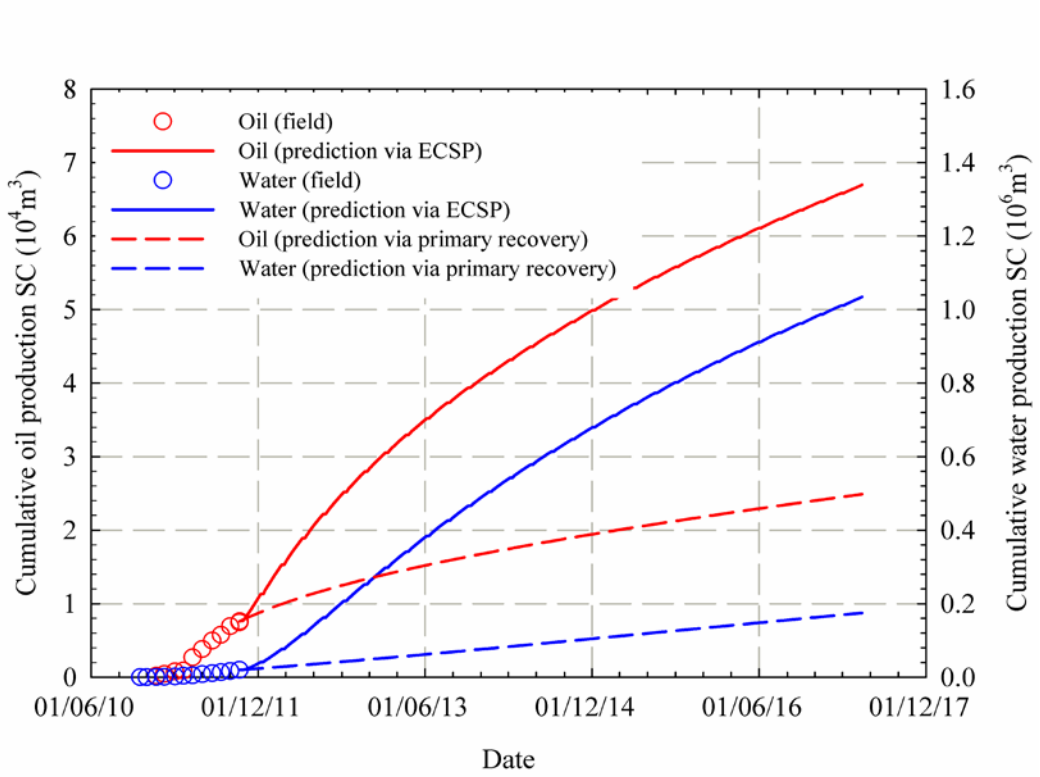

FIGURE 5-10: Predicted cumulative oil production and cumulative water production

time during the whole 5 and half years of production. This is mainly due to synergetic mechanisms for improving heavy oil recovery, i.e., solution-gas-drive caused by CH_4 injection, viscosity reduction together with swelling effect due to C_3H_8 dissolution, and the foamy oil behavior due to the released solvent from heavy oil.

FIGUREs 5-11 to **13** show the oil, water, and gas distribution in the second layer before (i.e., right after primary-depletion production) and after the ECSP, respectively. As can be seen from **FIGURE 5-11**, the oil saturation decreases in the whole second layer even far from the production wells due to the exsolution of solution gas from heavy oil, while decreasing significantly near the wellbore because of the good oil production near the wellbore. It can be seen from **FIGURE 5-12** that, in general, the water saturation in the second layer after ECSP treatment is much lower than that prior to the ECSP initiation mainly due to the fact that a large amount of water has been produced during the ECSP (See **FIGURE 5-10** for the cumulative water production). Since gas solvents (i.e., CH_4 and C_3H_8) are cyclically injected and produced from the same wellbore, the gas saturation adjacent to the wellbore experiences a dramatic increase as presented by **FIGURE 5-13**. As such, the above field-scale simulations clearly indicate that the proposed ECSP scheme is a highly effective method for improving the heavy oil recovery.

5.4 Summary

Simulation techniques have been developed to evaluate field-scale ECSP application in a targeted reservoir (i.e., the Pelican oilfield). Once history matching is accomplished,

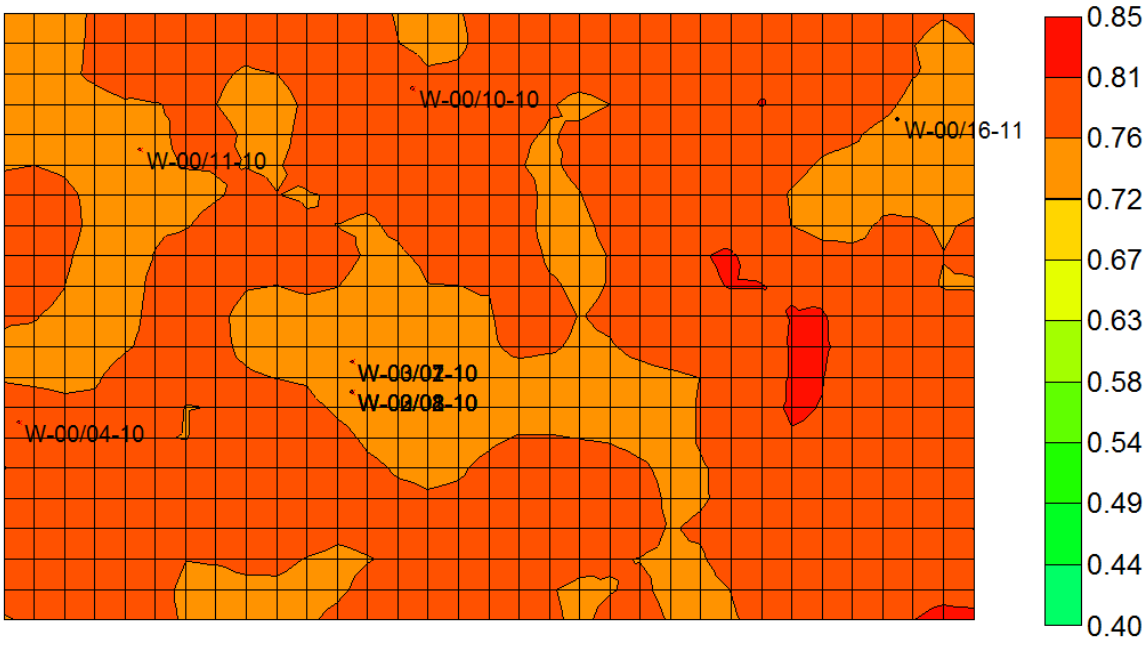

(a)

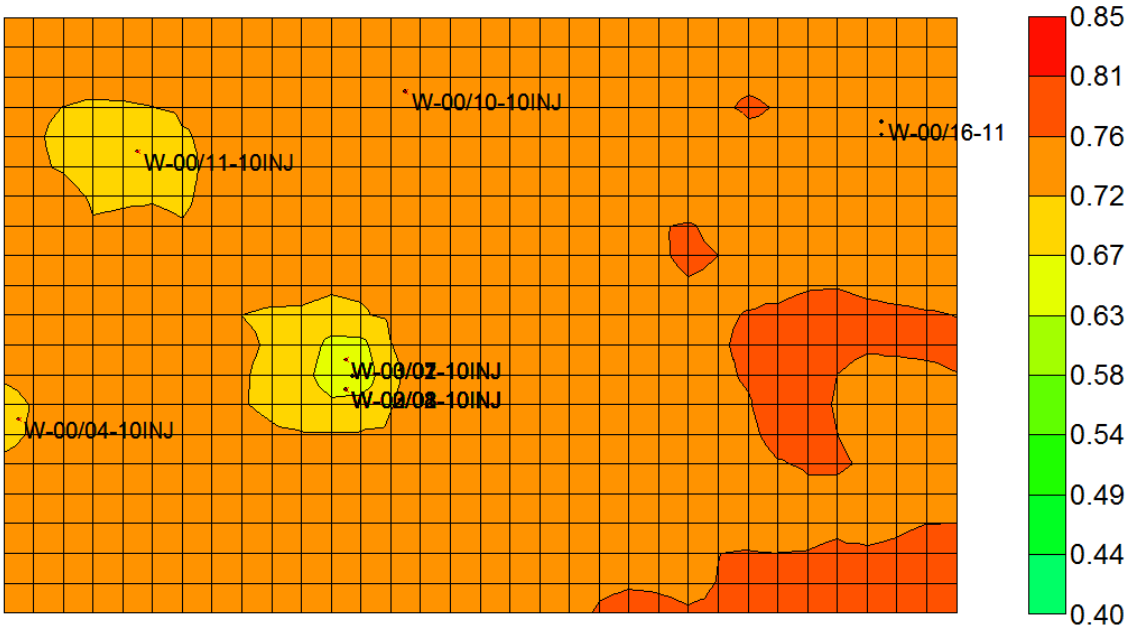

(b)

FIGURE 5-11: Oil saturation distribution in the second layer **(a)** before and **(b)** after the ECSP initialization

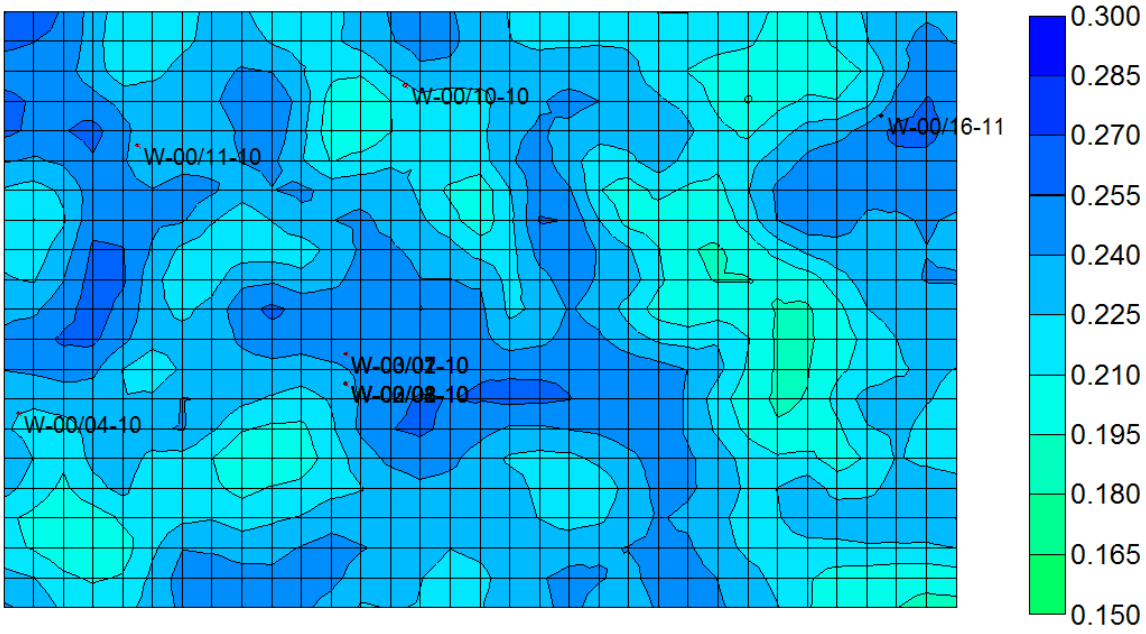

(a)

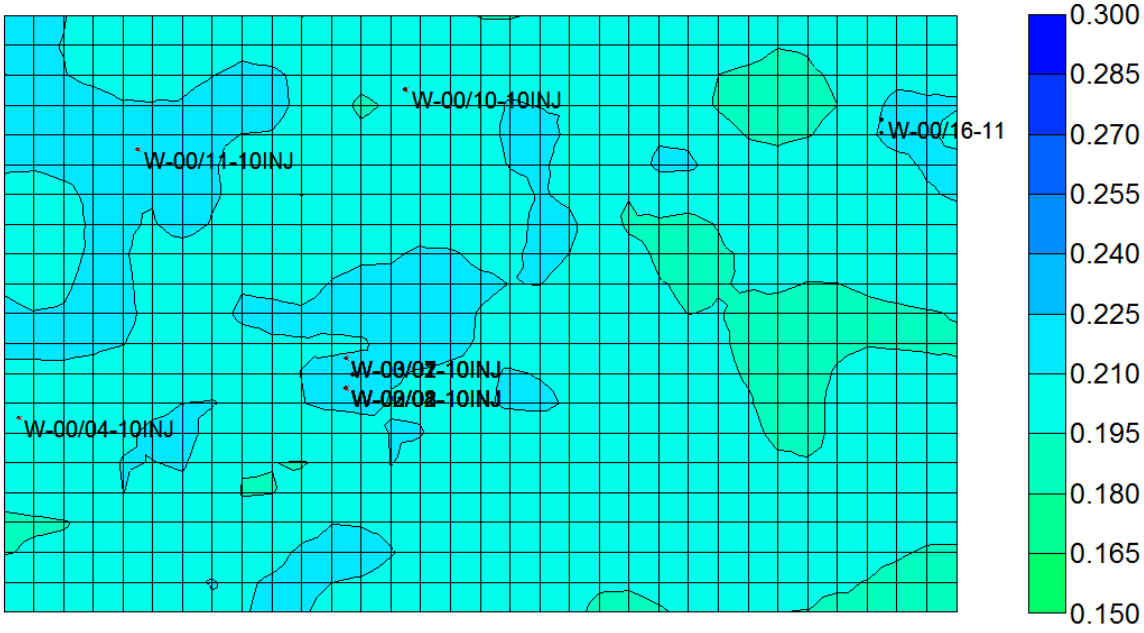

(b)

FIGURE 5-12: Water saturation distribution in the second layer **(a)** before and **(b)** after the ECSP initialization

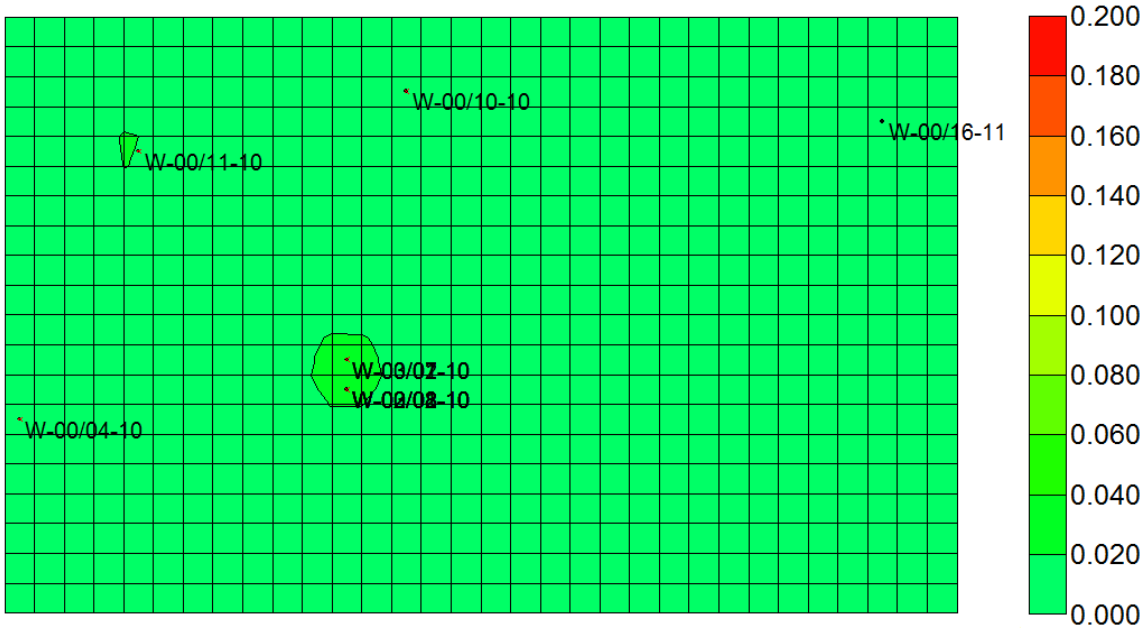

(a)

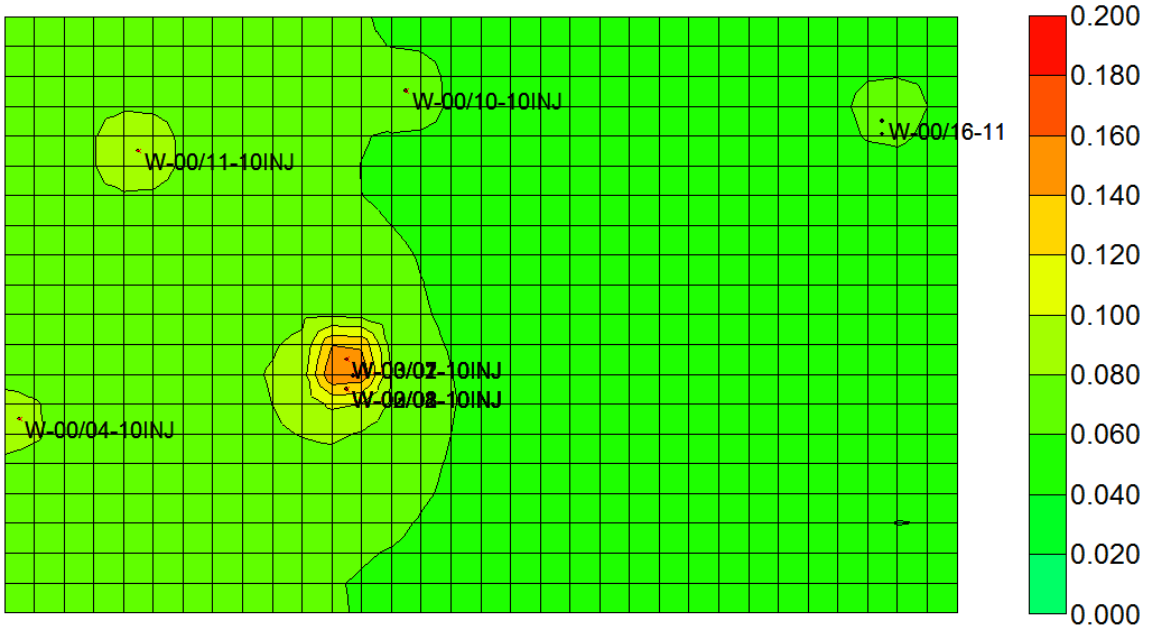

(b)

FIGURE 5-13: Gas saturation distribution in the second layer **(a)** before and **(b)** after the ECSP initialization

the history-matched reservoir model is used to predict the future field production performance for the CH_4-C_3H_8 ECSP scheme by using the optimized operational parameters obtained from the orthogonal design method.

There exists a good agreement between the simulated production profiles and the observed field data. The highest recovery efficiency can be achieved when 1) the injection rate of CH_4 is 200-500 Sm^3/day and the injection time of CH_4 is 2 days; 2) the injection rate and injection time of C_3H_8 are 100 Sm^3/day and 3 days, respectively, while the soaking time is 3 days and the minimum well bottomhole pressure is 200 kPa. The minimum well bottomhole pressure is the most sensitive parameter and should be carefully set at a proper value for each specific scenario. The injection time of CH_4 and C_3H_8, and soaking time are also subject to relatively large sensitivities and hence should be carefully selected as well.

As for the production prediction, the cumulative oil production increases quickly with time since the ECSP is initiated. Afterwards, the increasing rate in cumulative oil production slows slightly after 2 years of production. Meanwhile, the cumulative water production is increased with time during the whole 5 and half years of production. The oil saturation decreases due to good oil production near the wellbore and the exsolution of solution gas from heavy oil. The water saturation after ECSP treatment is much lower than that prior to the ECSP initiation mainly due to the fact that a large amount of water has been produced during the ECSP while the gas saturation adjacent to the wellbore experiences a dramatic increase since gas solvents are cyclically injected and produced from the same wellbore.

CHAPTER 6 CONCLUSIONS AND RECOMMENDATIONS

6.1 Conclusions

In this thesis study, techniques have been developed to comprehensively evaluate the performance of ECSP in the laboratory- and field-scale. The major conclusions that can be drawn from this study are summarized as follows,

(1) For the CH_4-C_3H_8-heavy oil mixture, the swelling factor of heavy oil maintains at a relatively high value for each test temperature, while the measured saturation pressures are also found to have high values, indicating that the dissolved methane comes out of solution easily when the pressure decreases. Meanwhile, the heavy oil viscosity can still be maintained to be low at a low pressure because C_3H_8 has a high solubility even at low pressures.

(2) The parameters in the PR EOS (1978) and the modified Pedersen (1987) corresponding states viscosity model are regressed using the experimentally measured phase behaviour data. The tuned PR EOS (1978) model can be used to reproduce the saturation pressures and swelling factors with an average relative error of 3.68% and 3.76%, respectively, while the modified viscosity model is able to predict the viscosity of solvent(s)-heavy oil systems with an average relative error of 10.74%.

(3) The ultimate oil recovery for the two ECSP tests using CH_4-C_2H_6 and CH_4-C_3H_8 are measured to be 18.7% and 41.1%, respectively. The ECSP

performance is enhanced significantly when C_2H_6 is replaced with C_3H_8 because C_3H_8 has a higher solubility at the same condition and can reduce the oil viscosity and swell the oil to a larger degree. The dominant mechanisms of ECSP using CH_4-C_3H_8 to enhance oil recovery are solution gas drive due to the more volatile solvent (i.e., CH_4), viscosity reduction and swelling effect due to the enhanced dissolution of more soluble solvent (C_3H_8) in heavy oil.

(4) There exists a good agreement between the experimental and numerical results for each individual ECSP test, indicating that the mechanisms governing the ECSP has been largely captured in the numerical simulations. As for ECSP using CH_4 and C_3H_8, the deeper penetration of gas into the sandpack and larger gas saturation in the sandpack result in a larger contact area between solvent and heavy oil so that more solvent can be dissolved in the heavy oil.

(5) A minor impact on the oil recovery is observed when the diffusion coefficients are in the order of 10^{-9} to 10^{-10} m^2/s, but the dispersion coefficient imposes a strong impact on the oil recovery factor. The oil recovery factor first increases with the dispersion coefficient, and then tends to level off when dispersion coefficient falls in the order of 10^{-6} m^2/s. The reaction frequency factor (RFF) for gas exsolution from bubble to gas phase almost shows no influence on the oil recovery. In comparison, the RFFs for gas dissolution and exsolution from oil phase to bubble affect the oil recovery to a larger extent.

(6) The orthogonal design method is used to optimize the operational parameters in ECSP using CH_4 and C_3H_8. The highest recovery efficiency can be achieved when: 1) the injection pressure of C_3H_8 is 1150.0 kPa and the injection time of

C_3H_8 is 5.0 hour; 2) the injection pressure and time of CH_4 are 7000.0 kPa and 10.0 hours, respectively; 3) the soaking time is 24.0 hours; and 4) the minimum production pressure is 101.0 kPa. The injection pressure of CH_4 and minimum production pressure are found to be the most sensitive parameters.

(7) There exists a good agreement between the simulated production profiles and the observed field data. The highest recovery efficiency can be achieved when 1) the injection rate of CH_4 is 200-500 Sm^3/day and the injection time of CH_4 is 2 days; 2) the injection rate and injection time of C_3H_8 are 100 Sm^3/day and 3 days, respectively, while the soaking time is 3 days and the minimum well bottomhole pressure is 200 kPa. The minimum well bottomhole pressure is the most sensitive parameter while the injection time of CH_4 and C_3H_8, and soaking time are also subject to relatively large sensitivities.

(8) As for the field-scale production prediction, the cumulative oil production increases quickly with time since the ECSP is initiated. Afterwards, the increasing rate slows slightly after 2 years of production. Meanwhile, the cumulative water production is increased with time during the whole 5 and half years of production. After ECSP treatment, the oil saturation decreases due to good oil production near the wellbore and the exsolution of solution gas from heavy oil. The water saturation is much lower than that prior to the ECSP initiation mainly due to the fact that a large amount of water has been produced during the ECSP while the gas saturation adjacent to the wellbore experiences a dramatic increase since gas solvents are cyclically injected and produced from the same wellbore.

6.2 Recommendations

Based on this study, the following recommendations are listed for future research as follows:

(1) Since the ECSP may be a potential post-CHOPS EOR method, it is essential that modelling CHOPS be performed in a systematic manner. Difficulties in modelling CHOPS result from the representation of foamy oil behaviour and wormhole network growth. Although foamy oil behaviour has been captured in this study, geomechanical effects that mainly refer to dynamic wormhole network growth should be considered in the oilfield application of this method.

(2) The ECSP performance has been evaluated for directional wells in the Pelican oilfield in this study, but horizontal wells may be more efficient to recover heavy oil by using the ECSP in this oilfield and the design of well pattern is also very critical to maximize the potential of ECSP. Therefore, future research could focus on the application of ECSP on horizontal wells together with optimization of well patterns.

(3) In this study, even though ECSP has greatly enhanced oil recovery in both laboratory- and field-scale, the NPV has not been calculated, which reflects the economic benefit. Thus, the NPV associated with the ECSP in an oilfield could be considered in future research according to the cost and profit. Also, it can be compared with the NPVs obtained from other EOR methods.

REFERENCES

Abukhalifeh, H. *Determination of Concentration-Dependent Dispersion of Propane in Vapor Extraction of Heavy Oil*. PhD Dissertation, Ryerson University, Canada, 2010.

Adams, D.M. Experiences with Waterflooding Lloydminster Heavy-Oil Reservoirs. *J. Pet. Tech*. 34 (8), 1643-1650, 1982.

Alvarez, J. and Coates, R. Heavy Oil Recovery-Cyclical Solvent Injection (CSI). *ROGTEC Oil & Gas News*, May 27, 2009.

Ambastha, A.K. and Kumar, M. New Insights Into In-Situ Combustion Simulation for Heavy Oil Reservoirs. Paper SPE 56543, presented at the SPE Annual Technical Conference and Exhibition, Houston, TX, October 3-6, 1999.

Arhuoma, M., Yang, D., Dong, M., Li, H., and Idem, R. Numerical Simulation of Displacement Mechanisms for Enhancing Heavy Oil Recovery during Alkaline Flooding. *Energy Fuels* 23 (12), 5995-6002, 2009a.

Arhuoma, M., Yang, D., Dong, M., Li, H., and Idem, R. Determination of Increase in Pressure Drop and Oil Recovery Associated with Alkaline Flooding for Heavy Oil Reservoirs. Paper PETSOC 2009-053, presented at the Canadian International Petroleum Conference, Calgary, AB, June 16-18, 2009b.

Badamchi-Zadeh, A., Yarranton, H.W., Maini, B.B., and Satyro, M.A. Phase Behaviour and Physical Property Measurements for VAPEX Solvents: Part II. Propane, Carbon Dioxide and Athabasca Bitumen. *J. Can. Pet. Technol*. 48 (3), 57-65, 2009.

Barrufet, M.A. and Setiadarma, A. Reliable Heavy Oil-Solvent Viscosity Mixing Rules for Viscosities up to 450K, Oil-Solvent Viscosity Ratios up to 4×10^5, and Any Solvent Proportion. *Fluid Phase Equilib*. 213 (1-2), 65-79, 2003.

Bijeljic, B., Muggeridge, A.H., and Blunt, M.J. Multi-Component Mass Transfer across Water Films during Hydrocarbon Gas Injection. *Chem. Eng. Sci.* 58 (11), 2377-2388, 2003.

Bohannon, J.M. A linear Programming Model for Optimum Development of Multi-Reservoir Pipeline Systems. *J. Pet. Tech*. 22 (11), 1429-1436, 1970.

Boustani, A. and Maini, B.B. The Role of Diffusion and Convective Dispersion in Vapour Extraction Process. *J. Can. Pet. Technol*. 40 (4), 68-77, 2001.

Bowers, B. and Drummond, K.J. Conventional Crude Oil Resources of the Western Canada Sedimentary Basin. *J. Can. Pet. Technol.* 36 (2), 56-63, 1997.

Butler, R.M. and Mokrys, I.J. A New Process (VAPEX) for Recovering Heavy Oils Using Hot Water and Hydrocarbon Vapour. *J. Can. Pet. Technol.* 30 (1), 97-106, 1991.

Butler, R.M. and Jiang, Q. Improved Recovery of Heavy Oil by Vapex with Widely Spaced Horizontal Injectors and Producers. *J. Can. Pet. Technol.* 39(1), 48-56, 2000.

CAPP. *Statistical Handbook for Canada's Upstream Petroleum Industry*. Calgary, AB, Canada, 2013.

Carroll III, J.A. and Horne, R. Multivariate Optimization of Production Systems. *J. Pet. Tech*. 44 (7), 782-789, 1992.

Chang, J. and Ivory, J. Field Scale Simulation of Cyclic Solvent Injection (CSI). Paper SPE 157804, presented at the SPE Heavy Oil Conference, Calgary, AB, June 12-14, 2012.

Chang, J. Understanding HW-CSS for Thin Heavy Oil Reservoir. Paper SPE 165386, presented at the SPE Heavy Oil Conference, Calgary, AB, June 11-13, 2013.

Chen, J. and Maini, B. Numerical Simulation of Foamy Oil Depletion Tests. Paper PETSOC 2005-073, presented at the Petroleum Society's Canadian International Petroleum Conference, Calgary, AB, June 7-9, 2005.

Chen, S. *Integrated Optimization of CO_2 Enhanced Oil Recovery and Storage under Uncertainty*. PhD Dissertation, University of Regina, Canada, 2012.

Chugh, S., Baker, R., and Telesford, A. Mainstream Options for Heavy Oil: Part I-Cold Production. *J. Can. Pet. Technol.* 39(4), 31-39, 2000.

Computer Modelling Group Ltd. STARS Advanced Process and Thermal Reservoir Simulator. Calgary, AB, Canada, 2011.

Computer Modelling Group Ltd. WinProp Phase Property Program. Calgary, AB, Canada, 2011.

Coskuner, G., Naderi, K., and Babadagli, T. An Enhanced Oil Recovery Technology as a Follow Up to Cold Heavy Oil Production with Sand. Paper SPE 165385, presented at the SPE Heavy Oil Conference, Calgary, AB, June 11-13, 2013.

Cuthiell, D., Mccarthy, C., Frauenfeld, T., Cameron, S., and Kissel, G. Investigation of the VAPEX Process Using CT Scanning and Numerical Simulation. *J. Can. Pet. Technol.* 42 (2), 41-49, 2003.

Dake, L.P. *Fundamentals of Reservoir Engineering*. Elsevier Publishing Company, Amsterdam, 2010.

Das, S.K. and Butler, R.M. Mechanism of the Vapor Extraction Process for Heavy Oil and Bitumen. *J. Pet. Sci. Eng*. 21 (1-2), 43-59, 1998.

Denbina, E.S., Baker, R.O., Gegunde, G.G., Klesken, A.J., and Sodero, S.F. Modelling Cold Production for Heavy Oil Reservoirs. *J. Can. Pet. Technol.* 40 (3), 23-29, 2001.

Deo, M.D., Wang, C.J., and Hanson, F.V. Solubility of Carbon Dioxide in Tar Sand Bitumen: Experimental Determination and Modelling. *Ind. Eng. Chem. Res.* 30 (3), 532-536, 1991.

Dong, M., Huang, S., and Hutchence, K. Methane Pressure-Cycling Process with Horizontal Wells for Thin Heavy-Oil Reservoirs. *SPE Res. Eva. & Eng*. 9 (2), 154-164, 2006.

Dong, M., Ma, S., and Li, A. Sweep Efficiency Improvement by Alkaline Flooding for Pelican Lake Heavy Oil. Paper SPE 148971, presented at the SPE Canadian Unconventional Resources and International Petroleum Conference, Calgary, AB, November 15-17, 2011.

Dong, M., Mahinpey, N., Maini, B.B., Yang, D., Yadali Jamaloei, B., Guo, Z., and Yang, P. Enhanced Cyclic Solvent Process (ECSP) for Thin Heavy Oil Reservoirs. Final Report submitted to the Petroleum Technology Research Centre (PTRC), Regina, SK, 2013.

Dunn, S.G., Nenniger, E.H., and Rajan, V.S.V. A Study of Bitumen Recovery by Gravity Drainage Using Low Temperature Soluble Gas Injection. *Can. J. Chem. Eng*. 67 (6), 978-991, 1989.

Efron, B. and Stein, C. The Jackknife Estimate of Variance. *Ann. Stat.* 9 (3), 586-596, 1981.

El-Haj, R., Lohi, A., and Upreti, S.R. Experimental Determination of Butane Dispersion in Vapor Extraction of Heavy Oil and Bitumen. *J. Pet. Sci. Eng*. 67 (1-2), 41–47, 2009.

Fontaine, T., Hayes, L., and Reese, G. Development of Pelican Lake Area Using Horizontal Well Technologies. *J. Can. Pet. Technol.* 32 (9), 44-49, 1993.

Forth, R., Slevinsky, B., Lee, D., and Fedenczuk, L. Application of Statistical Analysis to Optimize Reservoir Performance. *J. Can. Pet. Technol*. 35 (8), 36-42, 1996.

Fossey, J.P., Morgan, R.J., and Hayes, L.A. Development of the Pelican Lake Area: Reservoir Considerations and Horizontal Technologies. *J. Can. Pet. Technol.* 36 (6), 53-56, 1997.

Frauenfeld, T.W.J., Kissel, G, and Zhou, S.B. PVT and Viscosity Measurements for Lloydminster-Aberfeldy and Cold Lake Blended Oil Systems. Paper SPE 79018, presented at the SPE International Thermal Operations and Heavy Oil Symposium and International Horizontal Well Technology Conference, Calgary, AB, November 4-7, 2002.

Freitag, N.P. Evidence That Naturally Occurring Inhibitors Affect the Low-Temperature Oxidation Kinetics of Heavy Oil. *J. Can. Pet. Technol*. 49 (7), 36-41, 2010.

Fujii, H. and Horne, R. Multivariate Optimization of Networked production Systems. *SPE Prod. Facil.* 10 (3), 165-171, 1995.

Ganapathy, R. *Solubility and Diffusivity Study for the Light Gases in Heavy Oil and Its Fractions*. MASc Thesis, University of Regina, Canada, 2009.

Grabowski, A., Nercessian, O., Fayolle, F., Blanchet, D., and Jeanthon, C. Microbial Diversity in Production Waters of a Low-Temperature Biodegraded Oil Reservoir. *FEMS Microbiol. Ecol.* 54 (3), 427-443, 2005.

Harding, T.J., Radcliffe, N.J., and King, P.R. Optimization of Production Strategies Using Stochastic Search Methods. Paper SPE 35518, presented at the SPE European 3-D Reservoir Modelling Conference, Stavanger, Norway, April 16-17, 1996

Hedayat, A.S., Sloane, N.J.A., and Stufken, J. *Orthogonal Arrays: Theory and Applications*. Springer Series, NY, USA, 1999.

Ivory, J., Chang, J., Coates, R., and Forshner, K. Investigation of Cyclic Solvent Injection Process for Heavy Oil Recovery. *J. Can. Pet. Technol.* 49 (9), 22-33, 2010.

Jameson, C.E. The Lloydminster Heavy Oil Area. *J. Can. Pet. Technol*. 12 (3), 16-19, 1973.

James, L.A., Rezaei, N., and Chatzis, I. VAPEX, Warm VAPEX and Hybrid VAPEX-The State of Enhanced Oil Recovery for In Situ Heavy Oils in Canada. *J. Can. Pet. Technol.* 47 (4), 1-7, 2008.

Jha, K.N. A Laboratory Study of Heavy Oil Recovery with Carbon Dioxide. *J. Can. Pet. Technol.* 25 (2), 54-63, 1986.

Kalla, S. and White, C.D. Efficient Design of Reservoir Simulation Studies for Development and Optimization. *SPE Res. Eva. & Eng*. 10 (6), 626-637, 2007.

Kasrale, M., Sammon, P.H., and Jespersen, P.J. Field Development Options for a Waterflooded Heavy-Oil Reservoir. *J. Pet. Tech.* 45 (9), 888-894, 1993.

Ko, S.C.M., Domier, D.B., and MacDermott, R.N. Waterflood Optimization of the Buffalo Coulee Bakken Heavy Oil Pool of Southwestern Saskatchewan. Paper SPE 30285, presented at the SPE International Heavy Oil Symposium, Calgary, AB, June 19-21, 1995.

Lee, A.S. and Aronofsky, J.S. A Linear Programming Model for Scheduling Crude Oil Production. *J. Pet. Tech*. 10 (7), 51-54, 1958.

Li, H., Zheng, S., and Yang, D. Enhanced Swelling Effect and Viscosity Reduction of Solvents-CO_2-Heavy Oil Systems. *SPE J.* 18 (4), 695-707, 2013.

Li, H. and Yang, D. Phase Behaviour of C_3H_8-n-C_4H_{10}-Heavy Oil Systems at High Pressures and Elevated Temperatures. *J. Can. Pet. Technol*. 52 (1), 30-40, 2013.

Li, H. *Phase Behaviour and Mass Transfer of Solvent(S)-CO_2-Heavy Oil Systems under Reservoir Conditions*. PhD Dissertation, University of Regina, Canada, 2013.

Lim, G.B., Kry, R.P., Harker, B.C., and Jha, K.N. Cyclic Stimulation of Cold Lake Oil Sand with Supercritical Ethane. Paper SPE 30298, presented at International Heavy Oil Symposium, Calgary, AB, June 19-21, 1995.

Lim, G.B., Kry, R.P., Harker, B.C., and Jha, K.N. Three-Dimensional Scaled Physical Modelling of Solvent Vapor Extraction of Cold Lake Bitumen. *J. Can. Pet. Technol*. 35 (4), 32-40, 1996.

Liu, Q., Dong, M., and Ma, S. Alkaline/Surfactant Flood Potential in Western Canadian Heavy Oil Reservoirs. Paper SPE 99791, presented at the SPE/DOE Symposium on Improved Oil Recovery, Tulsa, OK, April 22-26, 2006.

Luo, P. and Gu, Y. Effects of Asphaltene Content and Solvent Concentration on Heavy Oil Viscosity. Paper SPE 97778, presented at the SPE/PS-CIM/CHOA International Thermal Operations and Heavy Oil Symposium, Calgary, AB, November 1-3, 2005.

Luo, P. *Asphaltene Precipitation and Its Effects on a Solvent-Based Heavy Oil Recovery Process*. PhD Dissertation, University of Regina, Canada, 2009.

Marsh, R. and Hein, F. Canada's Extra-heavy (Bitumen) and Heavy Oil Resources, Reserves and Development. *J. Can. Pet. Technol.* 47(5), 7-11, 2008.

Marufuzzaman, M. *Solubility and Diffusivity of Carbon Dioxide, Ethane and Propane in Heavy Oil and Its Sara Fractions*. MASc Thesis, University of Regina, Canada, 2010.

Mehrotra, A.K. and Svrcek, W.Y. Correlations For Properties of Bitumen Saturated with CO_2, CH_4 and N_2, and Experiments with Combustion Gas Mixtures. *J. Can. Pet. Technol*. 21 (6), 95-104, 1982.

Mehrotra, A.K., Patience, G.S., and Svrcek, W.Y. Calculation of Gas Solubility in Wabasca Bitumen. *J. Can. Pet. Technol.* 28 (3), 81-83, 1989.

Milha, K.A. Interim Progress Report on Husky's Pikes Peak Steam Pilot. *J. Can. Pet. Technol*. 25(2), 41-46, 1986.

Miller, K.A. EOR Pilot Review-Husky Experience. Paper PETSOC SS-87-11, presented at the 1st Annual Technical Meeting of the South Saskatchewan Section, Regina, October 6-8, 1987.

Miller, K.A. Improving the State of the Art of Western Canadian Heavy Oil Waterflood Technology. *J. Can. Pet. Technol*. 45 (4), 7-11, 2006.

Nghiem, L.X., Kohse B.F., and Sammon, P.H. Compositional Simulation of the VAPEX Process. *J. Can. Pet. Technol.* 40 (8), 54-61, 2001.

Olenick, S., Schroeder, F.A., Haines, H.K., and Monger-McClure, T.G. Cyclic CO_2 Injection for Heavy-Oil Recovery in Halfmoon Field: Laboratory Evaluation and Pilot Performance. Paper SPE 24645, presented at the SPE Annual Technical Conference and Exhibition, Washington, DC, October 4-7, 1992.

Padamsey, R. and Railton, J. CO_2 Capture and Use for EOR in Western Canada-4. Economic Results and Conclusions. *Energy Convers. Manage.* 34 (9-11), 1165-1175, 1993.

Pan, Y., Chen, Z., Sun, J., Bao, X., Xiao, L., and Wang, R. Research Progress of Modelling on Cold Heavy Oil Production with Sand. Paper SPE 133587, presented at the SPE Western Regional Meeting, Anaheim, CA, May 27-29, 2010.

Pedersen, K.S. and Fredenslund, A. An Improved Corresponding States Model for the Prediction of Oil and Gas Viscosities and Thermal Conductivities. *Chem. Eng. Sci.* 42 (1), 182-186, 1987.

Peng, D.Y. and Robinson, D.B. A New Two-Constant Equation of State. *Ind. Eng. Chem. Fundam.* 15 (1), 59-64, 1976.

Qi, J. and Polikar, M. Optimal Solvent and Well Geometry for Production of Heavy Oil by Cyclic Solvent Injection. Paper PETSOC 2005-194, presented at the Canadian International Petroleum Conference, Calgary, AB, June 7-9, 2005.

Robinson, D.B. and Peng, D.Y. The Characterization of the Heptanes and Heavier Fractions for the GPA Peng-Robinson Programs, Research Report 28, Gas Producers Association (GPA), Tulsa, 1978.

Saskatchewan Energy and Resources. *Oil and Gas Industry Facts*, Regina, SK, Canada, 2008.

Satter, A. and Thakur, G.C. *Integrated Petroleum Reservoir Management: A Team Approach*. PennWell Publishing Company, Tulsa, OK, USA, 1994.

Sawatzky, R.P., Lillico, D.A., London, M.J., Tremblay, B.R., and Coates, R.M. Tracking Cold Production Footprints. Paper PETSOC 2002-86, presented at the Petroleum Society's Canadian International Petroleum Conference, Calgary, AB, June 11-13, 2002.

Shrivastava, V.K. *Physical Dispersion in Compositional Reservoir Simulation*. PhD Dissertation, University of Calgary, Canada, 2003.

Simant, R.U. and Anil, K.M. Diffusivity of CO_2, CH_4, C_2H_6 and N_2 in Athabasca bitumen. *Can. J. Chem. Eng.* 80 (1), 116-225, 2002.

Srivastava, R.K. and Huang. S.S. A Laboratory Evaluation of Suitable Operating Strategies for Enhanced Heavy Oil Recovery by Gas Injection. *J. Can. Petrol. Tech.* 36 (2), 33-41, 1997.

Srivastava, R.K., Huang, S.S., and Dong, M. Comparative Effectiveness of CO_2, Produced Gas, and Flue Gas for Enhanced Heavy-Oil Recovery. *SPE Res. Eva. & Eng*. 2 (3), 238-247, 1999.

Tavallali, M., Maini, B., Harding, T., and Busahmin, B. Assessment of SAGD Well Configuration Optimization in Lloydminster Heavy Oil Reserve. Paper SPE 153128, presented at the SPE/EAGE European Unconventional Resources Conference and Exhibition, Vienna, Austria, March 20-22, 2012.

Teja, A.S. and Sandler, S.I. A Corresponding States Equation for Saturated Liquid Densities. II. Applications to the Calculation of Swelling Factors of CO_2-crude Oil Systems. *AIChE J*. 26 (3), 341-345, 1980.

Thomas, S., Farouq Ali, S.M., Scoular, J.R., and Verkoczy, B. Chemical Methods for Heavy Oil Recovery. *J. Can. Pet. Technol*. 40 (3), 56-61, 2001.

Wassmuth, F.R., Green, K., Arnold, W., and Cameron, N. Polymer Flood Application to Improve Heavy Oil Recovery at East Bodo. *J. Can. Pet. Technol*. 48 (2), 55-61, 2009.

West, J. Performance Review of In Situ Oil Sands Scheme Approval 9404P. Report, Calgary, March 21, 2012.

Whitson, C.H. Characterizing Hydrocarbon Plus Fractions. *SPE J.* 23 (4), 683-694, 1983.

Wong, F.Y., Anderson, D.B., O'Rourke, J.C., Rea, H.Q., and Scheidt, K.A. Meeting the Challenge to Extend Success at the Pikes Peak Steam Project to Areas With Bottomwater. *SPE J.* 6 (3), 157-167, 2003.

Wu, H., Chang, B. and Zhu, C. A Special Case of Genetic Algorithm-Orthogonal Experimental Design Method (In Chinese). *J. Softw*. 12 (1), 148-153, 2001.

Xiao, W., Liu, Z., Jiang, M., and Shi, Y. Multiobjective Linear Programming on Injection Oilfield Recovery System. *Comput. Math. Appl*. 36 (5), 127-135, 1998.

Yadali Jamaloei, B., Dong, M., Mahinpey, N., and Maini, B.B. Enhanced Cyclic Solvent Process (ECSP) for Heavy Oil and Bitumen Recovery in Thin Reservoirs. *Energy Fuels* 26 (5), 2865-2874, 2012.

Yadali Jamaloei, B., Dong, M., Yang, P., Yang, D., and Mahinpey, N. Impact of Solvent Type and Injection Sequence on Enhanced Cyclic Solvent Process (ECSP) for Thin Heavy Oil Reservoirs. *J. Pet. Sci. Eng.*, in press.

Yang, C. and Gu, Y. New Experimental Method for Measuring Gas Diffusivity in Heavy Oil by the Dynamic Pendant Drop Volume Analysis (DPDVA). *Ind. Eng. Chem. Res.* 44 (12), 4474-4483, 2005.

Yang, C. and Gu, Y. Diffusion Coefficient and Oil-Swelling Factors of Carbon Dioxide, Methane, Ethane, Propane, and Their Mixtures in Heavy Oil. *Fluid Phase Equilib.* 243 (1-2), 64-73, 2006.

Yang, C. and Gu, Y. A Novel Experimental Technique for Studying Solvent Mass Transfer and Oil-Swelling Effect in the Vapour Extraction (VAPEX) Process. *J. Can. Pet. Technol*. 46 (9), 44-49, 2007.

Yang, P., Li, H., and Yang, D. Phase Behaviour of CH_4-C_3H_8-Heavy Oil Systems under Reservoir Conditions. Paper SPE 165502, presented the SPE Heavy Oil Conference, Calgary, AB, June 11-13, 2013.

Yang, X., Ma, C., and Deng, D. Orthogonal Test of Injection and Production Parameter Optimization of N_2 Simulation (In Chinese). *Xinjiang Oil & Gas* 7 (2), 63-65, 2011.

Yaws, C.L. Yaws' Handbook of Thermodynamic and Physical Properties of Chemical Compounds. Knovel Corporation, 2003; http://www.knovel.com/knovel2/Toc.jsp

Yazdani, J.A. and Maini, B.B. Measurements and Modelling of Phase Behaviour and Viscosity of a Heavy Oil/Butane System. *J. Can. Pet. Technol.* 49 (2), 9-14, 2010.

Zan, C., Ma, D., Wang, H., Li, X., Guo, J., Li, M., Jiang, H., and Luo, J. Experimental and Simulation Studies of Steam Flooding Process in Shallow, Thin Extra-Heavy Oil Reservoirs. Paper SPE 131942, presented at the CPS/SPE international Oil and Gas Conference and Exhibition, Beijing, China, June 8-10, 2010.

Zeng, F., Knorr, K.D., and Ryan R.W. Enhancing Oil Rate in Solvent Vapour Extraction Processes Through Tee-Well Pattern. Paper SPE 117528, presented at the SPE International Thermal Operations and Heavy Oil Symposium, Calgary, AB, October 20-23, 2008.

Zhao, R., Wu, X., Wang, R., Jiao, S., and Yang, S. Bubble Nucleation and Growth Mechanism in Heavy Oil Cold Production (In Chinese). *Special Oil & Gas Reservoirs* 18 (3), 101-104, 2011.